Aus dem Institut für Biochemie
der Medizinischen Fakultät Charité – Universitätsmedizin Berlin

DISSERTATION

The Role of Afadin Signaling in the Assembly of Spinal Locomotor Circuits

zur Erlangung des akademischen Grades Doctor of Philosophy (PhD)
im Rahmen des
International Graduate Program Medical Neurosciences

vorgelegt der
Medizinischen Fakultät Charité – Universitätsmedizin Berlin

von
Sophie Skarlatou
aus Athen, Griechenland

Datum der Promotion: 05.03.2021

PREFACE

The work presented in this thesis has been partly used for the manuscript "Afadin Signaling at the Spinal Neuroepithelium Regulates Central Canal Formation and Gait Selection" (hereafter cited as: Skarlatou et al., 2020), which has been published in Cell Reports on June 9th 2020.

TABLE OF CONTENTS

Preface ..... **II**

Table of contents ..... **III**

List of figures ..... **VI**

List of tables ..... **VIII**

List of abbreviations ..... **IX**

Abstract ..... **XIII**

Zusammenfassung ..... **XIV**

1. Introduction **1**

1.1 Definition of locomotion 2

1.2 Organization of the locomotor system 4

1.3 Supraspinal control of locomotion 6

1.4 Sensory feedback systems 7

1.5 Spinal control of locomotion 9

1.5.1 Development of the spinal cord 10

1.5.2 Diversification of spinal neurons 10

1.5.3 Axon guidance systems in the spinal cord 14

1.5.4 Spinal circuits for locomotion 15

1.5.4.1 Rhythm generation 16

1.5.4.2 Flexor/extensor alternation 17

1.5.4.3 Left/right alternation 18

1.5.4.4 Intersegmental control of locomotion 20

1.5.4.5 Modulation of motor output 21

1.5.4.6 Spinal topographic maps and sensory targeting 22

1.6 Afadin/nectin cell-adhesive recognition system 25

2. Aims of the project **27**

3. Material and methods **28**

3.1 Buffers and solutions 28
3.2 *In-situ* hybridization buffers 30
3.3 Mice 32
3.4 Genotyping 33
3.5 Embryonic spinal cord dissection 36
3.6 Perfusion and postnatal spinal cord dissection 36
3.7 Embedding 37
3.8 Immunohistochemistry 38
3.9 *In-situ* hybridization probe labeling 39
3.10 *In-situ* hybridization 40
3.11 Contralateral interneurons tracing 42
3.12 Cultivation of BHK-B19G and HEK293T cells 42
3.13 Rabies virus-mCherry amplification 44
3.14 Rabies virus-mCherry concentration 45
3.15 Rabies virus-mCherry titer determination 45
3.16 Intramuscular injections 46
3.17 Gait analysis 47
3.18 Three-dimensional positional analysis 47
3.19 Statistical analysis 48
3.20 List of chemicals and material 48
3.21 List of equipment 51
3.22 List of software 53
4. Results 54
4.1 Validation of *afadin* $^{fl/fl}$ mutant mice 54
4.2 Characterization of locomotor gait pattern 55
4.3 Analysis of motor neuron organization upon conditional afadin elimination 58
4.4 Afadin function at the neuroepithelium 61

4.5 Afadin function in postmitotic motor neurons 66
4.6 Expression of axon guidance cues in presence of a double central canal .. 67
4.7 Commissural axons trajectory upon reduction of Netrin-1 signal 70
4.8 Contralateral axonal projections upon disruption of Ephrin B3 signaling 72
4.9 Analysis of forelimb premotor connectivity 73
4.10 Identification of aberrantly wired interneurons populations 76
4.11 Analysis of hindlimb premotor connectivity 83
5. Discussion 86
5.1 Cell-cell adhesion and the organization of motor neurons 86
5.2 Afadin as a regulator of lumen formation 88
5.3 Roles of afadin in motor neuron synaptic specificity 90
5.4 Double central canal and the wiring of spinal motor circuits 91
5.5 Ephrin B3 dependency of interneurons wiring profiles 93
5.6 Influence of ectopic connections on sensory-motor integration 95
5.7 Organization of Intersegmental control of locomotion 96
5.8 Future perspectives 97
References 99
Appendix 119
Appendix I 119
Appendix II 121
Appendix III 122
Statutory Declaration 125
Curriculum vitae 127
Publications list 128
Acknowledgements 129

LIST OF FIGURES

Figure 1: Phases of a quadrupedal step cycle **3**

Figure 2: Basic components of the locomotor system **5**

Figure 3: Diversification of spinal neurons during development **12**

Figure 4: Spinal topographic map of the hindlimb **24**

Figure 5: Spinal cord embedding guidelines **38**

Figure 6: Afadin expression and motor neuron generation in control and *afadin* $^{fl/fl}$ mice **55**

Figure 7: Quantitative description of the gait pattern of control and *afadin* $^{fl/fl}$ mice **57**

Figure 8: Three-dimensional positional analysis of motor neurons at e13.5 ..... **59**

Figure 9: Three-dimensional positional analysis of motor neurons in adult mice ... **60**

Figure 10: Central canal development in control and *afadin* $^{fl/fl}$ mice **62**

Figure 11: Development of the actin network in control and *afadin* $^{fl/fl}$ mice **63**

Figure 12: Central canal development in e14.5 control and *afadin* $^{fl/fl}$*; Wnt1 (afW) embryos* **64**

FIgure 13: Central canal development in e16.5 control and *afadin* $^{fl/fl}$*; Wnt1 (afW) embryos* **65**

Figure 14: Central canal development and quantitative gait analysis in *afadin* $^{fl/fl}$*; ChAT (afC)* mice **67**

Figure 15: Netrin-1 mRNA expression at e13.5 and p1 ..... **68**

Figure 16: Ephrin B3 protein expression during development **69**

Figure 17: Commissural axons trajectory as identified by TAG-1 and Robo3 expression during development **71**

Figure 18: RDA tracing of spinal interneurons at e15.5 ..... **72**

Figure 19: Comparison of ECR premotor connectivity in control and *afadin* $^{fl/fl}$ mice **75**

Figure 20: Premotor connectivity of Lbx1^{+} interneurons in control and *afadin* $^{fl/fl}$ mice **77**

Figure 21: Premotor connectivity of Lhx1^{+}/FoxD3^{-} interneurons in control and *afadin* $^{fl/fl}$ mice.....**78**

Figure 22: Premotor connectivity of Lhx1^{+}/FoxD3^{+} interneurons in control and *afadin* $^{fl/fl}$ mice.....**79**

Figure 23: Premotor connectivity of ChAT^{+} interneurons in control and *afadin* $^{fl/fl}$ mice **81**

Figure 24: Premotor connectivity of Chx10^{+} interneurons in control and *afadin* $^{fl/fl}$ mice **82**

Figure 25: Identified ectopic interneurons complement contralateral control premotor map.....**83**

Figure 26: Comparison of GS and TA premotor connectivity in control and *afadin* $^{fl/fl}$ mice **84**

LIST OF TABLES

Table 1: Mouse strains employed in this study **33**

Table 2: Oligonucleotides used for genotyping **34**

Table 3: Annealing temperatures and extension times used for genotyping programs **36**

Table 4: Primary antibodies employed in this study **39**

Table 5: Secondary antibodies employed in this study **39**

Table 6: ISH-probes employed in this study **40**

Table 7: Cell lines employed in this study **42**

Table 8: Locomotor parameters in control, *afadin* $^{fl/fl}$ and *afadin* $^{fl/fl}$*; ChAT* mice ... **119**

Table 9: Afadin and grey matter measurements in e14.5 control and *afadin* $^{fl/fl}$*; Wnt1* mice **121**

Table 10: Afadin, phalloidin and grey matter measurements in e16.5 control and *afadin* $^{fl/fl}$*; Wnt1* mice **121**

Table 11: Number of neurons labeled in each ECR RV tracing experiment **122**

Table 12: Number of neurons labeled in each GS and TA RV tracing experiment **124**

LIST OF ABBREVIATIONS

ACSF = artificial cerebrospinal fluid

AJ = adherens junction

BCIP = 5-bromo-4-chloro-3-indolyl phosphate

Bmp = bone morphogenetic protein

CAM = cell-cell adhesion molecule

Cdc42 = cell division control protein 42

cDNA = complementary DNA

ChAT = choline acetyltransferase

Chx10 = ceh-10 homeodomain-containing homologue

Cno = Canoe

CNS = central nervous system

CPG = central pattern generator

CST = corticospinal tract

CTB = cholera toxin subunit B

Dbx (1/2) = developing brain homeobox protein (1/2)

DDC = deleted in colorectal carcinoma

DMEM = Dulbecco's modified Eagle medium

DMRT3 = Doublesex- and Mab3-related transcription factor

DNA = deoxyribonucleic acid

dNTP = deoxynucleoside triphosphate

DSCT = dorsal spinocerebellar tract

DV = dorsoventral

e = embryonic day

ECR = extensor carpis radialis

En1 = Engrailed-1

EDTA = ethylenediamine tetraacetic acid

FBS = fetal bovine serum

FGF = fibroblast growth factor

Fgfr1 = fibroblast growth factor receptor 1

FL = floxed

FoxD3 = fordkead box D3

FoxP1 = forkhead box protein 1

G = rabies virus glycoprotein

GABA = γ-aminobutyric acid

GATA2 = GATA-binding protein 2

Gi = gigantocellular nucleus

GM = grey matter

GS = gastrocnemius

Hb9 = basic helix-loop-helix domain containing, class B, 9

HBSS = Hanks' balanced salt solution

HINGS = heat inactivated normal goat serum

Irx3 = Iroquois-class homeobox protein 3

ISH = *in-situ* hybridization

Lbx1 = ladybird homeobox protein 1

Lhx (1/3) = LIM homeobox (1/3)

LMC = lateral motor column

LMCl = lateral LMC

LMCm = medial LMC

LPGi = lateral paragigantocellular nucleus

LPN = long projecting neuron

Mc = magnocellular nucleus

ML = mediolateral

MMC = medial motor column

NBT = nitro blue tetrazolium chloride

Olig (2/3) = oligodendrocyte transcription factor (2/3)

p = postnatal day

PAJ = puncta adherentia junction

Pax (3/6/7) = paired boxed protein (3/6/7)

PB = phosphate buffer

PBS = phosphate buffer saline

PCR = polymerase chain reaction

PFA = paraformaldehyde

Plxnd1 = Plexin D1

PTN = pyramidal tract neuron

RA = retinoic acid

RC = rostrocaudal

RDA = tetramethyl-rhodamine dextran

RNA = ribonucleic acid

Robo3 = roundabout guidance receptor 3

RV = rabies virus

RVΔG = G-deficient rabies virus

SCI = spinal cord injury

SDS = sodium dodecylsulfate

Sema3e = class 3 semaphorin 3

Shh = sonic hedgehog

Shox2 = short stature homeobox protein 2

SIM1 = single-minded homologue 1

SSC = saline sodium citrate

TA = tibialis anterior

TAG-1 = contactin 2

TAE = tris-acetate-EDTA

TE = tris-EDTA

vGlut2 = vesicular glutamate transporter 2

VP = virus particles

Wnt1 = Wnt family member 1

WT = wild-type

WT1 = Wilms' tumor protein 1

ABSTRACT

Coordinated movement sequences, such as locomotor episodes, are defined by the precisely orchestrated timing of muscle activation. The basic pattern of motor rhythm is determined by spinal circuits comprising sets of interneurons that modulate distinct aspects of motor neuron activity. The accuracy that underlies such motor behaviors implies strict connectivity patterns in the spinal cord that arise through the interplay of different developmental programs, including cellular diversification, axon guidance and neuronal positioning. Cell adhesive cadherin/catenin and afadin signaling have been found to be involved in the assembly of motor circuits by regulating the organization of motor neurons during development. However, the implications of disrupted cell-adhesive signaling for motor behavior are still largely unknown. In this study, we sought to better understand the role of afadin in the assembly of locomotor circuits. For this purpose, afadin was conditionally eliminated from motor neuron progenitors, which led to a striking locomotor phenotype: the alternation of left and right limbs during on-ground locomotion was replaced by synchronous stimulation of paired appendages. Surprisingly, our data showed that the perturbed gait pattern was not a consequence of mispositioned motor neurons, but rather that of disrupted central canal morphogenesis. As a result, animals that lacked afadin in the motor neuron progenitor zone displayed a split central canal, which affected the expression of Ephrin B3, one of the main regulators of axonal trajectories across the spinal cord midline. Finally, analysis of limb premotor connectivity using rabies virus tracing demonstrated the presence of aberrant connections arising from the contralateral side of the spinal cord of different interneurons subtypes, including dI4-dI5s, putative V0s, V0cs and V2as, thus contributing to changes in the balance of motor neuron activation across the two halves of the body. Together, these results show that afadin signaling plays a crucial role in the development of locomotor circuits by regulating the generation of the central canal and thereby also maintaining the balance that ensures coordinated left/right movements.

ZUSAMMENFASSUNG

Koordinierte Bewegungssequenzen, wie sie beispielsweise bei Fortbewegungsabläufen gegeben sind, werden durch präzise abgestimmte Muskelaktivierungen definiert. Das Grundschema des motorischen Rhythmus wird durch spinale Netwerke bestimmt, die Gruppen von Interneuronen umfassen, die ihrerseits verschiedene Aspekte der Motoneuronenaktivität modulieren. Die Genauigkeit, die solchen Bewegungen zugrunde liegt, deutet auf strikte Konnektivitätsmuster im Rückenmark hin, die durch das Zusammenspiel unterschiedlicher Entwicklungsprogramme entstehen. Dazu gehören die zelluläre Diversifizierung, die axonale Wegfindung und die neuronale Positionierung. Die Zelladhäsionssysteme der Cadherine/Catenine und Afadin sind an der Zusammensetzung von motorischen Netwerken beteiligt, indem sie die Ansiedlung von Motoneuronen während der Entwicklung regulieren. Allerdings, sind die Auswirkungen einer gestörten Zelladhäsion auf das motorische Verhalten größtenteils noch unbekannt. Ziel dieser Studie war es, die Rolle von Afadin in der Entwicklung von lokomotorischen Netzwerken besser zu verstehen. Zu diesem Zweck, wurde Afadin konditional in motorischen Vorläuferzellen eliminiert, was einen markanten lokomotorischen Phänotyp zur Folge hatte: das Alternieren der linken und rechten Gliedmaßen während der Fortbewegung auf festem Boden wurde durch eine synchrone Stimulierung von gepaarten Körperteilen ersetzt. Interessanterweise, zeigten unsere Daten, dass sich das Bewegungsverhalten nicht aufgrund fehlpositionierter Motoneuronen änderte, sondern eher eine Konsequenz der gestörten Zentralkanalmorphogenese war. Folglich, weisten Tiere ohne Afadin in der Motoneuronenvorläuferzone einen geteilten Zentralkanal auf, wodurch die Expression von Ephrin B3, eines der wichtigsten molekularen Merkmale, die die Navigation von Axonen über die Mittellinie des Rückenmarks steuern, unterbrochen war. Schließlich, zeigte eine Analyse der prämotorischen Konnektivität mittels Tollwutvirus-Tracing das Vorhandensein von aberranten kontralateralen Verbindungen verschiedener Interneuronen, einschließlich dI4-dI5, mutmaßlichen V0, V0c und V2a, was zu einer Verlagerung des Gleichgewichts der Motoneuronaktivierung zwischen den beiden Körperhälften führte.

Zusammenfassend, zeigen die Ergebnisse dieser Studie, dass Afadin eine entscheidende Rolle in der Entwicklung lokomotorischer Netzwerke spielt indem es die Bildung des Zentralkanals reguliert und damit auch das Gleichgewicht aufrechterhält, welches koordinierte links/rechts Bewegungen gewährleistet.

1. INTRODUCTION

Vertebrates display a wide spectrum of behaviors that allow them to interact with their surroundings and generate suitable responses to external stimuli that are essential for their survival. From the apparently simple and repetitive innate breathing movements through the more complex premeditated motor behavior of grasping an object to the subtle act of communicating through facial expressions - what we see is the result of a precise sequence of muscle contractions. Each of these behaviors relies on the communication between appropriately interconnected neurons comprised in the central nervous system (CNS) and the propagation of these signals to the executing organs, the muscles.

Understanding the organization and functional operation of neuronal circuits underlying specific behaviors is a major challenge in neuroscience that promises to provide new insights into the principles governing movement and new entry points for therapeutic strategies. Every year, 250 000 to 500 000 people worldwide are diagnosed with a condition that compromises the function of spinal circuits, including, but not limited to, spinal cord injury (SCI), neurodegenerative diseases and other genetic disorders that interfere with motor coordination and/or sensory perception (World Health Organization, 2011). Affected patients experience difficulties in everyday activities due to loss of basic body functions and have a higher mortality risk. The available treatments to date aim at ameliorating the symptoms through pharmacological intervention and promoting the reconstitution of cell connections that integrate sensory signals and direct movement through physical training. However, the success rate is very low and there is high demand for more effective methods.

The focus of this study will be the circuits that control locomotion, one of the most susceptible behaviors. The high degree of precision and reliability with which the automated and coordinated movement sequences are executed during locomotion imply stringent connectivity patterns underlying the function of spinal motor circuits. Elucidating the molecular mechanisms determining cell type specification and circuit formation during development will equip us with the knowledge and tools to more accurately restore neuronal networks and activity in the spinal cord and, thus, give these patients a chance of better recovery in the future.

1.1 DEFINITION OF LOCOMOTION

Locomotion is not only the motor action that allows an organism to move from A to B, but it also endows it with the mechanistic ability to perform evolutionary important tasks, such as food retrieval or escape. Many forms of locomotion have evolved in the course of time based on the environmental circumstances and needs of different animals, ranging from swimming to flying, crawling and walking. Nevertheless, they all have in common rhythmic and alternating movements of the body or its appendages, making locomotion one of the most conserved motor programs across species (Kandel et al., 2013; Ferreira-Pinto et al., 2018).

A locomotor episode can be divided into three temporarily separate phases: initiation, behavioral phase and termination (Ferreira-Pinto et al., 2018). Initiation reflects the transition from a stationary state to an actively moving state, which in the case of locomotion aims at bringing the body to a different place in space. It can be triggered by external stimuli, e.g. the sighting of a predator, or it can be the result of a changing internal state, e.g. hunger (Takakusaki, 2013). Similarly, the reasons for termination, which represents the opposite course of action, can vary depending on the context. The movement sequence of locomotion takes place during the behavioral phase. It consists of a series of stereotyped and repetitive sequential muscle contractions that are carefully coordinated along the two sides of the body and, in tetrapods, also between forelimbs and hindlimbs. Every repetition of this sequence is termed gait cycle and in every gait cycle each limb undergoes a complete step cycle, which can be broken down to four stages: the support phase or stance, the lift-off, the transfer phase or swing and the touchdown (Figure 1). Each of these stages has different biomechanical demands on the limb muscles, which is why the timing of their activation has to be tightly controlled.

Locomotor behavior can be further described by various attributes, each representing parameters that have to be regulated and adapted to the immediate surroundings and the given situation. The most relevant of these attributes are the spatiotemporal characteristics of limb placement that give rise to distinct footfall patterns and provide the substrate for different locomotor activities. Four types of gaits can be disinguished for quadrupeds on the basis of phenotypic limb

coordination: walk, which is defined as a movement where diagonal limbs are sequentially lifted while maintaining three feet simultaneously in contact with the ground; trot, where diagonal pairs of limbs move forward at the same time and opposite pairs of limbs alternate; bound, which is characterized by synchronous movement of forelimbs and hindlimbs; and gallop, which is an intermediate gait that expresses trot and bound features (Bellardita and Kiehn, 2015). Interestingly, the different footprint patterns are displayed at distinct ranges of speed, suggesting that the frequency of locomotion, which is determined by the behavioral context, is intimately related to the generated gait pattern. Accordingly, each speed range can be assigned a so-called attractor gait, which represents the state at which the biomechanical constraints underlying muscle contraction are stabilized. Based on these observations, out-of-phase walk, trot and full bound are robust gait patterns that are preferentially manifested in tetrapod locomotion at low, intermediate and high speeds, respectively (Lemieux et al., 2016). Finally, locomotion, being a purposeful behavior, is also characterized by its directionality (Ferreira-Pinto et al., 2018). The trajectory of a locomotor episode is a context-dependent function of extrinsic and intrinsic factors that direct movement and, thus, can exhibit variable degrees of straightforwardness, even within a single event. For example, exploratory behavior does not require a fixed direction and is continuously modified in line with incoming sensory input about the surroundings of the subject while high-speed escape running is a goal-directed movement with a clear direction until the encounter of an obstacle or the onset of termination.

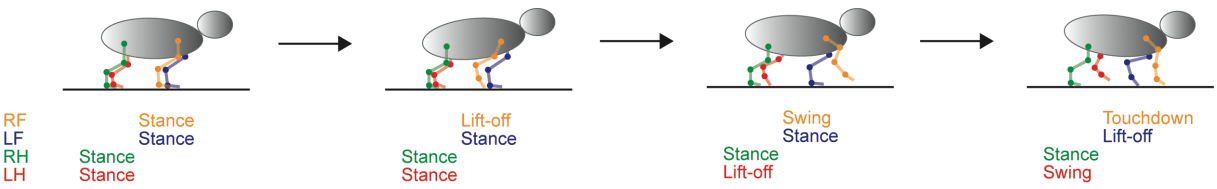

Figure 1. Four phases of a quadrupedal step cycle. In legged locomotion, the phases of the leg movement in a cycle are typically divided into four phases: stance, lift-off, swing, and touchdown, which are sequentially repeated. Before the onset of locomotion, all four limbs are in contact with the ground (stance). When locomotion begins, one of the forelimbs is lifted (lift-off) and then extended to the front (swing) before being placed again on the ground (touchdown). The other limbs undergo the same transformations, whereas their exact timing relative to the reference forelimb will vary depending on the gait pattern.

1.2 ORGANIZATION OF THE LOCOMOTOR SYSTEM

Breaking locomotion down to its individual components, it becomes apparent that the seemingly simple and repetitive motor sequences are in fact more complex and depend on many factors. The locomotor system must therefore be regulated by a multitude of interleaved circuit modules with dedicated functions that engage different parts of the CNS.

Early anatomical experiments showed that decerebrate animals, where the brainstem is completely transected at the level of the midbrain, maintain their ability to produce spontaneous walking episodes (Langworthy, 1924). In addition, the cortex is not essential for locomotion, as animals that completely lack a cortex can still walk, display exploratory behavior and survive for many years (Goltz, 1892; Schaltenbrand and Cobb, 1931; Ten Cate and Van Herk, 1933; Bjursten et al., 1976). On the other hand, coordinated patterns of motor activity could also be evoked in animals that had undergone a spinal transection at the lower thoracic levels, suggesting that the spinal cord harbors all the necessary components to compute the rhythmicity of locomotion (Philippson, 1905; Sherrington, 1906; Sherrington, 1910). Finally, it was demonstrated that the generation of alternating muscle contractions does not depend on sensory input from the limbs (Graham Brown, 1911; Graham Brown, 1914).

Together, these findings provided first insights into the framework and function of the neural pathways that elicit and modulate motor behavior. Thanks to recent technological advances a more detailed study of the structures and control mechanisms involved in locomotion has been enabled. Nowadays, it is known that the vertebrate locomotor system can be divided into three main modules: the supraspinal centers that are responsible for planning and initiating behavior, the spinal circuits that produce the basic pattern of motor activity and the sensory feedback systems that adjust the locomotor output to the environmental circumstances (Figure 2). In order to understand how the different rhythmic motor patterns are encoded for and executed within this system, it is necessary to study the developmental and genetic programs that instruct its organization and connectivity. The following sections shall give a brief overview of the state of knowledge about the roles of different CNS regions.

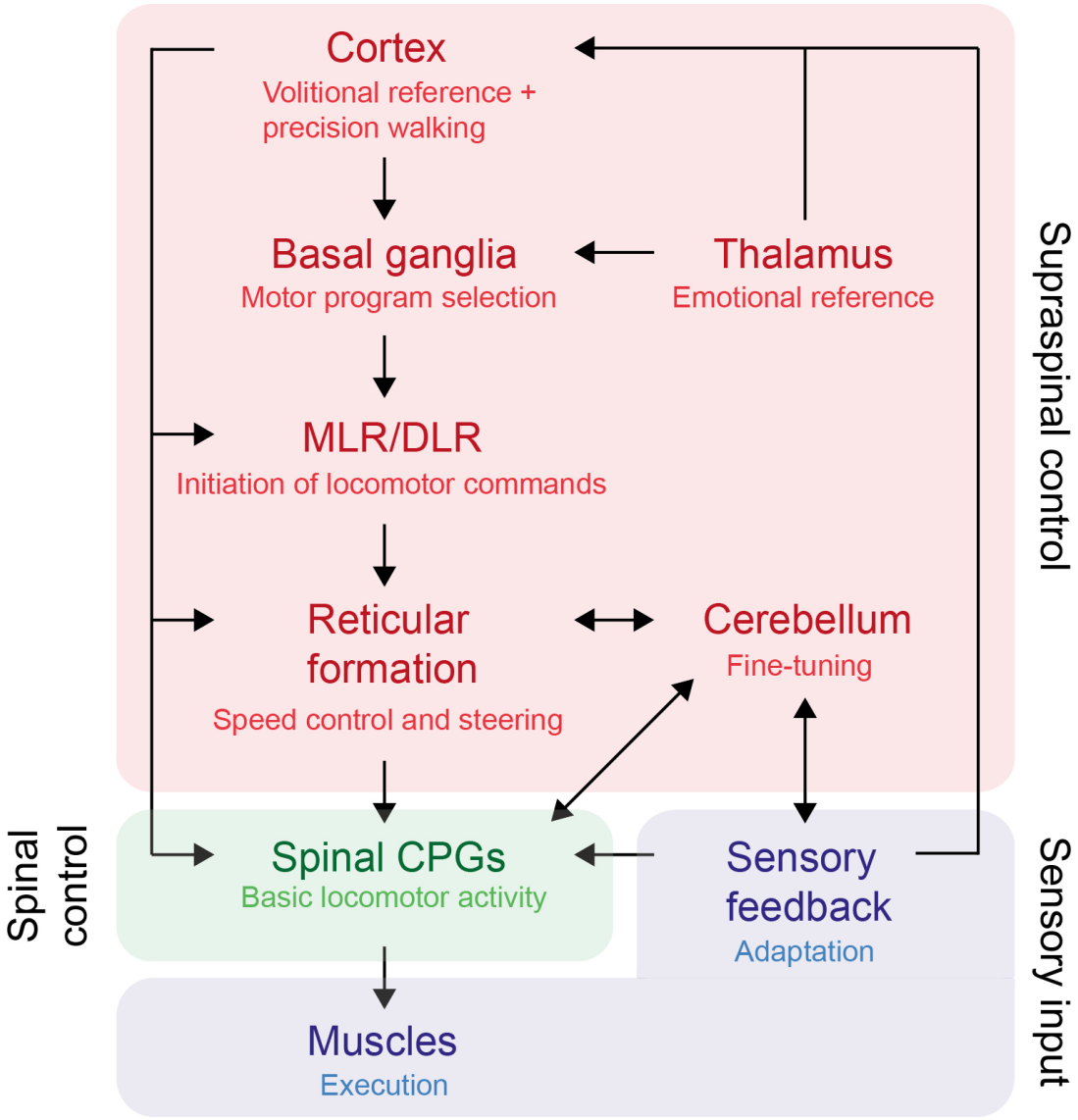

Figure 2. Basic components of the locomotor system. Locomotion engages the function of different parts of the CNS that can be roughly divided into supraspinal control, spinal control and sensory feedback systems. The basal ganglia select the appropriate basic locomotor pattern on the basis of thalamic (emotional reference) or cortical (volitional reference) input. Their output acts on the MLR or DLR, which in turn stimulate reticulospinal neurons in the LPGi that control spinal CPGs. The interneurons in the spinal circuits determine the rhythm of motor neuron activation, which ultimately generate the motor output by eliciting the corresponding muscle contractions. The cortex is in charge of planning the limb trajectory and foot placement when the surroundings demand more specialized gait movements. Sensory feedback mechanisms that are in direct contact with the CPGs in the spinal cord are able to adjust behavior according to external stimuli bypassing higher centers. CPG = central pattern generator, MLR = mesencephalic locomotor region, DLR = diencephalic locomotor region, LPGi = lateral paragigantocellular nucleus.

1.3 SUPRASPINAL CONTROL OF LOCOMOTION

In the twentieth century it was established that neuronal networks in the spinal cord are capable of generating intrinsic patterns of motor activity independently of sensory (Graham Brown, 1911; Graham Brown, 1914) or descending input (Kudo and Yamada, 1987). This gave rise to the concept of spinal central pattern generators (CPGs) that control and command rhythmic axial and limb movements (Goulding, 2009), ruling out a role for supraspinal areas for the production of basic activity patterns. Nevertheless, communication between spinal circuits and supraspinal centers is essential for the planning and initiation as well as for the adaptation of motor programs.

Depending on the situation, the stimulus that elicits locomotion can have a cognitive reference, that arises in the cerebral cortex, or an emotional reference that originates in the limbic hypothalamus (Takakusaki, 2013). Regardless of the source, the command is transmitted to the basal ganglia, a set of forebrain nuclei whose main role is to select the appropriate motor program for a context-specific behavior. The striatum, which represents the input layer of the basal ganglia, receives excitatory signals from the cortex and thalamus that activate γ-aminobutyric acid (GABA)-expressing striatal spiny projection neurons. In turn, these cells deactivate the output neurons in the globus pallidus interna and substantia nigra pars reticulata that maintain the downstream locomotor regions in the mesencephalon and diencephalon under tonic inhibition (DeLong, 1972; Garcia-Rill et al., 1981; Swanson et al., 1983; Carpenter, 1984; Takakusaki et al., 2003). As a consequence, an activating signal is induced in the mesencephalic or diencephalic locomotor region, which is conveyed to the spinal cord through excitatory reticulospinal neurons of the lower brainstem (Deniau & Chevalier, 1985; Dubuc et al., 2008; Jordan et al., 2008; Roberts et al., 2008).

While this pathway provides the direct command for triggering the locomotor CPG networks, the functional interplay of additional brain regions is required to fine-tune or adjust the locomotor output to unknown territory or unpredictable conditions. Pyramidal tract neurons (PTNs) of the corticospinal tract (CST) have been attributed roles in postural control and voluntary gait modifications (Beloozerova and Sirota,

1993; Drew, 1993; Widajewicz et al., 1994; Beloozerova et al., 2005). PTNs can directly interact with CPG interneurons in the spinal cord or exert indirect influence on motor networks through brainstem circuits (Orlovsky et al., 1999; Lemon, 2008). In addition, to evaluate the necessity of a change in limb trajectory and/or foot placement, the locomotor apparatus also requires visual guidance. Studies have shown that cells in area 5 of the posterior parietal cortex alter their discharge activity in anticipation of the actual onset of a gait modification (Beloozerova and Sirota, 2003), an observation that was not affected by interruption of the visual perception or later removal of an obstacle (McVea & Pearson, 2006; Marigold & Drew, 2011). The ability to maintain a representation of the encountered impediment is particularly important for guiding the hindlimbs, when the visual contact is not given anymore. On the other hand, locomotor parameters, such as the speed or the direction, are regulated by additional brainstem neurons. Two regions have been shown to establish connections with both cervical and lumbar spinal CPGs: the magnocellular nucleus (Mc) and the gigantocellular nucleus (Gi) (Esposito et al., 2014). Different cell populations in an Mc subdomain called lateral paragigantocellular nucleus (LPGi) have been implicated in inducing fast locomotion or behavioral arrest, respectively, (Bouvier et al., 2015; Capelli at el., 2017) whereas Chx10 expressing Gi neurons have been proposed to control left/right locomotor asymmetries (Cregg et al., 2019). Finally, the cerebellum is responsible for fine-tuning the locomotor output on a step-by-step basis. Cortical signals are integrated along with input from the dorsal and ventral spinocerebellar tracts that convey sensory information about the state of the limbs and dynamic information about the CPG commands during each step cycle (Arshavsky et al., 1972a; Arshavsky et al., 1972b). Its output neurons project back to vestibular and reticular nuclei, but can also contact spinal cord neurons, thus having a direct influence on the specific control of limb movements and muscle tone.

1.4 SENSORY FEEDBACK SYSTEMS

Although sensory input is dispensable for the expression of rhythmic activity patterns, afferent feedback can dynamically interact with the locomotion-generating centers in a state- and phase-dependent manner. Thus, locomotion is the result of

centrally generated motor patterns that are being constantly adapted to the environmental circumstances through feedback mechanisms. The feedback originates from cutaneous or proprioceptive afferents in the muscles as well as other sensory senses, like vision and audition, and can affect both the supraspinal regulation of locomotion and the timing and coordination of motor neuron activity at spinal levels (Rossignol et al., 2006).

Proprioceptive input plays an important role during normal step cycles as it ensures that the sequence of motor neuron activation is precisely timed based on the biomechanical state of the limbs (Pearson, 2004). For example, the swing phase of a stepping event is only initiated when the load on the extensor muscle has been attenuated. This information is conveyed by sensory neurons in the corresponding muscles. Group Ia/II muscle spindles, that function as stretch receptors and detect the length of the muscle, in cooperation with group Ib Golgi tendon organs (GTOs), that sense changes in muscle tension, influence locomotor activity via mono- or disynaptic pathways (Duysens et al., 1980; Pearson, 1995; Akay et al., 2014). In addition, proprioceptive control can also help to maintain the equilibrium and generate an appropriate response to a perturbation by advancing or delaying specific components of the step cycle, which endows an animal with the ability to regulate its speed (Rossignol et al., 2006).

The main role of cutaneous afferents is to monitor precise foot placement, in particular when the behavioral context requires adaptive modifications. Interestingly, the same stimulus might induce different reactions depending on the initial position or phase of the limb that is being excited (Rossignol et al., 2006; Grillner & El Manira, 2020). This is observed when an animal encounters an obstacle: if the impediment of movement is registered during the swing phase, the result will be an enhanced flexion that should allow the animal to overcome the obstacle; if, on the other hand, the stimulus is sensed during the stance phase, the extensor activity will be prolonged. This phase-dependent regulation was shown to be mediated by skin afferents (Forssberg et al., 1975; Mayer & Akay, 2018).

Sensory control over the final motor output is exerted either directly on neuronal components of the CPGs or through upstream circuits. Proprioceptors are known to form monosynaptic connections with motor neurons in the spinal cord in a highly precise fashion, selectively targeting those innervating synergistic muscles and

avoiding those with antagonistic functions (see section 1.5.4.6; Eccles et al., 1957). This enables rapid reactions called reflexes that take place without supraspinal involvement. Moreover, both proprioceptive and skin afferents contact spinal interneurons that are either themselves an integral part of the rhythmogenic complex or can modulate its activity by changing its rhythm and pattern (Lundberg, 1979; Moschovakis et al., 1992; Degtyarenko et al., 1998; Zampieri et al., 2014). Through ascending projections, sensory afferents also send signals to cerebellar and reticulospinal neurons (Valle et al., 2017). The latter integrate descending commands and sensory input and, thereafter, produce an adequate stimulation of the downstream executive centers. Finally, cutaneous input also modulates cortical activity during locomotion in order to generate the appropriate gait modifications (Marple-Horvat et al., 1993; Marple-Horvat & Armstrong, 1999).

1.5 SPINAL CONTROL OF LOCOMOTION

The broad behavioral repertoire exhibited by vertebrates is made possible through the precise interplay of the three main modules of the motor system: the supraspinal motor centers, the sensory feedback systems and the spinal neuronal networks. The latter are charged with the task of integrating descending and sensory input in order to produce the activity that will drive motor neurons to stimulate their muscle targets sequentially in a coordinated manner in order to generate an appropriate motor output (Kiehn, 2006; Goulding, 2009; Arber, 2012). In particular, the relative timing of left and right limb activation, which has to be regulated both intra- and intersegmentally, provides the basis for different locomotor outputs, ranging from swimming to walking and running (Grillner, 2006; Kiehn, 2016).

It is still not fully understood exactly how this information is encoded in the spinal cord, but recent advances in electrophysiological and molecular approaches have paved the way of identifying the key players and decoding the structure of the neuronal networks regulating the rhythm and pattern of locomotor behavior. It is believed nowadays that spinal CPGs underlie a modular organization, where different interconnected sets of interneurons are responsible for modulating specific facets of

locomotion. However, the precise interplay between parallel developmental programs controlling their assembly and ensuring their wiring specificity remains elusive.

1.5.1 DEVELOPMENT OF THE SPINAL CORD

The formation of the spinal cord begins after the three main cell layers of embryogenesis (endoderm, mesoderm and ectoderm) have developed and the neural differentiation of ectodermal cells is induced through disinhibition of TGFβ signaling by the mesoderm (Spemann & Mangold, 1924; Hemmati-Brivanlou & Melton, 1994; Hemmati-Brivanlou et al., 1994). The neural cells that are generated upon initiation of neuralization are collectively called neural plate. During neurulation, the neural plate invaginates and gives rise to a cylindrical tube that extends along the rostrocaudal axis of the embryo. At the rostral end, the neural tube expands and forms the brain whereas the caudal regions become the structure that we know as the spinal cord. As development proceeds, cells in the neural tube proliferate and populate the spinal cord in a conserved pattern that is regulated by the presence of molecular signals in the environment.

1.5.2 DIVERSIFICATION OF SPINAL NEURONS

Cell specification during spinal cord development is orchestrated by signaling pathways along the three main axes of the embryonic body plan: rostrocaudal (RC), dorsoventral (DV) and mediolateral (ML). In addition, different types of cells arise during temporally restricted periods, adding a fourth dimension to the establishment of cell fate (Arber, 2012; Lu et al., 2015). Together, these developmental programs control the emergence of a high number of functionally distinct subpopulations of interneurons that are able to support the wide range of tasks that spinal motor circuits need to perform (Figure 3).

At early stages of development, opposing concentration gradients of retinoic acid (RA) and fibroblast growth factor (FGF) secreted by the paraxial mesoderm confer a rostral or caudal identity, respectively, by acting as regulators of *Hox* genes expression (Figure 3A; Liu et al., 2001; Bel-Vialar et al., 2002; Catela et al., 2015). Based on the RA/FGF-mediated RC patterning, Hox proteins shape the cervical,

brachial, thoracic or lumbar regional character and specify the identity of postmitotic motor neurons according to the tissue that they will eventually innervate. The role of RC positional information for the development of interneuronal subtypes remained elusive for many years, since most of the interneurons found in the spinal cord are represented at all RC levels. Recently, it was shown that V2a interneurons are subdivided into two types that are arrayed in counter-gradients along the RC axis and control forelimbs and hindlimbs differently (Hayashi et al., 2018). This indicates that other classes of interneurons might display an analogous complexity.

Similarly, DV patterning is governed by graded signals along the midline of the neural tube. Ventralizing sonic hedgehog (Shh) produced by the notochord and cells in the floor plate and dorsalizing bone morphogenetic proteins (Bmps) emanating from the roof plate and surface ectoderm form gradients along the DV axis that activate different transcriptional programs (Figure 3A; Ericson et al., 1997; Jessell, 2000). This results in the spatial subdivision and differentiation of five ventral (p0 - 03, pMN) and six dorsal (pd1 - pd6) progenitor pools at conserved DV positions (Figure 3B). The boundaries between these progenitor zones are established and maintained by cross-repressive interactions among pairs of homeodomain proteins that respond differently to Shh signals (Briscoe et al., 2000; Balaskas et al., 2012). Class I proteins are expressed dorsally and are repressed by Shh while Class II proteins are induced by Shh and are found more ventrally (Briscoe et al., 2000). These topographically and genetically defined progenitor domains give rise to the ten cardinal classes of interneurons and motor neurons. The first can, in turn, be roughly divided into ventral interneurons (V0 - V3) that provide the main cellular substrate for the spinal motor circuits along with motor neurons, and dorsal interneurons (dI1 - dI6) that relay sensory input from the periphery. The postmitotic neurons arising from each domain are characterized by the combinatorial expression of unique sets of markers (Figure 3C) and can be further categorized on the basis of their neurotransmitter profile. However, increasing evidence points towards an even higher degree of subtype diversity within individual classes of interneurons (Zagoraiou et al., 2009; Borowska et al., 2013; Bikoff et al., 2016; Sweeney et al., 2017; Hayashi et al., 2018).

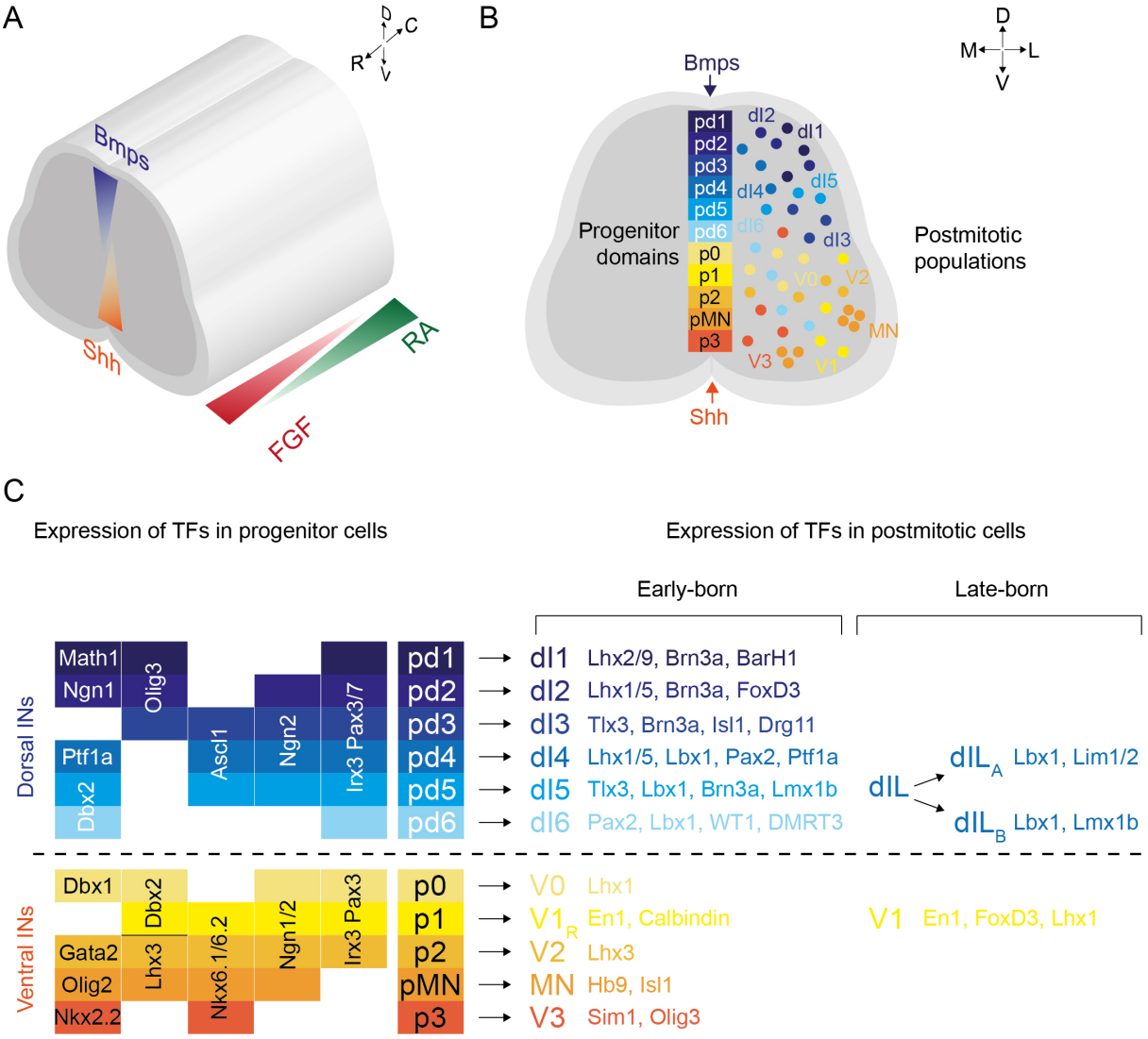

Figure 3. **Diversification of spinal neurons during development.** A) Opposing graded signals of FGF-RA and Bmps-Shh confer regional character along the RC and DV axis, respectively. B) Shh from the floor plate and Bmp from the roof plate define 11 progenitor domains along the DV axis of the spinal cord midline. Each of these domains will give rise to either a cardinal class of interneurons (dI1 - dI6, V0 - V3) or to motor neurons (MNs). C) Transcription factor profiles of progenitor and postmitotic spinal neurons. Note that only the main class identifiers are shown here and that each class can be further subdivided into subgroups, which can be characterized by specific markers. An additional layer of diversification is given by the time of neurogenesis. FGF = fibroblast growth factor, RA = retinoic acid, Bmps = bone morphogenetic proteins, Shh = sonic hedgehog.

The organization along the ML axis divides neurons into progenitor cells, which are located medially near the lumen, and postmitotic cells, which migrate laterally until they assume their target destination (Figure 3B; Lu et al., 2015). The exact mechanisms that control the rate of proliferation at the midline are not known

yet, but Notch signaling seems to be needed for the maintenance of a progenitor state (Appel et al., 2001). The regulation of Notch signaling, in turn, involves inputs from the RC (Akai et al., 2005) and possibly also the DV patterning programs, highlighting the dynamic nature of the processes establishing cell fate. On the other hand, the cellular and molecular underpinnings of neuronal migration in the spinal cord have also not been fully elucidated yet. Although radial migration seems to be the first step away from the progenitor zone (Leber & Sanes, 1995), distinct migration modes are required in order to achieve the stereotyped distribution of motor neurons and interneurons in the spinal cord. The underlying mechanisms are beginning to be understood for motor neuron settlement, where cell-adhesive proteins and their effector molecules, including cadherins/catenins and afadin, play a prominent role (see section 1.5.4.6; Demireva et al., 2011; Dewitz et al., 2018). Moreover, the ML distribution of interneurons can also correlate with their connectivity and function. In the dorsal spinal cord, premotor interneurons connected to extensor motor neurons are located more medially than interneurons directly contacting flexor motor neurons, thus suggesting an anatomical plan that distinguishes antagonistic circuits (Tripodi et al., 2011).

Finally, the timing of neurogenesis acts as an additional determinant of diversification (Figure 3C). Different waves of newborn neurons can later develop into subtypes of a single interneuron class exhibiting distinct transcriptional profiles. The most prominent example is the V1 class, where early-born En1-labeled cells from the p1 progenitor domain become Renshaw cells, clearly segregated both functionally and molecularly from other later-born $En1^+$ V1 interneurons (Benito-Gonzalez & Alvarez, 2012; Stam et al., 2012). Similar differences according to birthdate have also been observed for neurons arising from the $Lbx1^+$ progenitor zone (dI4 - dI6) (Gross et al., 2002). Finally, the time of neurogenesis can also be predictive of the functional properties of the cells since extensor and flexor premotor interneurons can not only be identified by their ML distribution, but also by their birthdate (Tripodi et al., 2011).

1.5.3 AXON GUIDANCE SYSTEMS IN THE SPINAL CORD

The fidelity with which motor circuits are assembled implies the necessity of axon guidance systems that facilitate target selection and the establishment of correct synapses. In particular, the choice of either extending axons ipsilaterally or contralaterally within the spinal locomotor network is crucial for the balanced excitation and inhibition across the two sides that ensures coordinated left/right movements. Thus, signaling systems that direct neural connectivity are an essential element of locomotor circuit wiring.

Ipsilateral glutamatergic interneurons drive the rhythm of activity and provide direct excitation on motor neurons (see section 1.5.4.1). One of the key mechanisms that controls ipsilateral projections in the spinal cord is the repulsive interaction between Ephrin B3 and EphA4. Ephrin B3 is found at the neuroepithelium along the midline and serves as a barrier to interneurons expressing its receptor EphA4, thereby ensuring the unilaterality of their projections. The same strategy is also used for the guidance of corticospinal pathways that provide communication between the spinal cord and the cortex (Kullander et al., 2001; Paixão et al., 2013). Recent studies have shown that eliminating one interacting partner or downstream effectors of EphA4, like α-Chimaerin, is enough to abolish left/right alternation both *in vitro* and *in vivo* (Dottori, et al., 1998; Kullander et al., 2001; Beg et al., 2007; Iwasato, et al., 2007; Satoh et al., 2016). Interestingly, it is the spinal, and not the forebrain, function of Ephrin B3/EphA4 signaling that is essential for proper organization of the locomotor circuitry (Borgius et al., 2014).

On the other hand, commissural inhibitory interneurons provide bilateral communication critical for the alternation of motor activity (see section 1.5.4.2; Grillner & El Manira, 2020). The main feature of commissural interneurons is that they project their axons across the midline to contact cells on the contralateral side. The navigation of their axons is subject to a temporal sequence of responsiveness towards attractive and repulsive cues emanating mainly from the floor plate. Initially, their axonal trajectory is guided ventrally by attractive signals, including nectin-3, Netrin-1 and Shh (Serafini, et al., 1996; Charron et al., 2003; Okabe et al., 2004; Wu et al., 2019). These signals are interpreted by migrating axons through interactions

with nectin-1, the Netrin receptor DCC and the Shh mediator Smoothened, respectively. Next, the axons interact with local cells that guide them to the other side and, upon crossing, they become responsive to repulsive signals derived from the floor plate, which prevent them from turning back (Pignata et al., 2016). This repulsion is modulated by the tightly regulated Slit/Robo signaling pathway. The importance of regulating commissural axon navigation becomes apparent when the involved mechanisms are disrupted. Indeed, mice deficient in either Netrin-1 or DCC display major motor deficits in the form of uncoordinated left/right activity (Rabe et al., 2009; Rabe-Bernhardt et al., 2012; Peng et al., 2017).

Axon pathfinding is not only important for spinal interneurons, but also for motor neurons that need to innervate their specific muscle targets. In the spinal cord, motor neurons are organized in a hierarchical fashion during development based on their peripheral connectivity (see section 1.5.4.6). To ensure that motor axons find their destination, each motor column expresses a different code of transcription factors, which helps them choose their route according to their muscle target. For example, medial motor column (MMC) neurons depend on the activity of Lhx3 in order to reach the axial muscles (Sharma et al., 2000). Lhx3 regulates the expression of Fgfr1, turning MMC axons responsive to FGF coming from the dermamyotome (Shirasaki et al., 2006). Neurons of the lateral motor column (LMC) have to select a dorsal or ventral path within the limb. In this case, the choice is directed by the presence of members of the Ephrin/Eph signaling system. Lateral LMC (LMCl) neurons express EphA4, which favors a dorsal route avoiding EphrinA5 repulsive signals from the ventral limb (Helmbacher et al., 2000). Conversely, medial LMC (LMCm) axons extend ventrally in accordance with repulsive interactions between their EphB1 receptor and EphrinB2 originating from dorsal cells (Luria et al., 2008).

1.5.4 SPINAL CIRCUITS FOR LOCOMOTION

One of the major tasks of spinal circuits is to coordinate muscle contractions in the limbs in a way that will give rise to smooth and robust locomotor behaviors. These neuronal networks, also known as CPGs, consist of a variety of spinal interneurons, which can either directly or indirectly modulate motor neuron activity, thus producing the basic pattern of muscle activation (Grillner & Jessell, 2009;

Gosgnach, 2017). The mammalian locomotor network relies on interconnected CPGs that govern the three main aspects of locomotion: rhythmicity, flexor/extensor alternation and left/right alternation (Kiehn, 2016). In addition, the intersegmetal control of limb activation ensures the stabilization of posture and the production of coordinated locomotor movements. In this context, molecular and positional cues play a key role in determining the connectivity patterns between interneurons, motor neurons, sensory afferents and muscles and endow the system with the necessary precision required for its modular mechanics.

1.5.4.1 RHYTHM GENERATION

Rhythmogenic interneurons are characterized by their ability to initiate and/or change the frequency of motor neuron firing. In the spinal cord, the generation of locomotor rhythm relies primarily on excitatory activity from ipsilaterally projecting neurons in the ventral spinal cord (Kjaerulff & Kiehn, 1996; Whelan et al., 2000; Hägglund et al., 2010; Talpalar & Kiehn, 2010). Confining the optogenetic activation of vGlut2^{+} excitatory neurons unilaterally to a restricted region in the spinal cord associated with either a flexor (lumbar segment L2) or extensor muscle (lumbar segment L5) limits the rhythmic output to the corresponding motor neurons, thus suggesting that each motor pool is controlled by its own rhythmogenic module (Hägglund et al., 2013). This arrangement provides the necessary flexibility to allow for the sequential recruitment of different flexor and extensor muscles. Nevertheless, flexor bursting seems to play a dominant role in patterning the rhythmic output and can occur even in the absence of extensor activity (Hinckley et al., 2015; Machado et al., 2015).

One population of excitatory cells that has been implicated in the generation of locomotor rhythm is the Shox2^{+} population. Expression of Shox2 partly overlaps with that of Chx10, which is the canonical marker for V2a interneurons in the spinal cord, leading to the classification of three groups of excitatory interneurons: V2a Shox2^{-}, V2a Shox2^{+} and non-V2a Shox2^{+}. Blocking the input of Shox2-expressing interneurons alters the rhythm of motor output significantly, without affecting the relative burst pattern across the two sides of the spinal cord (Dougherty et al., 2013).

On the other hand, ablation of $Chx10^+$; $Shox2^+$ cells (V2a $Shox2^+$) does not perturb the rhythm, indicating that non-V2a $Shox2^+$ neurons are responsible for regulating this feature. Another class that contributes to the modulation of locomotion is the one expressing the transcription factor Hb9. These cells are ipsilateral and excitatory and have direct connections to motor neurons. Selective silencing of glutamatergic transmission from $Hb9^+$ interneurons leads to a decrease in the frequency of motor bursts, suggesting that they also participate in the rhythm-generating circuit for spinal locomotion (Caldeira et al., 2017).

Moreover, rhythm generation does not only depend on interactions between neurons, but also on cellular properties that can endow them with pacemaker functions. This mechanism relies on the fact that some neurons have inherent rhythmic bursting capabilities (Kiehn, 2016). Indeed, blocking the persistent sodium current, which is native to many spinal cord neurons, including motor neurons, perturbs the rhythmic motor output (Tazerart et al., 2007; Zhong et al., 2007). Further studies are required in order to discern whether this alteration is due to interneuron or motor neuron activity.

1.5.4.2 FLEXOR/EXTENSOR ALTERNATION

The control of flexor and extensor muscles both around single joints and across multiple joints has to be timed precisely in order to enable flexion of the limb at the onset of the swing phase followed by its extension to support the stance phase. From a network point of view, this means that flexors and extensors need to be activated in an alternating pattern while at the same time the counterpart needs to be inhibited. This regulation is driven by rhythm-generating circuits that are organized in layers, thus, on the one hand, ensuring the direct control of motor neurons and, on the other, the reciprocal inhibition of antagonistic networks.

The inhibition or excitation of motor neurons is mediated by interneurons that are monosynaptically connected to them. Analysis of the premotor connectivity of flexor and extensor motor neurons revealed spatial segregation of their corresponding networks, indicating that different neuronal classes provide input to different motor pools (Tripodi et al., 2011). Two groups of inhibitory interneurons have

been shown to function in an opposing manner to control flexor/extensor movements: V1 interneurons, originating from the $En1^+$ progenitor domain, and V2b interneurons that derive from cells expressing GATA2. Combined silencing of the output of both populations severely perturbs flexor/extensor alternation while maintaining left/right alternation (Zhang et al., 2014). Furthermore, specific deletion of either V1 or V2b interneurons in the spinal cord revealed differential control of flexor/extensor activity, with V1 neurons controlling flexor motor output and V2b neurons inhibiting extensors (Britz et al., 2015). Interestingly, V1 and V2b neurons account for all Ia interneurons in the spinal cord, which are directly upstream of motor neurons and are stimulated by Ia afferents from muscle spindles coming from the same muscle that their targeted motor pool innervates (see section 1.5.4.6). These cells are rhythmically active during locomotion and provide reciprocal inhibition to antagonistic motor neurons. Thus, the cells belonging to the V1 and V2b classes exert a two-fold control over flexor/extensor alternation. In contrast, the different sources of excitatory input on motor neurons regulating opposing activities has not been clarified yet, but is likely to involve V2a $Shox2^+$ neurons, dI3 neurons and dorsal interneurons arising from the $Lbx1^+$ progenitor domain (Stepien et al., 2010; Tripodi et al., 2011).

The speed of locomotion also influences the coordination of flexor and extensor muscles. An increase in the frequency of locomotion causes shorter stance phases, which could be explained by stronger bursting activity from flexor circuits. Indeed, V1 interneurons have been implicated in the control of locomotor speed as well (Gosgnach et al., 2006), however, the precise neuronal architecture of the asymmetric modulation of stance and swing phase is still unknown.

1.5.4.3 LEFT/RIGHT ALTERNATION

The ability to coordinate limb movements across the two sides of the body is a prerequisite for successful locomotion. In particular, in limbed animals changes in locomotor speed are accompanied by modifications in the gait pattern, which represent a biomechanically more stable state (see section 1.1; Bellardita and Kiehn, 2015; Lemieux et al., 2016). This, in turn, means that the underlying neuronal circuits must be able to compute speed-dependent left/right-coordinating recruitments.

In order to be able to monitor bilateral activity, there must be lines of communication that link the two halves of the spinal cord. This is given by commissural interneurons, which constitute a diverse group of cells in terms of projection patterns, neurotransmitter identities and functions (Kiehn, 2016). The best studied class of commissural interneurons originates from $Dbx1^{+}$ progenitors, but later separates into a ventral excitatory (V0v) and a dorsal inhibitory (V0d) subpopulation that can be distinguished molecularly. Genetic ablation of all V0 cells disrupts left/right coordination independently of the locomotor frequency (Talpalar et al., 2013), which is consistent with a deletion of Dbx1 from spinal neurons (Lanuza et al., 2004). However, the targeted elimination of either V0v or V0d interneurons revealed a modular control of left/right activities. Specifically, V0d interneurons secure alternation at low speeds while V0v neurons fulfill the same function at higher speeds (Talpalar et al., 2013). This suggests that the two subtypes are recruited sequentially as the locomotor frequency increases. Another group of excitatory commissural interneurons is the $SIM1^{+}$ population of V3 neurons. These interneurons are not involved in the establishment of alternating left/right movements, but rather in balancing the excitation of flexor/extensor circuits between opposite body halves (Zhang et al., 2008). Finally, dI6 interneurons emerging from the dorsal progenitor domain that expresses Lbx1 have also been implicated in left/right locomotor pattern formation. dI6 interneurons diversify into distinct subgroups postmitotically that can be characterized by the expression of WT1 and/or DMRT3 and their deletion generates irregular fictive locomotor outputs with non-coherent left/right and flexor/extensor alternation (Haque et al., 2018; Schnerwitzki et al., 2018). In addition, *in vivo* observations in horses have shown that mutations in the *DMRT3* gene, that result in a truncated protein, lead to the expression of gaits with deregulated left/right alternation, which are normally not part of their repertoire (Andersson et al., 2012).

Besides commissural interneurons, also ipsilaterally projecting neurons play a role in the coordination of paired limb movements. Work in zebrafish and mice has shown that V2a interneurons are necessary for appropriate locomotor output at high speeds (Crone, et al., 2008; Crone et al., 2009; Ausborn et al., 2012). Interestingly, V2a interneurons directly connect to both V0v and motor neurons (Crone et al., 2009; Stepien et al, 2010), suggesting that they might drive the V0v pathway when locomotion speed increases. On the other hand, ipsilateral dorsal premotor

interneurons coming from Lbx1^{+} progenitors function as a hub for integrating sensory information and adapting motor output accordingly. Genetic manipulation of their axonal projections by specifically eliminating EphA4 in Lbx1-derived interneurons causes aberrant contralateral connectivity to motor neurons while maintaining unilateral sensory input (Satoh et al., 2016). As a consequence, the gait phenotype changes in a context-dependent manner, displaying left/right limb synchronization only when proprioceptive signaling relies exclusively on muscle spindles, for example during swimming or air-stepping (see section 5.6). This indicates that the robustness of locomotor pattern generation also depends on sensory relay interneurons.

1.5.4.4 INTERSEGMENTAL CONTROL OF LOCOMOTION

The ability to successfully generate coordinated movement, in particular that of quadruped animals, relies on interactions between circuits across different spinal cord levels that influence many aspects of motor output, such as the speed, balance and posture (Grillner, 2006). While supraspinal motor centers can send commands for intersegmental coordination, reciprocal communication pathways between segmental neuronal circuits are likely to provide faster information exchange that allows for the fine-tuning of locomotion.

Descending and ascending cross-segmental interactions are mediated by long propriospinal neurons (LPNs), which are defined as interneurons that originate and terminate within the spinal cord with projections that span over several spinal levels (Laliberte et al., 2019). They can influence motor neuron activity either directly by establishing premotor connections (Ni et al., 2014) or indirectly by targeting the ventral spinal territory, where most motor-related interneurons are located (Ruder et al., 2016). Both excitatory and inhibitory cells have been shown to project distally, however, excitatory connections travel mostly contralaterally in both directions, while inhibitory ones are mainly cervico-lumbar and confined to the ipsilateral side (Ruder et al., 2016). The developmental origin of the excitatory population has been traced back to Dbx1^{+} V0 and Shox2^{+} V2 identities, which surprisingly also exhibit mutually exclusive projection patterns, the first being contralateral and the latter ipsilateral (Ni et al., 2014; Ruder et al., 2016). On the other hand, a fraction of inhibitory LPNs were

found to belong to the V2b subtype (Flynn et al., 2017), but the identity of the remaining ones needs to be further clarified.

Work in isolated spinal cords has demonstrated that long ascending connections play a dominant role in coupling forelimb and hindlimb activity since pharmacological disruption of the caudal locomotor pattern has a direct effect on the cervical one, but not viceversa (Juvin et al., 2005). In addition, silencing them *in vivo* perturbs left/right alternation at each girdle, without affecting other features of locomotion, thus suggesting that they are functionally separated from the circuitry responsible for rhythm and intralimb coordination (Pocratzky et al., 2019). In contrast, ablation of descending LPNs leads to postural instability and a selective loss of left/right alternation in the hindlimbs when the locomotor frequency increases (Ruder et al., 2016). Another aspect that depends on long distance information flow is the rostrocaudal propagation of signals arising from sensory cues in order to generate responses involving multiple muscles. Excitatory interneurons originating from the dI3 progenitor domain have been shown to receive input from cutaneous and proprioceptive afferents and to contact motor neurons within adjacent segments at cervical and lumbar levels (Stepien et al., 2010; Bui et al., 2013; Bui et al., 2016), but long projecting dI3s have not been found (Ruder et al., 2016). This indicates that the long distance integration of sensory input must be distributed amongst different populations (Laliberte et al., 2019).

1.5.4.5 MODULATION OF MOTOR OUTPUT

The execution of motor behaviors not only requires the activation of motor neurons, but also a regulation of their output strength in order to ensure appropriate muscle contractions. Several spinal interneuron subtypes with direct connections to motor neurons have been shown to modulate motor activity.

The best known example is that of a small subset of V0v interneurons that becomes cholinergic (V0c) and is marked by the expression of Pitx2. These cells, although being partly commissural, have not been reported to interfere with left/right alternation, but they form large synapses called C-boutons onto motor neurons through which they are able to influence their output by regulating their excitability

(Miles et al., 2007; Zagoraiou et al., 2009; Nascimento et al., 2020). Moreover, in zebrafish they have different post-synaptic effects based on the motor neuron subtype that they innervate, providing an additional layer of flexibility (Bertuzzi & Ampatzis, 2018). V3 interneurons that contact both ipsilateral and contralateral motor neurons also play important roles in controlling the activity of motor output. Recently, it was shown that commissural ventral V3 interneurons together with ipsilateral motor neurons form a positive feedback microcircuit that could enhance information processing needed for movement production (Chopek et al., 2018). In addition, mice lacking V3 interneurons are unable to adjust the muscle strength to various locomotor tasks (Deska-Gauthier & Zhang, 2019), confirming their importance for this aspect of locomotion. On the other hand, the force of motor activity can also be regulated by inhibitory input. Subgroups of V1 interneurons, including Renshaw cells, exhibit stereotyped positions that are predictive of their joint-specific sensory input and the motor neurons they innervate, and differ in their electrophysiological properties, indicating that each inhibitory microcircuit is tailored to its muscle target (Bikoff et al., 2016).

Finally, through reciprocal connections between motor neurons and interneurons, motor neurons themselves can exert an instructive role in shaping the upstream circuits. This was demonstrated in zebrafish, where motor neurons regulate the recruitment of premotor V2a interneurons via gap junctions (Song et al., 2016), but also in the mouse spinal cord, either suppressing or stimulating motor neurons optogenetically significantly alters the locomotor rhythm (Falgairolle et al., 2017). Together, this suggests that motor neurons are not only passive executive elements, but rather active members of the CPGs (Dasen, 2017).

1.5.4.6 SPINAL TOPOGRAPHIC MAPS AND SENSORY TARGETING

Locomotion relies on the ability of neuronal circuits to engage the functionally relevant subtypes of motor neurons at the appropriate time during a step cycle. This temporal and functional coordination depends heavily on the wiring of sensory-motor contacts, which underlie stringent rules of connectivity and are at the basis of the stretch reflex arcs. Incoming axons of Ia sensory neurons that sense changes in the

length of muscle fibers (see section 1.4) enter the spinal cord from the dorsal funiculus and are faced with the task of discriminating between motor neurons with synergistic and antagonistic functions, in order to establish strong monosynaptic connections with motor neurons that innervate the same muscle, weaker connections with functionally related motor neurons and to inhibit motor neurons supplying opponent muscles via local inhibitory interneurons (Ia interneurons; Eccles, 1951). Taking into account that the mammalian limb consists of >50 muscles, each of which is innervated by its dedicated set of motor neurons, the assembly of this circuit design requires a high degree of precision.

One way to accomplish this is to use molecular labels as recognition cues for identifying correct synaptic partners. Neurons belonging to different motor pools can be distinguished by their transcription factor and surface protein profiles (Lin et al., 1998; Livet, et al., 2002; Price et al., 2002; De Marco Garcia & Jessell, 2008). Thus, attractive or repulsive interactions between molecular recognition systems can drive the wiring fidelity of sensory-motor connections. Sema3e and Plxnd1 have been shown to mediate such interactions. Modifying the expression of either Sema3e or Plxnd1 at brachial or lumbar levels of the spinal cord results in rewiring of monosynaptic connections, leading to ectopic input onto motor neurons (Pecho-Vrieseling et al., 2009; Fukuhara, et al., 2013). Similarly, different LIM homeodomain transcription factors in motor neurons regulate the expression of members of the Ephrin/Eph signaling system and thereby contribute to defining motor neuron axonal trajectories towards their peripheral targets (see section 1.5.3; Catela et al., 2015).

Another determinant of connectivity is positional information. Motor neurons occupy highly stereotyped positions within the ventral horn of the spinal cord, which are tightly linked to their connectivity pattern, thus establishing topographic maps. Along the RC axis, they are found in four longitudinal columns, which align with their peripheral targets: visceral preganglionic column and hypaxial motor column motor neurons at thoracic levels, that innervate sympathetic ganglia and intercostal and abdominal musculature, respectively; LMC motor neurons at lumbar levels that project to the limbs; and MMC motor neurons that are present at all RC levels and control dorsal epaxial musculature (Romanes, 1952; Jessell, 2000). In addition, LMC neurons can be further divided into a medial and a lateral division, according to whether they innervate the dorsal or the ventral half of the limb. At the highest level

of organization, all motor neurons that are connected to a single muscle are found segregated and clustered into structures termed pools that assume invariant positions within the spinal cord (Romanes, 1951; Romanes, 1964; Landmesser, 1978). Interestingly, motor pools that innervate muscles with related functions are grouped together into so-called columels, which are organized in a way that mirrors the proximodistal axis of the innervated limb as well as their function. This results in a grid, where medial pools correspond to flexor and lateral pools to extensor muscles and, on the DV axis, more ventrally positioned motor neurons innervate proximal limb muscles while progressively more dorsal motor neurons project to more distal limb muscles (Figure 4).

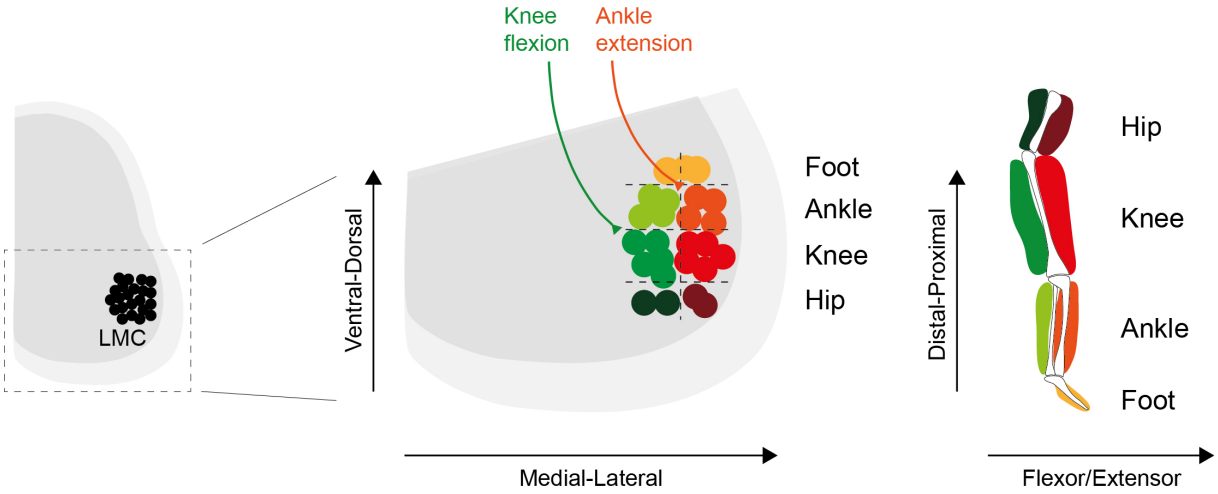

Figure 4. Spinal topographic map of the hindlimb. Motor neurons are organized in a hierarchical fashion in the spinal cord that reflects their function and connectivity pattern. At the highest level of organization, motor neurons are clustered into so-called motor pools, each being responsible for controlling the activity of a single muscle. The position of motor pools within the ventral horn of the spinal cord is highly stereotyped: the dorsoventral coordinates correlate with the distal-to-proximal axis of the limb while the mediolateral coordinates imply the function of the corresponding muscle. Incoming sensory afferents use this grid system to locate their appropriate synaptic partners. Adapted from: Sürmeli et al., 2011.

The axons of proprioceptive sensory neurons that invade the spinal cord during late embryogenesis use this coordinate system to locate their appropriate partners. In FoxP1 conditional mutants, where motor neurons are stripped from their molecular and positional identity, incoming sensory afferents still target discrete dorsoventral areas in the ventral horn, independently of motor neuron subtype or presence (Sürmeli et al., 2011). Moreover, the dendritic pattern of distinct motor pools, which is

also determined by their position, has been shown to be an additional factor defining the interactions between muscle-specific sensory and motor neurons (Balaskas et al., 2019). Loss of motor pool dendritic diversity, as seen for example in FoxP1 conditional mutants, affects the selectivity of sensory-motor connections as well. This indicates that motor neuron positioning according to the muscle target is an essential feature of circuit development ensuring that sensory-motor connectivity is established properly.

In previous work studying the positional organization of motor neurons during development it was shown that cell adhesion molecules (CAMs) are implicated in this process. Perturbation of classical cadherin function, through the inactivation of their transducer proteins β- and γ-catenin, or of nectin function, through the elimination of their scaffold protein afadin, disrupts motor pools clustering and settling (Demireva et al., 2011; Dewitz et al., 2018). In particular, coordinated afadin and catenin signaling orchestrates inside-out migration of motor neurons and layering of divisions while motor pool organization seems to be an afadin-independent process and instead relies on combined function of different types of cadherins (Dewitz et al., 2019).

1.6 AFADIN/NECTIN CELL-ADHESIVE RECOGNITION SYSTEM

Nectins are a family of CAMs with roles in many morphogenetic processes during development. They comprise four members, nectin-1 - 4, which can interact both homophilically and heterophilically with each other, but also with other immunoglobulin-like molecules (Takai et al., 2008). Structurally they are composed of an extracellular domain with three immunoglobulin-like loops, a transmembrane region and a cytoplasmic tail, which attaches to the PDZ domain of the F-actin binding protein afadin, thereby associating them with the actin cytoskeleton (Takahashi, et al., 1999). Afadin, in turn, serves as an adaptor protein that mediates interactions between nectins and other cell-cell adhesive signaling systems, such as cadherins. It can directly bind to α-catenin, which associates with β-catenin that anchors the C-terminal tail of cadherins into the cytoskeleton (Tachibana et al., 2000).

Nectins and afadin are found almost ubiquitously in the developing organism. They mainly localize at adherens junctions (AJs), which they stabilize in cooperation

with cadherins, but they are also expressed in tissues that lack cadherins, where they support dynamic functions, ranging from cell motility to proliferation and differentiation (Takai et al., 2008; Rikitake et al., 2012). In the developing CNS, nectins-mediated cell adhesions have been described between mossy fiber terminals and pyramidal cells in the hippocampus that are established by asymmetrical expression of nectin-1 and nectin-3 at the pre- and postsynaptic side, respectively (Mizoguchi, et al., 2002). The same *trans*-interaction between nectin-1 and nectin-3 is also found mediating weak cell adhesion between elongating commissural axons and floor plate cells in the neural tube, which is critical for their final trajectory (see section 1.5.3, Okabe, et al., 2004). Nevertheless, invidividual nectin KO mice are not lethal, probably due to functional redundancy between the family members. On the other hand, mice, where afadin has been constitutively eliminated, show improper organization of the ectoderm during embryogenesis and are not viable (Ikeda, et al., 1999). Afadin has been implicated in tubulogenetic processes and consequently, its removal severely perturbs tissue morphogenesis in a series of organs where lumen formation is critical for their function, including the kidneys and the pancreas (Yang et al., 2013; Azizoglu et al., 2017; Gao, et al., 2017). Moreover, conditional elimination of afadin in the developing brain leads to impaired synapse formation and neuronal migration (Beaudoin et al., 2012; Gil-Sanz et al., 2013; Miyata et al., 2017). Notably, a lack of afadin does not prevent neurons from exiting the ventricular zone, but rather slows them down and prematurely arrests their movement, thus leading to the formation of a hydrocephalus or a double-cortex (Yamamoto et al., 2013; Gil-Sanz et al., 2013; Gil-Sanz et al., 2014). In the spinal cord, afadin seems to fulfill a similar role in the correct positioning of motor neurons during development since deleting it from motor neuron progenitors selectively disrupts the migration of LMCl neurons (Dewitz et al., 2018). Taking into consideration the importance of positional cues for the assembly of sensory-motor circuits (see section 1.5.4.6), this could have major implications for their function. However, due to perinatal lethality of the so far available afadin mutant models, the effects of the resulting motor neuron mispositioning have not been investigated yet.

2. AIMS OF THE PROJECT

Elucidating the developmental mechanisms that coordinate the assembly and function of motor circuits in the spinal cord is one of the main challenges in neuroscience as it will help us understand how their organization correlates with specific behavioral outputs. Studies in the past have focused on the roles of specific interneurons or axon guidance molecules for the development of the locomotor circuitry (Kullander et al., 2001; Rabe et al., 2009; Zagoraiou et al., 2009; Dougherty et al., 2013; Talpalar et al., 2013; Britz et al., 2015; Satoh et al., 2016). Others have studied the relevance of the topographic organization of neurons in the spinal cord for wiring neuronal networks (Sürmeli et al., 2011; Hinckley et al., 2015; Bikoff et al., 2016). However, how a loss of positional identity can affect the architecture of motor circuits underlying locomotion has not been investigated to date.

In this thesis we aimed at analyzing the assembly of motor circuits upon perturbation of motor neuron organization. Previous mouse models with altered motor neuron positions have precluded postnatal analysis of mature circuits and motor behavior due to embryonic or perinatal lethality (Demireva et al., 2011; Dewitz et al., 2018). Here, a fully conditional afadin knock-out (KO) model was generated that survives until adulthood and exhibits a prominent defect in the coordination of left and right limbs. Using this model, following aims were undertaken:

Aim 1. Characterization of the locomotor phenotype of afadin mutant mice using quantitative gait analysis

Aim 2. Assessment of motor neuron organization in afadin mutant mice using three-dimensional positional analysis

Aim 3. Evaluation of the anatomical integrity of the spinal cord in afadin mutant mice using immunohistochemistry and *in-situ* hybridization methods

Aim 4. Analysis of the premotor connectivity in afadin mutant mice using retrograde rabies virus tracing

3. MATERIAL AND METHODS

3.1 BUFFERS AND SOLUTIONS

TAIL LYSIS BUFFER

Component	Mass/Volume	Final concentration
1 M Tris HCl pH 8.5	50 ml	100 mM
5 M NaCl	20 ml	200 mM
10% SDS	10 ml	0.2%
0.5 M EDTA pH 8.0	5 ml	50 mM

Fill up to 500 ml with ddH_2O and store at room temperature. Prior to use add Proteinase K at a final concentration of 0.1 mg/ml.

0.2 M PHOSPHATE BUFFER (PB)

Component	Mass/Volume	Final concentration
$NaH_2PO_4 * 2\ H_2O$	6.2 g	40 mM
$Na_2HPO_4 * 7\ H_2O$	42.88 g	160 mM

Dissolve in 1 l of ddH_2O, filter and store at room temperature.

4% PARAFORMALDEHYDE (PFA)

Component	Mass/Volume	Final concentration
1 M NaOH	200 µl	2 mM
PFA	4g	4%

Add 200 µl of 1 M NaOH to 50 ml of ddH_2O. Microwave for about 30 s, making sure it does not boil. Add PFA and stir under the hood until dissolved. Add 50 ml of 0.2 M PB, filter and store at 4ºC until further use. Use within 48 hrs.

30% SUCROSE

Component	Mass/Volume	Final concentration
Sucrose	30 g	30%

Dissolve 30 g of sucrose in 70 ml of 0.1 M PB. Fill up to 100 ml with 0.1 M PB, filter and store at 4ºC.

PBX BUFFER

Component	Mass/Volume	Final concentration
Triton X-100	100 - 300 µl	0.1 - 0.3%

Use a cut 1 ml tip to add Triton X-100 to 100 ml of PBS and stir well until dissolved. The concentration of Triton X-100 to be used depends on the thickness of the sections (see section 3.8).

10X ARTIFICIAL CEREBROSPINAL FLUID (ACSF)

Component	Mass/Volume	Final concentration
NaCl	74.22 g	127 mM
KCl	2.24 g	3 mM
NaH_2PO_4 * 2 H_2O	1.95 g	1.25 mM
$NaHCO_3$	21.84 g	26 mM
Glucose	18.02 g	10 mM
2 M $CaCl_2$	1 ml	2 mM
1 M $MgCl_2$	1 ml	1 mM

Dissolve all dry ingredients in ddH_2O, adjust the pH value to 7.4 and fill up to 1 l. Store at 4ºC. Prior to use dilute 1/10 and oxygenate with 95% O_2/5% CO_2 for 10 min. Then add $CaCl_2$ and $MgCl_2$ while still oxygenating (solution can become cloudy, but should clear after a while).

KETAMINE/XYLAZINE MIX

Component	Mass/Volume	Final concentration
100 mg/ml Ketamine	120 µl	120 mg/ml
20 mg/ml Xylazine	50 µl	10 mg/ml

Mix Ketamine and Xylazine and fill up to 1 ml with 1x PBS. Store at 4ºC for up to one week.

3.2 *IN-SITU* HYBRIDIZATION BUFFERS

PROTEINASE K BUFFER

Component	Mass/Volume	Final concentration
1 M Tris HCl pH 7.5	20 ml	50 mM
0.5 M EDTA pH 8.0	4 ml	50 mM
10 mg/ml Proteinase K	40 µl	1 µg/ml

Mix Tris HCl and EDTA and fill up to 400 ml with ddH_2O. Autoclave and store at room temperature. Add Proteinase K just prior to use.

ACETYLATION BUFFER

Component	Mass/Volume	Final concentration
Triethanolamine	2.5 ml	1.25%
HCl	0.35 ml	0.175%
Acetic acid anhydride	0.5 ml	0.25%

Add triethanolamine and concentrated HCl to 197 ml of ddH_2O. Mix well and pour into glass chamber. Add acetic anhydride dropwise at the same time as the slides are dipped into the solution and mix by dipping them several times.

20X SALINE SODIUM CITRATE (SSC) BUFFER

Component	Mass/Volume	Final concentration
NaCl	175.3 g	3 M
Sodium citrate tribasic dihydrate	88.2 g	300 mM

Dissolve everything in ddH_2O, adjust the pH value to 7.0 and fill up to 1 l. Filter, autoclave and store at room temperature.

HYBRIDIZATION SOLUTION

Component	Mass/Volume	Final concentration
Formamide	25 ml	50%
20x SSC	12.5 ml	5x
Denhardt's solution	2.5 ml	5x
10 mg/ml Baker's yeast RNA	1.25 ml	0.25 mg/ml
10 mg/ml Salmon sperm DNA	0.5 ml	0.1 mg/ml

Mix everything and fill up to 50 ml with ddH_2O. Aliquot and store at -20ºC.

BUFFER B1

Component	Mass/Volume	Final concentration
1 M Tris HCl pH 7.5	100 ml	100 mM
5 M NaCl	30 ml	150 mM

Mix and fill up to 1 l with ddH_2O. Autoclave and store at room temperature.

BUFFER B3

Component	Mass/Volume	Final concentration
1 M Tris HCl pH 9.5	40 ml	40 mM
5 M NaCl	8 ml	40 mM
1 M $MgCl_2$	20 ml	20 mM

Mix and fill up to 400 ml with ddH_2O. Autoclave and store at room temperature.

BUFFER B4

Component	Mass/Volume	Final concentration
24 mg/ml Tetramisole hydrochloride	50 µl	0.24 mg/ml
100 mg/ml NBT	17.5 µl	0.35 mg/ml
50 mg/ml BCIP	17.5 µl	0.18 mg/ml

Add tetramisole hydrochloride, NBT and BCIP to 5 ml of Buffer B3. Mix well (solution will be a pale yellow) and keep in a dark place until use. Prepare fresh just before developing.

3.3 MICE

Mice were bred under standard husbandry and housing conditions. All experiments were performed in compliance with the German Animal Welfare Act and approved by the Regional Office for Health and Social Affairs Berlin (LAGeSo). The mouse strains used in this study are summarized in Table 1. *afadin* $^{fl/fl}$ and *RΦGT* were kept homozygous while all Cre-lines were kept heterozygous for the Cre-allele. The new lines generated by combination of *afadin* $^{fl/fl}$ with either of the Cre-lines were assessed according to LAGeSo guidelines. *afadin* $^{fl/fl}$*; Olig2::cre* $^{+/-}$ sporadically develop hydrocephalus and were sacrificed as soon as the disease was diagnosed.

Table 1. Mouse strains employed in this study.

Name used in this study	Official nomenclature	Reference
afadin $^{fl/fl}$	*Afdn* $^{tm1.1Lfr}$	Beaudoin et al., 2012
Olig2::cre	*Olig2* $^{tm1(cre)Tmj}$	Dessaud et al., 2007
Wnt1::cre	*H2az2* $^{Tg(Wnt1-cre)11Rth}$	Rowitch et al., 1999
ChAT::cre	*B6.129S-Chat* $^{tm1(cre)Lowl}$	Rossi et al., 2011
RΦGT	*B6.129P2-Gt(Rosa)26Sor* $^{tm1(CAG-RABVgp4,-TVA)Arenk}$	Takatoh et al., 2013

3.4 GENOTYPING

In general, animals were genotyped after weaning using the tissue obtained from the ear numbering system for DNA extraction. Animals used for tracing experiments were genotyped 1 - 2 days after birth by taking a tail biopsy. Animals used for immunohistochemistry or *in-situ* hybridization experiments at specific postnatal timepoints before postnatal day (p) 21 were genotyped 2 days prior to their use.

Material obtained from the animals was lysed for 3 hrs at 56ºC in 50 µl of tail lysis buffer (see section 3.1) complemented with Proteinase K. DNA samples were subsequently centrifuged for 1 min at 13000 rpm and stored at 4ºC over night (ON). 1/20 dilutions were used for polymerase chain reaction (PCR). 20 µM primer pair solutions were prepared in autoclaved ddH_2O for each genotyping reaction according to Table 2 and stored at -20ºC until further use. Note that the PCR reactions for the WT and the FL allele for the *RΦGT* line have to be run separately. Following PCR, samples were run in a 2% agarose gel in 1x TAE buffer for 1 h at 100 V. DNA bands were visualized with ethidium bromide.

Table 2. Oligonucleotides used for genotyping. bp = base pairs

Mouse strain	Oligonucleotide sequence	Fragment size
afadin $^{fl/fl}$	Fw: CCT TGG GAA CAA CAG GAC ACC Rv: TCA GTA CAG GGG AAC ACC AGG	WT allele: 188 bp FL allele: 315 bp
Olig2::cre	Fw: CGA CGG TGA CTT GAG CAG Rv: TCT GGA TTC ATC GAC TGT GG	Cre allele: 360 bp
Wnt1::cre	Fw: TAA GAG GCC TAT AAG AGG CGG Rv: AGC CCG GAC CGA CGA TGA A	Cre allele: 550 bp
ChAT::cre	Fw: CCT TCT ATC GCC TTC TTG ACG Rv: AGA TAG ATA ATG AGG GGC TC	Cre allele: 350 bp
RΦGT	Fw WT: AAG GGA GCT GCA GTG GAG TA Fw MUT: ATT GCA TCG CAT TGT CTG AG Rv common: CCG AAA ATC TGT GGG AAG TC	WT allele: 297 bp FL allele: 300 bp

3.4.1 *AFADIN* $^{FL/FL}$ GENOTYPING PROTOCOL

Following protocol was used for genotyping *afadin* $^{fl/fl}$ strain (for 1 assay):

Component	Mass/Volume	Final concentration
autoclaved ddH_2O	16.875 µl	-
5x Green GoTaq Reaction Buffer	5 µl	1x
Primer mix (20 µM each)	0.5 µl	0.4 µM (each)
dNTPs mix (10 mM each)	0.5 µl	0.2 mM (each)
GoTaq® DNA Polymerase (5 U/µl)	0.125 µl	0.025 U/µl
DNA	2 µl	-

Following PCR program was used:

Step	Temperature (ºC)	Time	
Initial denaturation	94	3 min	
Cycle denaturation	94	30 s	
Annealing	60	30 s	Repeat 36x
Extension	72	20 s	
Final extension	72	10 min	
Reaction stop	10	∞	

3.4.2 *OLIG2::CRE, WNT1::CRE, CHAT::CRE AND RΦGT* GENOTYPING PROTOCOL

Following protocol was used for genotyping *Olig2::cre, Wnt1::cre, ChAT::cre and RΦGT* strains (for 1 assay):

Component	Mass/Volume	Final concentration
autoclaved ddH_2O	10 µl	-
2x KAPA2G Fast Ready Mix	12.5 µl	1x
Primer mix (20 µM each)	0.5 µl	0.4 µM (each)
DNA	2 µl	-

Following PCR program was used:

Step	Temperature (ºC)	Time	
Initial denaturation	94	3 min	
Cycle denaturation	94	30 s	
Annealing	see Table 3	30 s	Repeat 39x
Extension	72	see Table 3	
Final extension	72	10 min	
Reaction stop	10	∞	

Table 3. Annealing temperatures and extension times used for genotyping programs.

Mouse strain	Annealing temperature (ºC)	Extension time (s)
Olig2::cre	60	45
Wnt1::cre	55	60
ChAT::cre	55	30
RΦGT	60	20

3.5 EMBRYONIC SPINAL CORD DISSECTION

Pregnant females were sacrificed by cervical dislocation and the uterus was removed and placed in a petri dish with ice-cold 1x PBS. Embryos were then removed from placenta and yolk sac and placed in a clean petri dish with ice-cold 1x PBS. Each embryo was thereafter processed individually in the same manner. First, the embryo was transferred to a Sylgard™ dissecting petri dish filled with ice-cold 1x PBS. The head was cut off and the body was pinned down ventral side up with four pins (one in each shoulder and leg). The rib cage and belly were open up and the skin removed. Using forceps, the visceral organs were pulled out, careful not to damage the spinal cord underneath. For embryos older than embryonic day (e) 13.5 ventral laminectomy had to be performed at this stage (see section 3.6). Embryo was then gently stretched, so that the spinal cord was straight, and the tail was cut and kept for genotyping (see section 3.4). Once all embryos had been dissected and pinned down, PBS was replaced by freshly made ice-cold 4% PFA (see section 3.1) and fixed for 90 min on ice. This was followed by three washes with ice-cold 1x PBS for 5 min each. After the last wash, embryos were incubated in 30% sucrose (see section 3.1) ON at 4ºC until embedding (see section 3.7).

3.6 PERFUSION AND POSTNATAL SPINAL CORD DISSECTION

Animals were first anesthetized by intraperitoneal injection of 0.1 ml ketamine/xylazine mix per 10 grams of weight (final concentrations: 120 mg/kg and

10 mg/kg, respectively). After sedation, animals were checked for toe-pinch reflex before any procedure was done. Once sedated they were pinned down ventral side up on top of a sterilized styrofoam plate. Following complete anesthesia, the animals were cut open below the diaphragm and the rib cage was cut rostrally to expose the heart. A small incision was made in the right atrium to allow flow. A 27-gauge needle was inserted into the left ventricle and the animal was first transcardially perfused with ice-cold 1x PBS until the liver was cleared of blood. Next, the animal was perfused with freshly made ice-cold 4% PFA (see section 3.1) until no tremors could be observed anymore. Amount of PBS and PFA needed for a complete fixation depends on the age and corporal composition of the animal.

After perfusion, animals were decapitated and the tail was cut. The belly was open up to expose all the visceral organs, which were afterwards removed with forceps, and the extremities were cut off. Finally, the skin and the fat of the back were removed. The remaining carcass was transferred to a Sylgard™ dissecting petri dish filled with ice-cold 1x PBS and was pinned down ventral side up for ventral laminectomy. Starting at the rostral end, the vertebral bodies covering the spinal cord were removed with small spring scissors, careful not to damage the spinal cord underneath. The tissue was then post-fixed in 6-well plates filled with 4% PFA for 90 min on ice. This was followed by three washes with ice-cold 1x PBS for 5 min each. After the last wash, cords were incubated in 30% sucrose (see section 3.1) ON at 4ºC for cryoprotection until embedding (see section 3.7).

3.7 EMBEDDING

On a Sylgard™ dissecting petri dish filled with cold 30% sucrose, excess muscle or bone tissue surrounding the spinal cord was trimmed. Figure 5 shows the sites where the cuts were performed depending on the segment that was embedded. The spinal cord pieces were then briefly equilibrated in Optical Cutting Temperature (OCT) compound, before being transferred to an embedding mold filled with OCT. Spinal cord pieces were embedded with either the rostral or caudal end facing the bottom of the mold (unless otherwise specified), so that transverse sections could be

acquired subsequently. Blocks were first frozen on dry ice and then kept at -80ºC until further use.

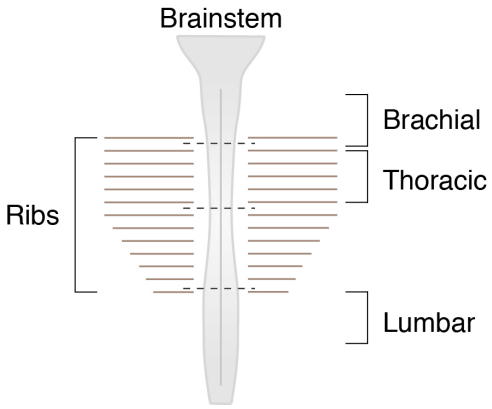

Figure 5. Spinal cord embedding guidelines. For the brachial part a cut was performed between the first and the second rib. Accordingly, the thoracic part started where the brachial cut was done and encompassed the spinal cord segments up to five ribs down. For the lumbar part, the spinal cord was transected just above the 13th rib and included the whole caudal end.

3.8 IMMUNOHISTOCHEMISTRY

In general, 16 µm transverse spinal cord cryosections were acquired with a Leica cryostat and collected on superfrost plus miscroscope slides. Slides were kept at room temperature for approximately 30 - 60 min to ensure good adhesion of the tissue on the glass. Afterwards, the sections were rehydrated with 1x PBS for 10 min before adding freshly prepared dilutions of the primary antibodies in 0.1% PBX (see section 3.1) as indicated in Table 4 for either 3 h incubation at room temperature or ON at 4ºC. Stainings against Ephrin B3 required blocking with 10% donkey serum; 2% BSA in 0.3% PBX for 1 h prior to incubation with the primary antibody in the same solution. After three washes with 0.1% PBX for 5 min each, the secondary antibodies diluted in 0.1% PBX as indicated in Table 5 were added for 1 h at room temperature. Sections were then washed twice with 0.1% PBX for 5 min, followed by a final wash with 1x PBS for 10 min. Slides were mounted with Vectashield® and coverslipped. Confocal images were acquired immediately afterwards to obtain the best possible signal.

For the analyses at postnatal stages 40 µm transverse spinal cord sections were acquired with a Leica cryostat. Immunohistochemistry procedure was performed as described above, but 0.3% PBX was used instead for more effective cell permeation.

Table 4. Primary antibodies employed in this study. SM = self-made, TJ = Thomas Jessell's laboratory, CB = Carmen Birchmeier's laboratory, GP = guinea pig, Go = goat, Rb = rabbit, Sh = sheep.

Target	Host	Source	Dilution
Afadin	GP	SM-TJ	1/20000
ChAT	Rb	SM-TJ	1/16000
Chx10	Sh	Abcam ab16141	1/500
Ephrin B3	Rb	Life Technologies 343600	1/100
FoxD3	GP	SM-CB	1/20000
Hb9	Rb	SM-TJ	1/8000
Isl1	GP	SM-TJ	1/30000
Lbx1	Rb	SM-CB	1/10000
Lhx1	Rb	SM-TJ	1/10000
ROBO3	Go	R&D Systems AF3076	1/200
TAG-1	Go	R&D Systems AF4439	1/200

Table 5. Secondary antibodies employed in this study. All secondary antibodies were purchased from Jackson laboratories. Cy = cyanine.

Target	Host	Conjugate	Catalog number	Dilution
GP	Donkey	Alexa-Fluor® 488	706-545-148	1/1000
		Cy™5	706-175-148	1/500
Go	Donkey	Cy™3	705-165-147	1/1000
Rb	Donkey	Alexa-Fluor® 488	711-545-152	1/1000
		Cy™3	711-165-152	1/1000
Sh	Donkey	Alexa-Fluor® 488	713-545-003	1/1000

3.9 *IN-SITU* HYBRIDIZATION PROBE LABELING

Fragments of interest were amplified from mouse cDNA clones using the primers listed in Table 6 and cloned into the vector pBluescript II SK^+ using the EcoRV restriction enzyme. Since EcoRV restriction results in blunt ends, the

fragments could be inserted either 3'-5' or 5'-3'. Positive clones were sequenced to clarify the direction of insertion. 20 µg of plasmid (pBluescript II SK^+ + ISH probe) were digested with a unique restriction site enzyme upstream of the 5' end of the ISH probe sequence in a 100 µl assay ON. DNA from the restriction reaction was purified using NucleoSpin® Gel and PCR Clean-Up Kit from Macherey-Nagel and resuspended in 50 µl ddH_2O.

Table 6. ISH-probes employed in this study. DB = Dario Bonanomi's laboratory, bp = base pairs.

Target	Primers	Probe size	Source
Netrin 1	Fw: CGT GAA CAT CAT CTC CGT GT Rv: GCA GTG GAG ACC AAA GCT G	858 bp	DB

For all subsequent steps surfaces and tools were treated with RNase AWAY™ decontaminant to prevent RNA loss due to degradation by RNases. Only filter tips were used. DIG-labeling reaction was set up using DIG RNA labeling kit from Roche according to the manufacturer's instructions and incubated for 2 h at 37ºC. Afterwards, 1 µl of DNase was added to the samples and they were incubated for further 15 min at 37ºC. Finally, 30 µl of TE Buffer were added and the probe labeling assays were centrifuged for 1 min at 13000 rpm. Samples were kept on ice until further use. Samples were purified using Microspin™ G-50 Columns from GE Healthcare according to manufacturer's instructions. Quality of purified probes was checked on a 1% agarose gel before use. 50 µl of hybridization buffer (see section 3.2) were subsequently added to the probes to avoid freezing.

3.10 *IN-SITU* HYBRIDIZATION

For *in-situ* hybridization (ISH) all solutions were autoclaved prior to use and surfaces and tools were treated with RNase AWAY™ decontaminant to prevent RNA loss due to degradation by RNases. Only filter tips were used. Unless otherwise specified, all steps were performed at room temperature. For buffer recipes see section 3.2.

12 µm transverse spinal cord sections were acquired with a Leica cryostat and collected on new sterile superfrost plus microscope slides. Slides were airdried for 30 min in a closed chamber before further use. Sections were first fixed with freshly made 4% PFA (see section 3.1) for 10 min, followed by three washes with 1x PBS for 3 min each. In the meantime, the required volume of Proteinase K buffer was complemented with Proteinase K. In general, approximately 1 ml per slide was used. Sections were then treated with Proteinase K solution for 5 min to degrade proteins and afterwards postfixed with 4% PFA for another 5 min. After three washes with 1x PBS for 3 min each, the sections were acetylated by incubating them in acetylation buffer for 10 min in a glass staining chamber while constantly stirring. This was followed by three washes with 1x PBS for 5 min each. Afterwards, the sections were equilibrated with 700 µl of hybridization buffer for 2 h in a chamber humidified with 5x SSC buffer. Shortly before the end of incubation time the probes were prepared. 1 µl of digoxigenin (DIG)-labeled probe (see Table 6 for information on the probes used in this study) was given to 100 µl of hybridization buffer (per slide) and incubated at 80ºC for 5 min, then kept on ice until use. The hybridization solution was poured off the slides and excess liquid removed by carefully wiping the edges of the slide with kimwipe tissue, before adding 100 µl of the probe and coverslipping. The slides were placed in a dark chamber humidified with 50% formamide; 5x SSC. The chamber was closed and taped to reduce evaporation and placed in a 70ºC incubator ON. The following day the coverslips were carefully removed and the slides incubated in pre-warmed 0.2x SSC buffer for 1 h at 72ºC. Afterwards, the slides were washed with room temperature 0.2x SSC for 5 min, followed by a 5 min wash with B1 buffer. Then they were equilibrated with 1 ml of 10% heat-inactivated normal goat serum (HINGS); B1 solution for 1 h. After three washes with B1 buffer for 5 min each, the anti-DIG antibody diluted 1/5000 in 1% HINGS; B1 was given (500 µl per slide) and the slides were incubated for 3 h at room temperature in a dark chamber humidified with 10% HINGS; B1. The slides were then rinsed three times with B1 buffer for 5 min each, followed by an equlibration with B3 buffer for 15 min. In the meantime B4 buffer was prepared. After the 15 min, the solution was poured off and excess liquid removed with a kimwipe tissue. 500 µl of B4 buffer were placed on the slides and coverslipped. The slides were kept in a dark chamber at room temperature and checked regularly for signal development. To stop the reaction, the slides wered

incubated in ddH_2O for 20 min four times and then mounted with Glycergel® pre-warmed at 65ºC and coverslipped. Slides were dried on a heating plate until the gel solidified and then imaged.

3.11 CONTRALATERAL INTERNEURONS TRACING

1x ACSF (see section 3.1) and 1% tetramethylrhodamine-dextran (RDA) solution were prepared. Only PFA-free tools were used. Pregnant females were sacrificed by cervical dislocation and e15.5 embryos were dissected as described in section 3.5 including ventral laminectomy. 0.5 µl of RDA solution were taken up with a glass capillary and injected unilaterally in the spinal cord between C5 and C8. Tails were kept for genotyping. Injected embryos were incubated in oxygenated 1x ACSF ON at room temperature, followed by 5 h of fixation in 4% PFA. Embryos were subsequently treated as described in section 3.5.

3.12 CULTIVATION OF BHK-B19G AND HEK293T CELLS

Table 7 summarizes the cell lines that were employed for the production of large-scale rabies glycoprotein (G)-deficient rabies virus (RVΔG) required for monosynaptic tracing (see sections 3.13 - 3.15). Cells were cultured in the corresponding medium described below in an incubator at 37ºC, 5% CO_2 and 95% of relative humidity.

Table 7. Cell lines employed in this study. EC = Edward Callaway's laboratory, ATCC = American Type Culture Collection.

Cell line	Description	Source
BHK B19G	Baby hamster kidney cells that express T7 polymerase, RV G-protein and nuclear GFP	EC
HEK293T	Homo sapiens embryonic kidney cells	ATCC CRL-3216™

Adherent cells were passaged at a confluency of about 90%. For this purpose, the medium was aspirated from the dish and the cells were washed with 10 ml of PBS. 2 ml of pre-warmed 0.25% trypsin-EDTA were added, followed by 5 min incubation at 37ºC, the optimal operating temperature of trypsin. The reaction was stopped by adding 5 ml of FBS-containing medium and gently dissociating the detached cells. The cell suspension was then centrifuged for 5 min at 1000 rpm and, after removal of the supernatant, the cell pellet was resuspended in 10 ml of pre-warmed medium. The required number of cells were subsequently seeded in a new dish with pre-warmed medium.

MEDIUM FOR BHK B19G CELLS

Component	Mass/Volume	Final concentration
DMEM w/ high glucose, L-glutamine and sodium pyruvate	245 ml	-
FBS	50 ml	10%
Penicillin-Streptomycin	5 ml	1%

Medium was filter-sterilized and stored at 4ºC.

MEDIUM FOR HEK293T CELLS

Component	Mass/Volume	Final concentration
DMEM w/ high glucose, L-glutamine, w/o sodium pyruvate	245 ml	-
FBS	50 ml	10%
Penicillin-Streptomycin	5 ml	1%

Medium was filter-sterilized and stored at 4ºC.

Because the quality of the RVΔG depends on the condition of the BHK B19G cells, it is important to generate frozen stocks at low-passage number regularly. For this purpose, cells were resuspended in 90% FBS; 10% DMSO and transferred to

cryotubes for 48 h storage in Mr. Frosty™ Freezing Container (Thermo Fisher Scientific) at -80ºC. For long-term storage, cells were transferred to liquid nitrogen. In order to thaw the cells, cryotubes were incubated at 37ºC for 2 min. The cells were then taken up in 9 ml of pre-warmed medium, centrifuged for 5 min at 1000 rpm and seeded as described above.

3.13 RABIES VIRUS-MCHERRY AMPLIFICATION

Rabies virus amplification was started from frozen stocks of amplified virus supernatant with a titer of at least 10^6 virus particles (VP)/ml. The day before infection BHK B19G cells were seeded in a T175 cell culture flask, so that they would reach 60% of confluency in 24 h (approximately $3*10^6$ cells). Prior to infection, the virus stock aliquot was thawed in a water bath at 37ºC. The medium of the cells was aspirated and the cells were washed with 15 ml of PBS. 20 ml of new medium complemented with 5 ml of the virus stock were then given to the cells. The multiplicity of infection (MOI), which gives the ratio between the number of virus particles and the number of cells should lie between 0.1 and 1. The dish was thereafter maintained in a humidified atmosphere at 35ºC and 3% CO_2 for four days. Cell growth and metabolism decrease under these conditions and the medium tends to last longer before turning acidic. Medium was checked every two days for acidity and 10 ml of additional fresh medium were added if needed. Rate of infection was checked under a fluorescence microscope. After four days, the medium with the secreted virus was collected (STM1), centrifuged for 5 min at 1000 rpm to remove cell debris and filtered. An aliquot of 2 µl was kept for titer determination (see section 3.15), the rest was stored at -20ºC. The procedure was repeated with 20 ml of fresh medium, which was collected after three days (STM2). In the meantime, ten T175 cell culture flasks were seeded with approximately $3*10^6$ BHK B19G cells. The following day, the ten flasks were infected with the virus-containing medium from the starter culture (STM1 and STM2 were mixed and a 5 ml aliquot was kept at -20ºC to restart a new batch). The cells were maintained in a humidified atmosphere at 35ºC and 3% CO_2 for four days, before collecting the medium (SUP1) and proceeding as described above. These steps were repeated with 20 ml of fresh medium two more times, until

a total of three supernatants were collected (SUP2 and SUP3). Because cells are kept for a long time in culture in the same flask during this procedure, morphology was regularly checked under the microscope and the medium was checked for acidity. If required, additional fresh medium was added or the time before collection was reduced.

3.14 RABIES VIRUS-MCHERRY CONCENTRATION

SUP1 - 3 were successively centrifuged for 2 h at 24000 rpm using an L-70 Ultracentrifuge (Beckman Coulter). The supernatant was removed by pouring it off and then resting the inverted tubes on paper towels to dispose of any remaining liquid. 400 µl of HBSS were used to resuspend the pellet with a pipette. The tubes were then covered with Parafilm® and incubated ON on a shaker at 4ºC. All subsequent steps were performed on ice. The following day, the resuspended pellets were pooled and additional 400 µl of HBSS were used to wash once every tube and added to the virus suspension. An Amicon® Ultra 4 ml Filter was first equilibrated with HBSS and then the virus suspension was applied in 2 - 3 ml steps by centrifuging for 5 - 15 min at 4000 rpm at 4ºC. As the virus particles accumulate at the bottom of the filter, the flowthrough becomes slower, so that some centrifugation steps have to be repeated. Once the remaining volume of virus suspension reached approximately 100 µl, the liquid was carefully transferred to a fresh tube. Additional 20 µl of HBSS were used to resuspend any residual virus particles on the filter and added to the concentrated virus suspension. 3 - 6 µl of virus aliquots were prepared and stored at -80ºC. A 2 µl aliquot was used for titer determination (see section 3.15).

3.15 RABIES VIRUS-MCHERRY TITER DETERMINATION

The day before infection for titer determination, a 24-well plate was coated with 1 mg/ml poly-L-lysine for 30 min at room temperature. Afterwards, the liquid was aspirated and the wells were washed once with sterile 1x PBS before seeding $5*10^4$ HEK293T cells per well in 500 µl of medium. Cells were cultured at 37ºC and 5% CO_2. The following day, 10^1 - 10^6 serial dilutions of the virus aliquot were

prepared. After checking that the condition of the cells was good, the medium was removed and 1 ml of fresh medium was added. 1 µl of virus dilution was given per well (duplicates for each dilution) and allowed three days for infection. Infected cells were counted and final titer was calculated under consideration of the dilution factors and expressed as VP/ml. Only titers with $5*10^9$ VP/ml and higher were used for intramuscular injections.

3.16 INTRAMUSCULAR INJECTIONS

Before surgery, the surgical tools were sterilized by autoclavation, followed by desinfection with 70% ethanol. The surgical site was also desinfected with 70% ethanol.

For motor pools analysis at adult stages, postnatal day (p) 60 animals were injected with 5 mg/kg of carprofen subcutaneously as preemptive analgesia 30 min prior to surgery. The animals were then initially anesthetized with 4% isoflurane and were checked for toe pinch reflex before any procedure was done. Once sedated, they were placed on top of a circulating warm water blanket maintained at 37ºC while keeping them under the effect of 2% isoflurane. Eye lubricant was applied to prevent their eyes from drying out. The head and body were gently fixed with tape to minimize movement during the surgery. To avoid any infection during the procedure, the area of the hindlimbs that was to be injected was treated with iodine solution. A small incision was made to the skin to reveal the specific muscles of the limb (gastrocnemius (GS) and tibialis anterior (TA)) and a glass capillary was used to introduce 2 µl of cholera toxin subunit B (CTB) conjugated to either Alexa Fluor®-488 or -555. Following injection, the skin was sutured with a nylon surgical suture. Animals were checked twice a day post-surgery and administered 5 mg/kg carprofen once a day for 48 h. They were sacrificed three days after surgery.

For monosynpatic tracing analyses at early postnatal stages, p4 animals were injected with 1.5 µl of RVΔG-mCherry in the extensor carpis radialis (ECR) muscle in the forelimbs or GS or TA muscles in the hindlimbs. The surgery and post-operative health controls were performed as described above, omitting the eye lubricant since

the animals have not opened their eyes yet at this age. Animals were sacrificed six days after surgery.

3.17 GAIT ANALYSIS

Quantitative gait analysis was performed as previously described (Mendes et al., 2015). Briefly, a customized acrylic glass walkway was constructed and surrounded by LED lights to generate the frustrated total internal reflection (fTIR) effect that is at the basis of the optical touch sensor that tracks the footprints. A lightbox was positioned above the walkway to visualize the body outline of the animals and a mirror was placed at a 45º angle below the walkway to reflect the signal to a high-speed camera. One week before data acquisition, the animals were habituated to the walkway setup and trained to walk straight from end to end. Three videos per animal were acquired and subsequently analyzed with the customized open-source MouseWalker software (http://biooptics.markalab.org/MouseWalker/) that registers the position of body, tail and each footprint in every frame and gives a list of quantifiable parameters.

3.18 THREE-DIMENSIONAL POSITIONAL ANALYSIS

Three-dimensional positional analysis was performed as previously described (Dewitz et al., 2018). Briefly, for the embryonic analysis lumbar levels L1 - L3 of e13.5 spinal cords were analyzed by cutting 16 µm consecutive cryosections and performing immunostaining (see section 3.8) with antibodies specific for the medial and lateral LMC motor neurons (Isl1 and Hb9, respectively). After acquisition of confocal images with widefield settings, x and y coordinates of motor neurons belonging to each division were obtained using the imaging software IMARIS. To account for differences in spinal cord size, orientation and shape, the datasets were rotated and normalized against a standardized spinal cord whose size was determined empirically (ML: 365 µm, DV: 340 µm). To align the datasets along the RC axis (z coordinate), the section where the first $Isl1^+$ medial LMC neurons were observed was defined as z = 0. The RC position of each neuron was then obtained

by keeping track of the order of the sections. The analysis was carried out for 512 µm in total. The x, y and z coordinates were then used to digitally reconstruct the distribution of the neurons (see section 3.19). The same method was applied to postnatal datasets (motor pools positional analysis and premotor connectivity analysis), omitting the immunostaining, since neurons were labeled with fluorophore-conjugated CTB or RV, respectively. In this case, the first cryosection was defined as z = 0 and the size of the standardized spinal cord was adjusted (ML: 1000 µm, DV: 700 µm for motor pools positional analysis and ML: 1000 µm, DV: 500 µm for RV tracing experiments).

3.19 STATISTICAL ANALYSIS

Positional datasets were analyzed using custom scripts in "R project" (R Foundation for Statistical Computing, Vienna, Austria, 2005). In particular, contour and density plots were generated using the "ggplot2" package, which estimates the two-dimensional Gaussian density for the distribution of the given values. Correlation analysis was done with the "corrplot" package, which calculates the similarity between pairs of experiments using the Pearson correlation coefficient. Datasets were clustered hierarchically. Additional statistical analyses were performed with GraphPad Prism v7.2.

3.20 LIST OF CHEMICALS AND MATERIAL

Product	Catalog number	Supplier
Acetic acid anhydride	CP28.1	Roth
Agarose Standard	3810.3	Roth
Ampicillin	K029.2	Roth
Amicon® Ultra 4 ml Centrifugal Filters	UFC8003	Merck Millipore
Anti-Digoxigenin antibody	11333089001	Roche
Baker's yeast tRNA	AM7119	Thermo Fisher

Bovine Serum Albumin	A7906	Sigma-Aldrich
5-Bromo-4-chloro-3-indolyl-phosphate	11383221001	Roche
Calcium chloride dihydrate	T885.2	Roth
Cholera Toxin subunit B-Alexa Fluor™ 488 conjugate	C34775	Thermo Fisher
Cholera Toxin subunit B-Alexa Fluor™ 555 conjugate	C22843	Thermo Fisher
DIG RNA labeling kit (SP6/T7)	11175025910	Roche
DMEM, w/ high glucose, L- glutamine, sodium pyruvate	11995073	Gibco
DMEM, w/ high glucose, L- glutamine, w/o sodium pyruvate	11965118	Gibco
D(+)-Glucose	HN06.3	Roth
50x Denhardt's solution	D2532	Sigma-Aldrich
Dimethyl Sulfoxide	A994.2	Roth
Disodium hydrogen phosphate heptahydrate	X987.2	Roth
dNTPs Mix	U1511	Promega
DPBS	A1285801	Gibco
D(+)-Sucrose	4661.1	Roth
EcoRV restriction enzyme	R0195	New England Biolabs
EDTA	6506.2	Roth
Ethanol	P075.2	Roth
Ethidium Bromide	2218.2	Roth
Fetal Bovine Serum	SH30070.03	HyClone
Formamide	P040.1	Roth
GeneRuler 1kb Plus	SM1331	Thermo Fisher
GoTaq® G2 DNA Polymerase Kit	M7848	Promega
Glycergel® Mounting Medium	C056330-2	Agilent
Hank's Balanced Salt Solution	14025092	Thermo Fisher
Heat Inactivated Normal Goat Serum	16210072	Thermo Fisher

HindIII restriction enzyme	R3104	New England Biolabs
Hydrchloric acid 37%	4625.1	Roth
Isofluran CP®	-	CP-Pharma
KAPA2G Fast Ready Mix Kit	KK5601	KAPA Biosystems
Ketamidor 100 mg/ml	-	WDT
LB agar	6675.2	Roth
LB broth	6673.2	Roth
Magnesium chloride hexahydrate	2189.1	Roth
Microspin™ G-50 Columns	27-5330-01	GE Healthcare
NeuroTrace™ 640/660	N-21483	Thermo Fisher
4-Nitro blue tetrazolium chloride, solution	11383213001	Roche
Normal donkey serum	ab7475	Abcam
NotI restriction enzyme	R0189	New England Biolabs
NucleoSpin® Gel and PCR Clean-Up Kit	740609.50	Macherey-Nagel
Optimum Cutting Temperature compound	4583	Tissue-Tek
Paraformaldehyde	0335.3	Roth
pBluescript II SK^+	212205	Addgene
10x PBS Liquid Concentrate	11666789001	Merck Millipore
Penicillin Streptomycin	15140163	Gibco
Phalloidin-FITC	P5282	Sigma-Aldrich
Poly-L-lysine	P4707	Sigma-Aldrich
Potassium chloride	6781.1	Roth
2-Propanol	AE73.2	Roth
Proteinase K	3115828001	Sigma-Aldrich
QIAGEN Plasmid Maxi Kit	12163	QIAGEN
Rimadyl	-	Pfizer
RNase AWAY™	7002	Thermo Fisher
Rompun 2%	-	Bayer
Rotiphorese 10x TAE buffer	T845.2	Roth

Sodium acetate	6773.2	Roth
Sodium citrate tribasic dihydrate	3580.1	Roth
Sodium chloride	3957.1	Roth
Sodium dihydrogen phosphate dihydrate	T879.2	Roth
Sodium dodecyl sulphate	4360.1	Roth
Sodium hydrogen carbonate	6885.1	Roth
Sodium hydroxide solution 1N	K021.1	Roth
Standard wall borosilicate glass capillaries	B100-50-10	Sutter Instrument®
Sylgard™ 184	101697	Dow Corning
Tetramethylrhodamine dextran 3000 MW	D3308	Thermo Fisher
Tetramisole hydrochloride	L9756	Sigma-Aldrich
Triethanolamine	6300.1	Roth
TRIS	4855.2	Roth
Triton X-100	3051.4	Roth
0.25% Trypsin, 1x phenol red	25200056	Thermo Fisher
UltraPure™ Salmon Sperm DNA Solution	15632011	Thermo Fisher
Vectashield®	H1000	Vector

3.21 LIST OF EQUIPMENT

Product	**Model**	**Supplier**
Analog peristaltic pump	73-2951	Hugo Sachs Elektronik
Basic Power/Voltage Supply	Power Pac 200	Bio-Rad
Binocular	MZ8	Leica
Cell Culture Hood	SAFE2020	Thermo Fisher

Confoca microscope	LSM 800	Zeiss
Cryostat	CM3050 S	Leica
Flaming/Brown Micropipette puller	Model P97, B	Sutter Instrument
Fluid aspiration system	Professional Vacuubrand	BVC
Fluorescence microscope	DFC3000 G	Leica
Fluorescence lamp	HXP 120V	Zeiss
Gel electrophoresis system	Owl™ Easycast™ B1 and B2	Thermo Fisher
Gel imager	C150	azure biosystems
High-speed camera	Grasshopper3 USB3	Point Grey®
High-speed centrifuge	5804	eppendorf
Hotplate stirrer	VMS-C7 advanced	VWR
Incubator	Series CB	Binder
Infrared lamp	SIL06	Sanitas
Inverted microscope	Eclipse TS100	Nikon
Lamp for Binocular	KL 1500LCD	Leica
MouseWalker walkway	-	Custom built
Mercury lamp	Ebq100 isolated	LEJ
Microcentrifuge	PerfectSpin Mini	peqlab
Nanodrop™	D-1000	peqlab
18 - 55 mm objective	EF-S 18-55mm f/3.5-5.6 IS STM	Canon
Orbital shaker	Sky Line	ELMI
PCR cycler	Mastercycler Nexus GX2	eppendorf
Platform shaker	Polymax 1040	Heidolph Instruments
Scale	PF	Shinko Denish
Tabletop centrifuge	541 SD	eppendorf
Thermomixer	Thermomixer comfort	eppendorf

Ultracentrifuge	L-70, Rotor: SW32Ti	Beckman Coulter
Warm water heating blanket	RightTemp® Jr.	Kent Scientific Corporation

3.22 LIST OF SOFTWARE

Product	Version	Supplier
Adobe Illustrator®	CS6	Adobe Inc.
Adobe Photoshop®	CS6	Adobe Inc.
Fiji	2.0.0-rc-69/1.52p	ImageJ
FlyCapture	2.0	Point Grey®
IMARIS	9.2.1	Bitplane
Microsoft Office	2011	Microsoft
MouseWalker software	-	http://biooptics.markalab.org/MouseWalker/
Prism	7.2	GraphPad
R	3.3.2	R Foundation for Statistical Computing
R studio®	0.99.893	R studio PBC
ZEN	2.3 (blue edition)	Zeiss

4. RESULTS

4.1 VALIDATION OF *AFADIN* $^{FL/FL}$ MUTANT MICE

Constitutive afadin inactivation leads to gross developmental defects in the ectoderm and mesoderm during embryogenesis and abortion by e10.5 (Ikeda et al., 1999). Thus, in previous work in our laboratory that studied the role of afadin in motor neuron organization, the protein was conditionally eliminated from motor neurons by crossing one copy of a floxed allele and one copy of a null allele with the *Olig2::cre* driver line, which targets motor neuron progenitors (hereafter referred to as *afadin* $^{fl/-}$, Dewitz et al., 2018). However, although this model allowed embryonic analyses, it was unsuitable for the study of motor behavior, because *afadin* $^{fl/-}$ mice die at perinatal stages of severe hydrocephaly. In an attempt to extend postnatal life span, a fully conditional afadin KO mouse model was generated by deleting two floxed alleles with the *Olig2::cre* driver (hereafter referred to as *afadin* $^{fl/fl}$). *Afadin* $^{fl/fl}$ mice were born at the expected Mendelian ratio and survived until adulthood. The efficiency of afadin elimination was confirmed by immunohistochemistry. In control e13.5 spinal cords, a timepoint when motor neuron development has finalized, afadin was ubiquitously expressed with more prominent localization along the neuroepithelium that lines the midline (Figure 6A). In contrast, in *afadin* $^{fl/fl}$ spinal cords the protein was missing in the motor neuron progenitor zone (pMN) at the midline and, accordingly, also from the motor neuron area in the ventral horn (Figure 6B). In order to assess whether this had an effect on motor neuron generation and subtype identity, the expression of transcription factors that are specific for medial and lateral LMC motor neurons (LMCm and LMCl) was assessed as previously described (Demireva et al., 2011; Dewitz et al, 2018). Neurons belonging to the LMCm division were identified by expression of Isl1 whereas LMCl neurons were identified by expression of Hb9. Consistent with observations in *afadin* $^{fl/-}$ mice, no significant differences were observed in the total number of LMCm and LMCl neurons, suggesting that the generation of motor neurons does not depend on afadin function (Figure 6C).

Thus, the implemented genetic strategy yielded effective removal of the protein from motor neuron progenitors while preserving the animal's ability to reach adulthood and enabling the study of mature motor circuits and motor behavior.

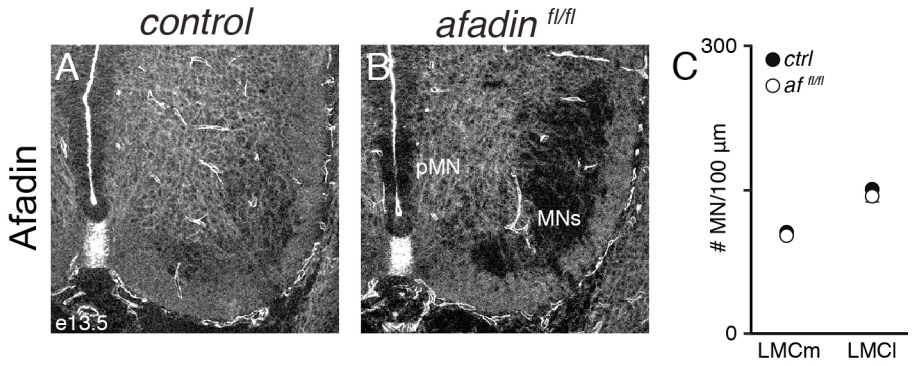

Figure 6. Afadin expression and motor neuron generation in control and *afadin* $^{fl/fl}$. A) Afadin expression in e13.5 control lumbar spinal cord. B) Afadin expression in e13.5 *afadin* $^{fl/fl}$ lumbar spinal cord. C) Number of medial (LMCm) and lateral LMC (LMCl) motor neurons in e13.5 control and *afadin* $^{fl/fl}$ spinal cords as identified by the expression of Isl1 and Hb9, respectively (n = 3, mean ± SEM, two-tailed unpaired t-test, $p > 0.05$). Adapted from: Skarlatou et al. 2020.

4.2 CHARACTERIZATION OF LOCOMOTOR GAIT PATTERN

Afadin $^{fl/fl}$ mice exhibit an altered locomotor gait pattern with variable degrees of a defect in the relative timing of left/right limb activation. In order to quantitatively describe this phenomenon, kinematic parameters were studied by analyzing video recordings of freely walking adult mice (for a detailed description see section 3.17 and Mendes et al., 2015). Using an algorithm that allows the tracking of each individual footprint, it is possible to generate a comprehensive description of locomotor features, such as the speed, the step frequency and the phase values that represent the left/right relationship between paired limb movements. Three control animals and a total of ten mutants were analyzed. For each subject, three representative videos with uninterrupted runs at similar velocities were evaluated and the quantifiable parameters averaged (Appendix I).

As expected, control animals showed consistent alternation between left and right extremities. No synchronous steps were observed in their gait pattern and both

forelimbs and hindlimbs displayed phase values of approximately 0.5, which is indicative of alternating movements (Figures 7A and 7E and Appendix I; Bellardita and Kiehn, 2015; Lemieux et al., 2016). Conversely, *afadin* $^{fl/fl}$ mutant mice exhibited diverse phenotypes and could be categorized into three groups, each representing roughly one third of the analyzed cohort. The first group used mostly alternating steps, but showed a significant increase in the incidence of synchronous steps compared to control littermates (hereafter referred to as *afadin* $^{fl/fl}$ *(alt)*, Figures 7B and 7E and Appendix I). The second group presented bouts of alternation intermixed with bouts of synchronization of paired limbs (hereafter referred to as *afadin* $^{fl/fl}$ *(mix)*, Figures 7C and 7E and Appendix I). Finally, the third group displayed an almost complete switch to synchronous activation of left and right limbs during locomotion (hereafter referred to as *afadin* $^{fl/fl}$ *(sync)*, Figures 7D and 7E and Appendix I). The forelimb and hindlimb phase values in the last cohort laid mostly around 0, suggesting a transition to bound gait (Bellardita and Kiehn, 2015; Lemieux et al., 2016). Accordingly, in *afadin* $^{fl/fl}$ *(sync)* mice the step frequency and speed were significantly increased while the step length and stance duration were decreased compared to both control animals and the other KO phenotypes (Figures 7F and 7G and Appendix I). This observation correlates well with the fact that tetrapods, including rodents, change their gait pattern from an alternating trot to a synchronous bound gait when the locomotor frequency increases (Bellardita and Kiehn, 2015; Lemieux et al., 2016). Moreover, in all analyzed animals, every limb displayed the full range of stepping movements, indicating that muscle connectivity and the temporal control of flexor/extensor muscle activation was not affected.

Together these data show that elimination of afadin from motor neuron progenitors selectively perturbs the function of locomotor circuits regulating the coordination of left and right appendages movement, resulting in a loss of alternation in favor of synchronization (Figure 7H).

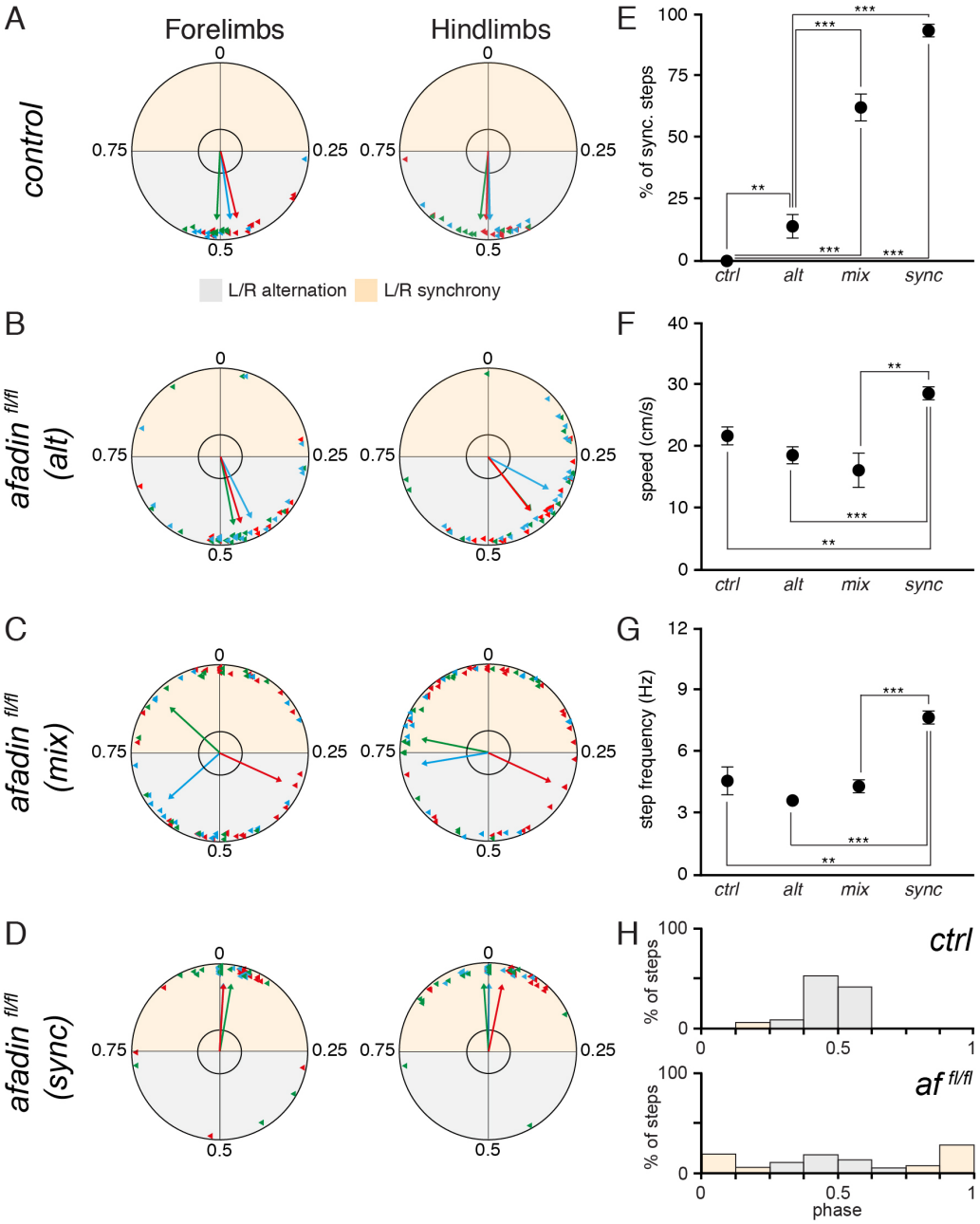

Figure 7. Quantitative description of the gait pattern of control and *afadin* $^{fl/fl}$ mice. A-D) Polar plots showing the left/right phase relationship in fore- and hindlimbs and the average orientation vector in individual control and *afadin* $^{fl/fl}$ mice (n = 3 for each group). *afadin* $^{fl/fl}$ mice were divided into three groups based on the penetrance of paired limb synchronization. E) Average percentage of synchronous steps in each group (n = 3, mean ± SEM, two-tailed unpaired t-test, ** = $p < 0.01$, *** = $p < 0.001$). F) Average speed in each group (n = 3, mean ± SEM, two-tailed unpaired t-test, ** = $p < 0.01$, *** = $p < 0.001$). G) Average step frequency in each group (n = 3, mean ± SEM, two-tailed unpaired t-test, ** = $p < 0.01$, *** = $p < 0.001$). H) Phase distribution histograms of all analyzed steps in control and *afadin* $^{fl/fl}$ mice (n = 3 for controls, n = 9 for *afadin* $^{fl/fl}$). From: Skarlatou et al., 2020.

4.3 ANALYSIS OF MOTOR NEURON ORGANIZATION UPON CONDITIONAL AFADIN ELIMINATION

The alterations in the locomotor gait pattern of *afadin* $^{fl/fl}$ mice suggest that the function of spinal motor circuits is perturbed. From previous work with afadin mutant mice, it was known that deleting afadin from motor neurons affects their ability to clearly segregate into a medial and a lateral division at limb levels of the spinal cord (Dewitz et al., 2018). Given that the spatial organization of motor neurons is an important determinant of sensory-motor connectivity (Sürmeli et al., 2011; Bikoff et al.; 2016), this developmental defect could have implications for the assembly of the motor circuits as well. In order to establish whether the fully conditional *afadin* $^{fl/fl}$ mouse model also displays disrupted motor neuron organization, three-dimensional quantitative analysis of motor neuron positions at embryonic stages was performed using specific markers to distinguish LMCm and LMCl neurons (for a detailed description see section 3.18 and Dewitz et al., 2018).

In e13.5 control embryos, the cell bodies of neurons belonging to LMCm and LMCl divisions were found at distinct ML positions in the ventral horn and did not present any differences in DV or RC distribution, consistent with the highly conserved stereotyped positioning of divisional subtypes (Figures 8A, 8C and 8E, Romanes, 1951; Landmesser, 1978). On the other hand, the ML separation of the two divisions was lost in *afadin* $^{fl/fl}$ mice (Figures 8B, 8D and 8F). The transverse and longitudinal contour plots show an increased overlap in the distribution of the cells along the ML axis while no variation could be detected on the DV or RC axes (Figures 8D and 8F). Interestingly, the average ML position of LMCm neurons was similar to that in control embryos whereas *afadin* $^{fl/fl}$ LMCl neurons were located at more medial positions, suggesting that the overlap is caused by a selective shift of the lateral division (Figures 8G and 8H). This observation recapitulates the positional defect described in *afadin* $^{fl/-}$ mice, albeit at a less penetrant level, and confirms the finding that afadin function has a specific role in controlling the settling position of LMCl neurons (Dewitz et al., 2018).

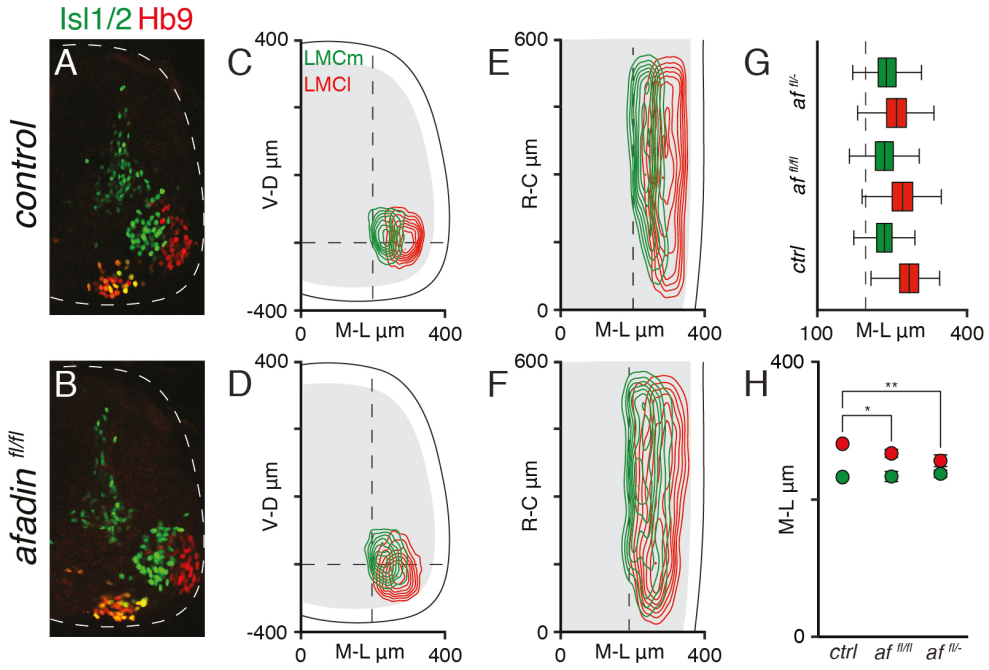

Figure 8. Three-dimensional positional analysis of motor neurons at e13.5. A-B) Representative images of transverse hemicords showing expression of Isl1 and Hb9 in e13.5 control (A) and *afadin* $^{fl/fl}$ (B) embryos. C-D) Transverse contour density plots of LMCm (green) and LMCl (red) neurons in e13.5 control (C) and *afadin* $^{fl/fl}$ (D) embryos (n = 3). E-F) Longitudinal contour density plots of LMCm and LMCl neurons in e13.5 control (E) and *afadin* $^{fl/fl}$ (E) embryos (n = 3). G) Box plots showing mediolateral distribution of LMCm (green) and LMCl (red) neurons in e13.5 control, *afadin* $^{fl/fl}$ and *afadin* $^{fl/-}$ embryos (*afadin* $^{fl/-}$ dataset from Dewitz et al., 2018; whiskers represent min/max). H) Average mediolateral position of LMCm (green) and LMCl (red) neurons in e13.5 control, *afadin* $^{fl/fl}$ and *afadin* $^{fl/-}$ embryos (*afadin* $^{fl/-}$ dataset from Dewitz et al., 2018; n = 3, mean ± SEM, two-tailed unpaired t-test, * = $p < 0.05$, ** = $p < 0.01$). Adapted from: Skarlatou et al., 2020.

Afadin $^{fl/-}$ mice die perinatally and do not allow the analysis of motor neuron organization at later stages when the assembly of motor circuits is concluded. Thus, in previous studies it was not possible to investigate whether the uncovered positional defect during development was permanent and influenced the formation of locomotor networks. Using the fully conditional *afadin* $^{fl/fl}$ mutant, the life expectancy was extended to adulthood, which enabled experiments in mice with completely established neuronal circuits. However, the expression of transcription factors that define specific groups of motor neurons is downregulated at postnatal stages. Instead, retrograde labeling with fluorophore-conjugated CTB was carried out to identify neurons belonging to distinct motor pools in adult mice (for a detailed description see section 3.16 and Sürmeli et al., 2011). Here, the gastrocnemius (GS)

and tibialis anterior (TA) muscles were chosen, which represent a medial and a lateral pool, respectively, and enable the assessment of ML segregation of motor neurons.

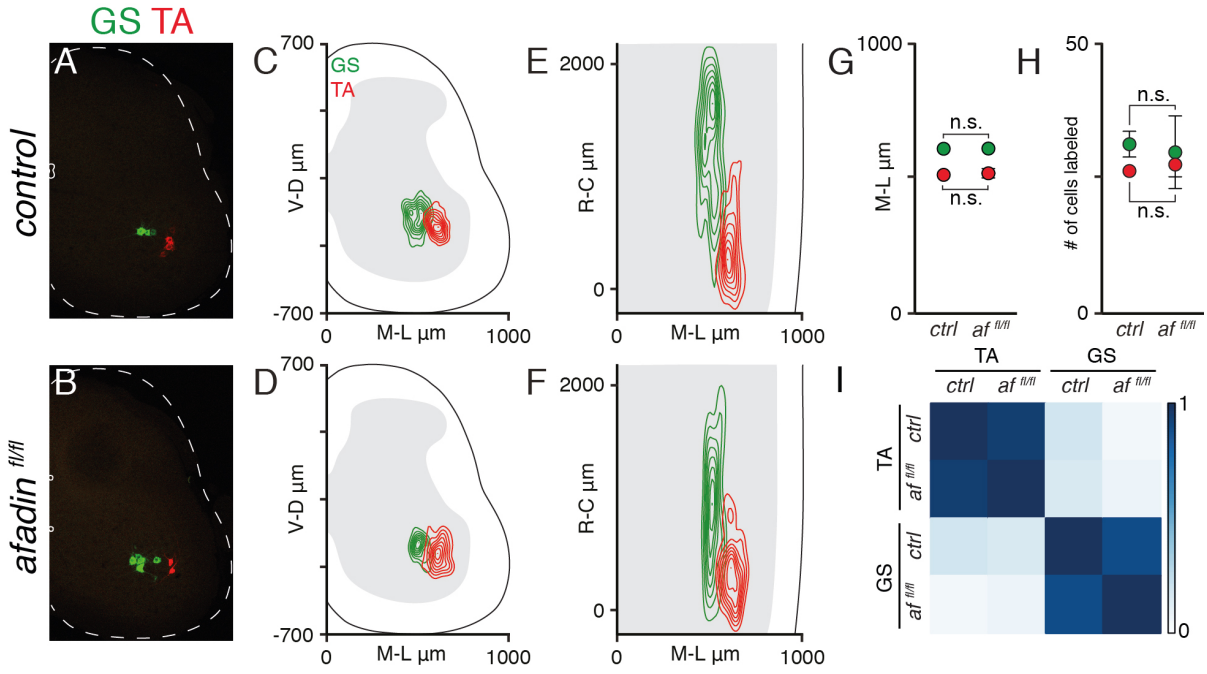

Figure 9. Three-dimensional positional analysis of motor neurons in adult mice. A-B) Representative images of transverse hemicords showing CTB-labeled GS and TA neurons in adult control (A) and *afadin* $^{fl/fl}$ (B) mice. C-D) Transverse contour density plots of GS (green) and TA (red) neurons in adult control (C) and *afadin* $^{fl/fl}$ (D) mice (n = 3). E-F) Longitudinal contour density plots of GS and TA neurons in adult control (E) and *afadin* $^{fl/fl}$ (F) mice (n = 3). G) Average mediolateral position of GS (green) and TA (red) neurons in adult control and *afadin* $^{fl/fl}$ mice (n = 3, mean ± SEM, two-tailed unpaired t-test, $p > 0.05$). H) Average number of GS and TA neurons in adult control and *afadin* $^{fl/fl}$ mice (n = 3, mean ± SEM, two-tailed unpaired t-test, $p > 0.05$). I) Correlation analysis of GS and TA neurons coordinates in adult control and *afadin* $^{fl/fl}$ mice. The scale bar indicates correlation values. Adapted from: Skarlatou et al., 2020.

GS and TA motor neurons were labeled efficiently and found at the expected rostral lumbar levels of the spinal cord both in control and *afadin* $^{fl/fl}$ mice (Figures 9A - B, 9E - F and 9H, McHanwell & Biscoe, 1981; Sürmeli et al., 2011). In control animals, the two motor pools were nicely clustered and clearly separated from each other along the ML dimension (Figure 9C). Surprisingly, the respective contour plots of *afadin* $^{fl/fl}$ mice presented a similar distribution (Figure 9D) and comparison of the average ML settling positions of GS and TA neurons revealed no significant

differences between control and mutant mice (Figure 9G). Moreover, correlation analysis of positional coordinates confirmed that the spatial organization of these motor pools was conserved in *afadin* $^{fl/fl}$ mice (Figure 9I). The coordinates of motor neurons belonging to each pool highly correlated with each other, independently of the genotype ($R = 0.89$ for GS and $R = 0.95$ for TA) while the correlation between different motor pools datasets was negligible ($R \leq 0.18$). This indicates that there is no significant overlap between the distributions of medial and lateral neurons.

Altogether, these experiments suggest that elimination of afadin from motor neuron progenitors causes a developmental delay in the layering of LMC divisions, which resolves over time and is no longer apparent at adult stages. Thus, the observed locomotor phenotype cannot be the result of altered motor neuron organization.

4.4 AFADIN FUNCTION AT THE NEUROEPITHELIUM

Afadin is expressed ubiquitously in the spinal cord during development (see Figure 6A), but is only localized around the central canal after birth. Strikingly, *afadin* $^{fl/fl}$ mice exhibit a double central canal at adult stages (see Figure 9B), which raised the question of how afadin might influence central canal morphology. In order to understand the underlying developmental process, afadin expression was analyzed at different timepoints (e10.5, e13.5, e15.5 and p1) to gain insight into the protein's function.

In controls afadin was expressed everywhere in the spinal cord with higher levels found at the neuroepithelium that extends along the whole DV extent up to e13.5 (Figures 10A - D). At e15.5 afadin signal was still detected at the midline (Figures 10E - F), which at this time has started constricting to form the tubular structure of the central canal that is apparent by p1. At postnatal stages afadin expression was restricted to lining the lumen of the central canal and blood vessels (Figures 10G - H). In *afadin* $^{fl/fl}$ mice conditional elimination of afadin from motor neuron progenitors resulted in disrupted protein expression at the neuroepithelium area representing the pMN, which was visible as early as e10.5 (Figures 10I - L). As a consequence, the morphology of the developing spinal cord was clearly perturbed

when tubulogenesis began. Two independent constricting structures, corresponding to the neuroepithelial areas with unaffected afadin expression, above and below the pMN, were observed (Figures 10M - N) and each formed a separate central canal (Figures 10O - P). The double central canal phenotype was maintained throughout adult life.

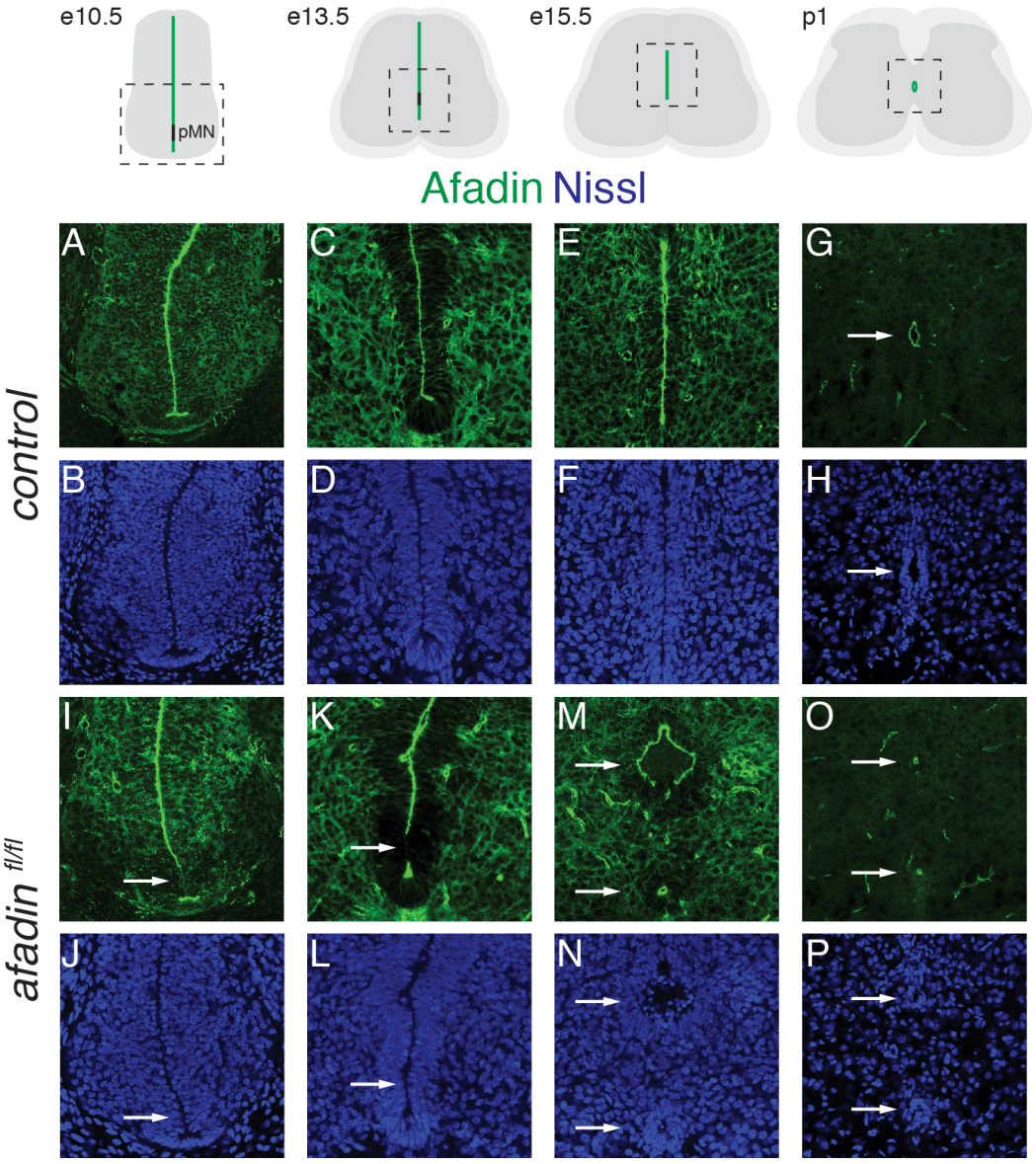

Figure 10. Central canal development in control and *afadin* $^{fl/fl}$ mice. A-H) Afadin expression and Nissl staining in e10.5 (A-B), e13.5 (C-D), e15.5 (E-F) and p1 (G-H) control spinal cords. Boxes in diagrams show magnified regions in A-H. Arrow in G points to the central canal. I-P) Afadin expression and Nissl staining in e10.5 (I-J), e13.5 (K-L), e15.5 (M-N) and p1 (O-P) *afadin* $^{fl/fl}$ spinal cords. Boxes in diagrams show magnified regions in I-P. Arrows in I and K point to the pMN. Arrows in M and O point to the two central canals. From: Skarlatou et al., 2020.

Moreover, phalloidin staining, which shows a high affinity for actin filaments, revealed an organized actin network both in control and *afadin* $^{fl/fl}$ animals up to e13.5 (Figures 11A - B and 11G - H). In particular, actin organization at the neuroepithelium was not affected by the deletion of afadin from motor neuron progenitors (Figure 11H). However, when lumen formation began afadin mutant spinal cords displayed a disruption in the overall integrity of the midline area with the emergence of amorphous tissue between the two central canals and an expansion of the DV extent of the grey matter (Figures 11C - F and 11I - L).

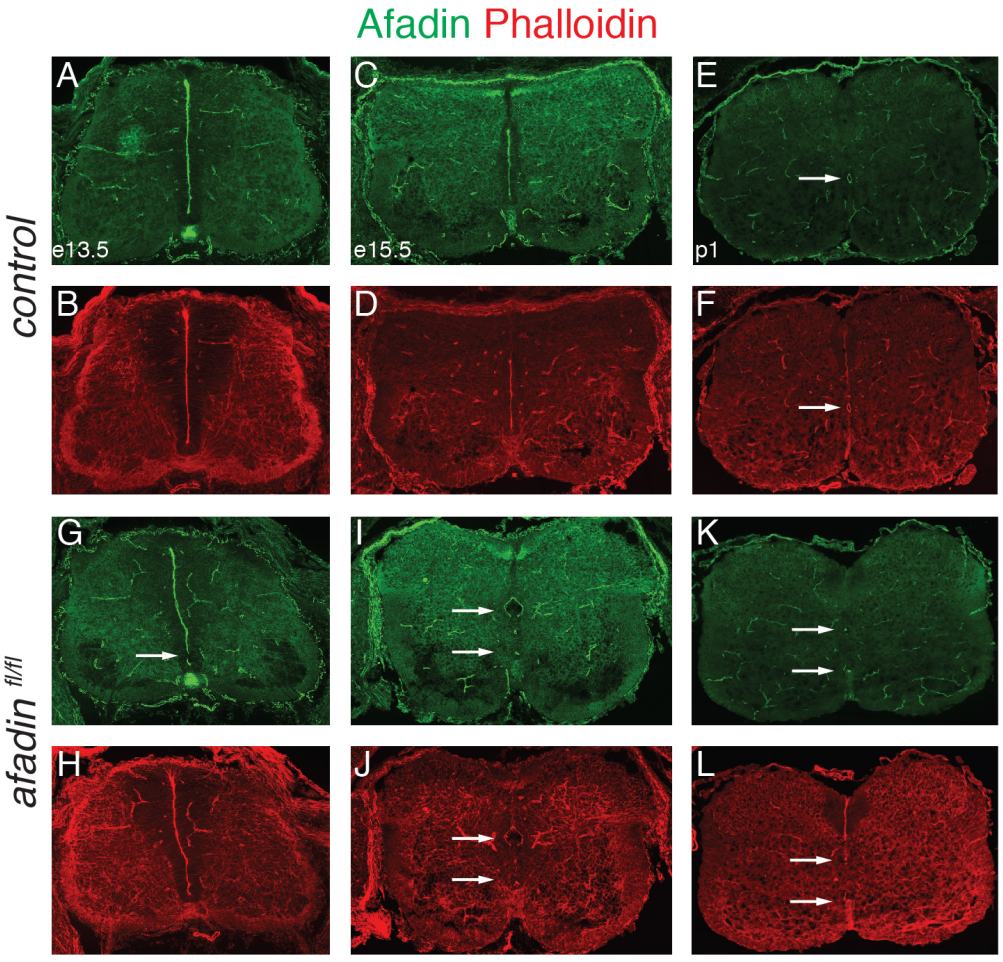

Figure 11. Development of the actin network in control and *afadin* $^{fl/fl}$ spinal cords. A-F) Afadin and phalloidin staining in e13.5 (A-B), e15.5 (C-D) and p1 (E-F) control spinal cords. Arrow in E-F points to the central canal. G-L) Afadin and phalloidin staining in e13.5 (G-H), e15.5 (I-J) and p1 (K-L) *afadin* $^{fl/fl}$ spinal cords. Arrow in G points to the pMN. Arrows in I-L point to the two central canals. From: Skarlatou et al., 2020.

The fact that a lack of afadin at the pMN disrupts central canal development suggests that afadin is indispensable for proper organization of the spinal cord midline. To further confirm this hypothesis, the *Wnt1::cre* mouse line was used to remove the protein from dorsal progenitor cells (hereafter referred to as *afadin* $^{fl/fl}$*; Wnt1*) and the development of the central canal was assessed by evaluating the expression of afadin. *Afadin* $^{fl/fl}$*; Wnt1* mice die at late embryonic stages as a result of exencephaly. At e14.5, when neuroepithelial constriction begins, a slight reduction in the extent of afadin localization at the midline was observed (Figures 12A - D). In order to measure this defect while accounting for differences in size and shape of the spinal cords, the extent of afadin signal was normalized against the total length of the midline grey matter (GM). Quantification showed that afadin expression was indeed reduced in *afadin* $^{fl/fl}$*; Wnt1* embryos, although the difference did not reach significance (Figure 12G). This was accompanied by an expansion of the dorsal GM, which differed significantly from that in control littermates (Figures 12E - F and 12H).

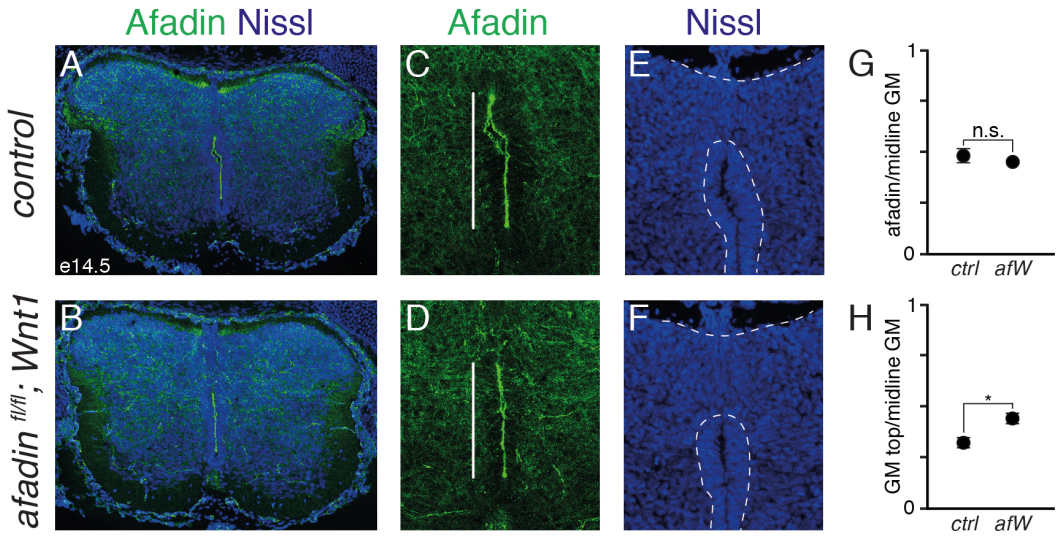

Figure 12. Central canal development in e14.5 control and *afadin* $^{fl/fl}$*; Wnt1* (*afW*) embryos. A-B) Representative images of transverse spinal cords showing expression of afadin in e14.5 control (A) and *afadin* $^{fl/fl}$*; Wnt1* (B) embryos. C-D) Afadin expression in the developing central canal area of the images in A (C) and B (D). Bars represent extent of afadin expression. E-F) Nissl staining in the dorsal midline area of the images in A (E) and B (F). Dashed lines delineate neuroepithelium and border between dorsal grey and white matter. G-H) Quantification of normalized afadin signal (G) and dorsal GM (H) extent in e14.5 control and *afadin* $^{fl/fl}$*; Wnt1* embryos (n = 3, mean ± SEM, two-tailed unpaired t-test, * = $p < 0.05$). Adapted from: Skarlatou et al., 2020.

The same anatomical alterations could also be observed later in development. In e16.5 *afadin* $^{fl/fl}$*; Wnt1* spinal cords the decrement in afadin and phalloidin expression was more pronounced and significantly different from controls (Figures 13A - D and 13J). In addition, the dorsal GM between the developing central canal and the white matter was significantly expanded (Figures 13E - F and 13K) while the ventral one was shrunk (Figures 13G - H and 13L), indicating a ventral shift of the central canal.

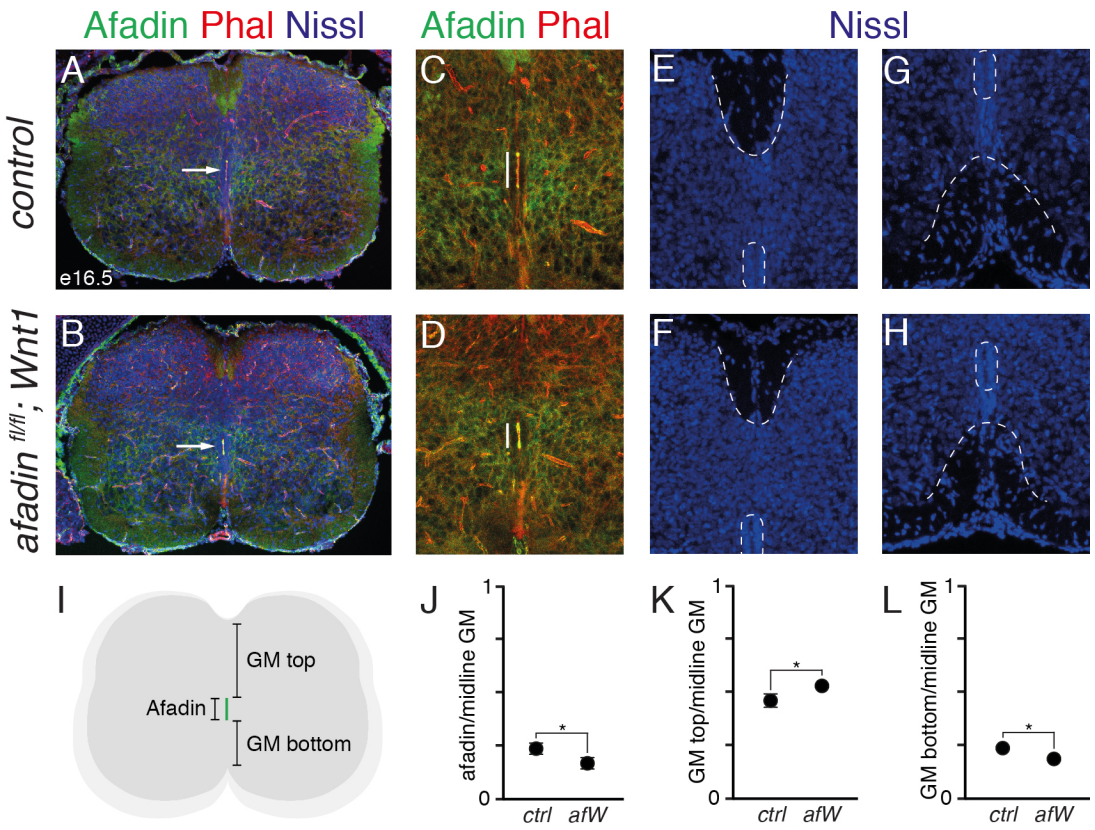

Figure 13. Central canal development in e16.5 control and *afadin* $^{fl/fl}$*; Wnt1* (*afW*) embryos. A-B) Representative images of transverse spinal cords showing expression of afadin and phalloidin in e16.5 control (A) and *afadin* $^{fl/fl}$*; Wnt1* (B) embryos. Arrow points to developing central canal. C-D) Afadin and phalloidin expression in the developing central canal area of the images in A (C) and B (D). Bars represent extent of afadin/phalloidin expression. E-F) Nissl staining in the dorsal midline area of the images in A (E) and B (F). Dashed lines delineate neuroepithelium and border between dorsal grey and white matter. G-H) Nissl staining in the ventral midline area of the images in A (G) and B (H). Dashed lines delineate neuroepithelium and border between ventral grey and white matter. I) Schematic spinal cord showing quantified areas. J-L) Quantification of normalized afadin signal (J), dorsal GM (K) and ventral GM (L) extent in e16.5 control and *afadin* $^{fl/fl}$*; Wnt1* embryos (n = 3, mean ± SEM, two-tailed unpaired t-test, * = $p < 0.05$). Adapted from: Skarlatou et al., 2020.

Together, these experiments demonstrate a role for afadin in the regulation of the developmental process that gives rise to the central canal. Loss of afadin in the spinal neuroepithelium abolishes its ability to correctly undergo apical constriction, which is at the basis of lumen formation. Accordingly, eliminating afadin from specific progenitor domains leads to their exclusion from the tubulogenetic process, thus altering the position and/or morphology of the final outcome.

4.5 AFADIN FUNCTION IN POSTMITOTIC MOTOR NEURONS

The elimination of afadin from motor neuron progenitors affects both the development of the central canal and that of motor circuits controlling locomotion. However, using the *afadin* $^{fl/fl}$ model it is not possible to discriminate between the role of afadin function in progenitor and postmitotic cells for the generation of gait pattern. Perturbations in the balance of motor neuron activation across the two sides of the spinal cord could also be attributed to defects in synapse formation between incoming proprioceptors and postmitotic motor neurons. In order to test whether the absence of afadin in mature motor neurons is sufficient to cause the locomotor defect, the *ChAT::cre* driver line was used to eliminate the protein (hereafter referred to as *afadin* $^{fl/fl}$*; ChAT*). With this strategy, motor neuron progenitors are spared and afadin is only deleted in motor neurons once they become cholinergic, around e12.5.

In agreement with the expectations based on the genetics, in *afadin* $^{fl/fl}$*; ChAT* animals the afadin expression pattern at the neuroepithelium resembled that of controls during development (Figures 14A - F, see also Figures 10A - F) and postnatally they exhibited a normal central canal morphology (Figures 14G - H). Quantitative gait analysis revealed that *afadin* $^{fl/fl}$*; ChAT* mice maintained left/right alternating limb movements during locomotion (Figure 14I) and their speed and step frequency was similar to that of controls (Figures 14J - K and Appendix I). In addition, no synchronous steps were observed (Appendix I).

These data indicate that afadin function in postmitotic motor neurons is not required for the correct assembly of locomotor circuits. Consequently, this suggests that the disruption of the alternating gait pattern in *afadin* $^{fl/fl}$ mice must be due to loss of afadin at the pMN and the resulting double central canal.

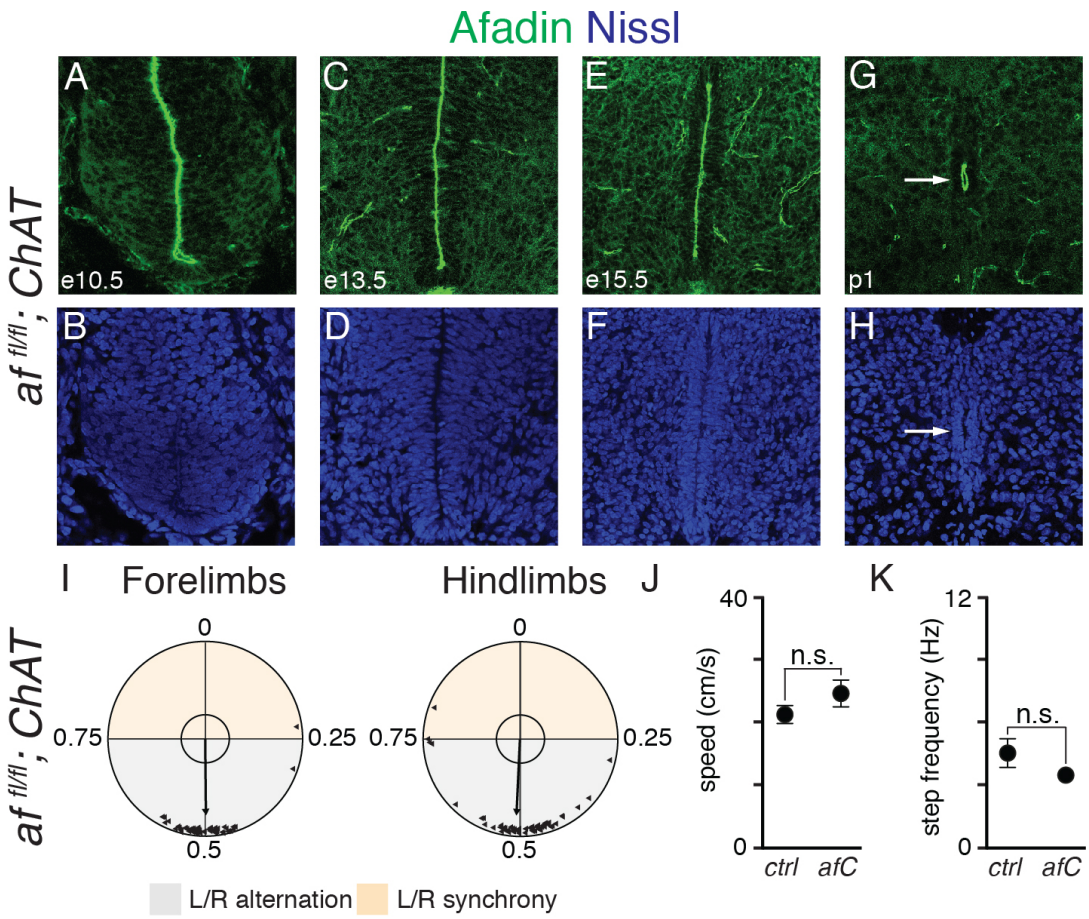

Figure 14. Central canal development and quantitative gait analysis in *afadin* $^{fl/fl}$*; ChAT* (*afC*) mice. A-H) Afadin expression and Nissl staining in e10.5 (A-B), e13.5 (C-D), e15.5 (E-F) and p1 (G-H) *afadin* $^{fl/fl}$*; ChAT* spinal cords. Ventral midline area is shown in A-D. Central canal area is shown in E-H. Arrow in G points to the central canal. I) Polar plots showing the left/right phase relationship in fore- and hindlimbs and the average orientation vector in *afadin* $^{fl/fl}$*; ChAT* mice (n = 3). J) Average speed in control and *afadin* $^{fl/fl}$*; ChAT* mice (n = 3, mean ± SEM, two-tailed unpaired t-test). G) Average step frequency in control and *afadin* $^{fl/fl}$*; ChAT* mice (n = 3, mean ± SEM, two-tailed unpaired t-test). Adapted from: Skarlatou et al., 2020.

4.6 EXPRESSION OF AXON GUIDANCE CUES IN PRESENCE OF A DOUBLE CENTRAL CANAL

The next question that was addressed was how a double central canal could influence the assembly of motor circuits. The midline of the spinal cord is a hub for axon guidance molecules that direct neural connectivity during development. Since the double central canal phenotype in *afadin* $^{fl/fl}$ mice changes the anatomical

architecture of that specialized region, it might also affect the localization of guidance cues and perturb the projection patterns of spinal neurons. Previous studies have shown that a lack of Netrin-1 or Ephrin B3 can alter the coordination of left and right motor neurons activation (Kullander et al., 2001; Rabe et al., 2009). Thus, the expression of Netrin-1 and Ephrin B3 was analyzed in afadin mutant mice by *in-situ* hybridization and immunohistochemistry, respectively.

At e13.5 Netrin-1 mRNA was found in similar extent and intensity at the floor plate of both control and *afadin* $^{fl/fl}$ embryos (Figures 15A - D). However, the presence of a double central canal in postnatal *afadin* $^{fl/fl}$ mice dramatically reduced the extent of Netrin-1 expression in the ventral segment of the midline (Figures 15E - H).

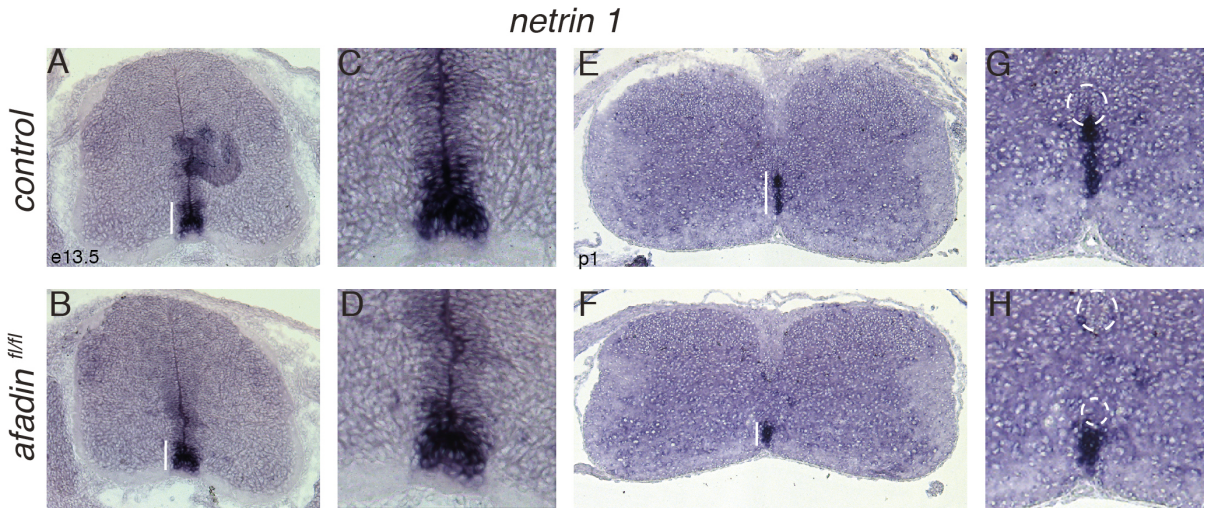

Figure 15. Netrin-1 mRNA expression at e13.5 and p1. A-B) Representative images of transverse spinal cords showing expression of Netrin-1 mRNA in e13.5 control (A) and *afadin* $^{fl/fl}$ (B) embryos. Bars represent extent of Netrin-1 signal. C-D) Magnification of ventral midline area from images in A (C) and B (D). E-F) Representative images of transverse spinal cords showing expression of Netrin-1 mRNA in p1 control (E) and *afadin* $^{fl/fl}$ (F) mice. Bars represent extent of Netrin-1 signal. G-H) Magnification of ventral midline area from images in E (G) and F (H). Dashed lines delineate the central canal. Adapted from: Skarlatou et al., 2020.

On the other hand, Ephrin B3 protein expression was first detected at e14.5 when lumen formation begins. In controls the area above and below the constricting neuroepithelium expressed Ephrin B3 (Figure 16A). In addition, some signal could also be seen in ventral cell populations, probably corresponding to early V3 interneurons (Laussu et al., 2017). In the course of development, Ephrin B3 expression along the midline became stronger and clearly delineated a separation of

the two halves of the spinal cord while its neuronal expression was downregulated (Figures 16C and 16E). In afadin mutants, the lower central canal has already emerged at e14.5 while the upper neuroepithelium is still constricting. At this stage Ephrin B3 was localized in the dorsal grey matter above the constricting cells and in migrating ventral interneurons, but was absent from the area between the two neuroepithelial structures and below the lower central canal (Figure 16B). The expression of Ephrin B3 at the ventral midline could be observed later in development, however, the tissue between the two central canals remained Ephrin B3-negative (Figures 16D and 16F).

Altogether, these results show that central canal morphology is tightly linked to the expression of signaling molecules with roles in establishing connectivity patterns in the spinal cord.

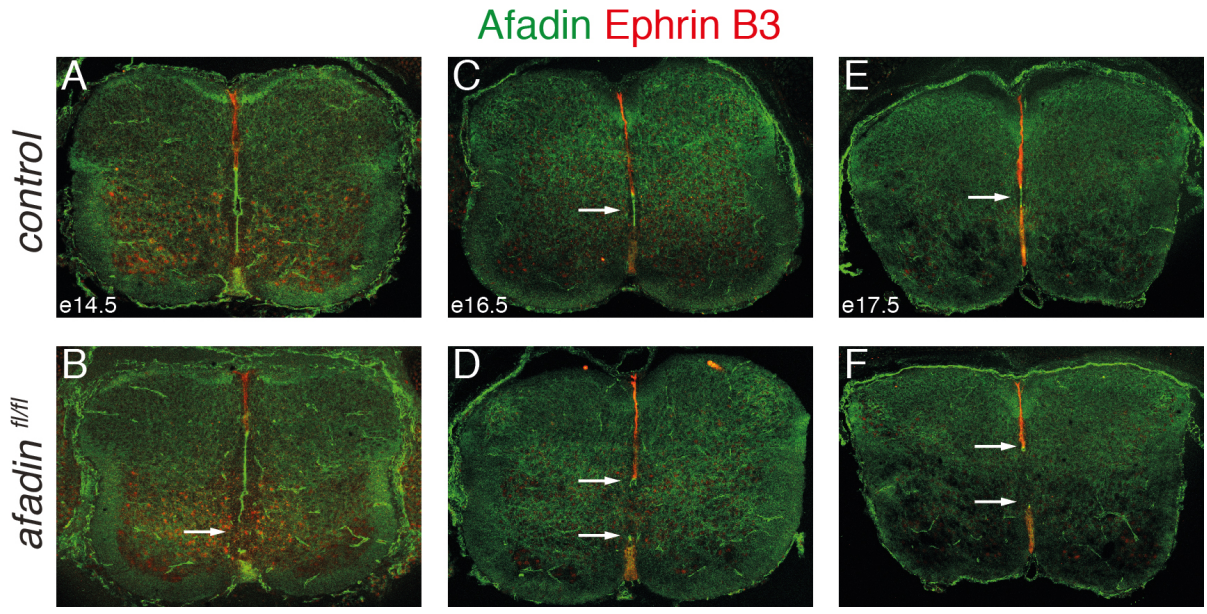

Figure 16. Ephrin B3 protein expression during development. A-B) Representative images of transverse spinal cords showing expression of Ephrin B3 in e14.5 control (A) and *afadin* $^{fl/fl}$ (B) embryos. Arrow in B points to the pMN devoid of afadin and Ephrin B3. C-D) Representative images of transverse spinal cords showing expression of Ephrin B3 in e16.5 control (C) and *afadin* $^{fl/fl}$ (D) embryos. Arrows point to the developing central canals. E-F) Representative images of transverse spinal cords showing expression of Ephrin B3 in e17.5 control (E) and *afadin* $^{fl/fl}$ (F) embryos. Arrows point to the developing central canals.

4.7 COMMISSURAL AXONS TRAJECTORY UPON REDUCTION OF NETRIN-1 SIGNAL

Netrin-1 emanating from the floor plate is known to guide dorsal commissural axons along their stereotyped pathway to the contralateral side of the spinal cord (Serafini et al., 1996). Commissural interneurons, in turn, participate in balancing the motor output across the two body halves and are, thus, likely to have altered functions in a network that favors left/right synchronization. Given the reduction of Netrin-1 signal in *afadin* $^{fl/fl}$ mice due to the presence of the double central canal, the trajectory pattern of commissural axons was studied. For this purpose, immunohistochemistry against TAG-1, which is a glycoprotein that is transiently expressed during development and promotes axonal growth, and Robo3, which is implicated in the Slit/Robo pathway directing crossing axons through the midline, was performed.

TAG-1 expression was detected in motor, commissural and dorsal root ganglion (DRG) axons in control e12.5 and e13.5 embryos (Figures 17A and 17C), but by e15.5 the signal was restricted to only incoming sensory afferents (Figure 17E). The same pattern was observed in *afadin* $^{fl/fl}$ spinal cords (Figures 17B, 17D and 17F). In addition, the thickness of the ventral commissure as measured by TAG-1 expression was quantified in control and *afadin* $^{fl/fl}$ embryos at e12.5 and e13.5 and no significant difference was found (Figures 17G - H). Robo3 signal was consistent with the migratory stream of dorsal commissural interneurons axons that approach the floor plate in order to navigate to the contralateral side up to e13.5 in control and mutant animals (Figures 17I - L). At e15.5 Robo3 expression was substantially weakened (Figures 17M - N). Quantification of the extent of Robo3 signal at the ventral commissure did not show significant differences either at e12.5 or e13.5 (Figures 17O - P).

Hence, despite the defect in Netrin-1 expression, commissural axon pathfinding and the organization of the ventral commissure are not affected in *afadin* $^{fl/fl}$ mice. This indicates that the underlying cause for the locomotor phenotype is not an imbalance due to reduced ventral crossing.

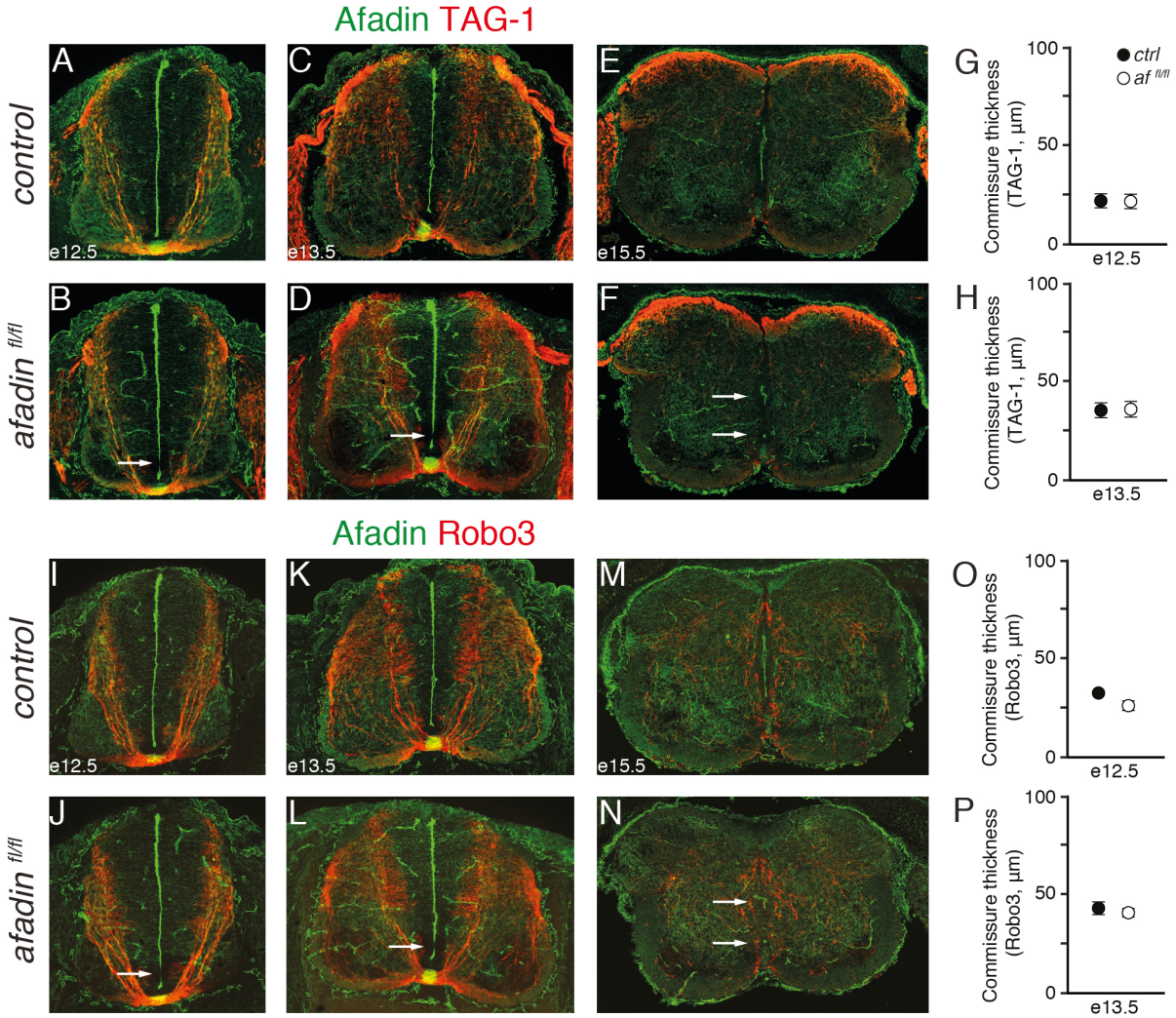

Figure 17. Commissural axons trajectory as identified by TAG-1 and Robo3 expression during development. A-B) Representative images of transverse spinal cords showing afadin and TAG-1 expression in e12.5 control (A) and *afadin* $^{fl/fl}$ (B) embryos. Arrow in B points to the pMN devoid of afadin. C-D) Representative images of transverse spinal cords showing afadin and TAG-1 expression in e13.5 control (C) and *afadin* $^{fl/fl}$ (D) embryos. Arrow in D points to the pMN devoid of afadin. E-F) Representative images of transverse spinal cords showing afadin and TAG-1 expression in e15.5 control (E) and *afadin* $^{fl/fl}$ (F) embryos. Arrows in F point to the two central canals. G-H) Quantification of TAG-1 signal at ventral commissure in e12.5 (G) and e13.5 (H) spinal cords (n = 3, mean ± SEM, two-tailed unpaired t-test). I-J) Representative images of transverse spinal cords showing afadin and Robo3 expression in e12.5 control (I) and *afadin* $^{fl/fl}$ (J) embryos. Arrow in J points to the pMN devoid of afadin. K-L) Representative images of transverse spinal cords showing afadin and Robo3 expression in e13.5 control (K) and *afadin* $^{fl/fl}$ (L) embryos. Arrow in L points to the pMN devoid of afadin. M-N) Representative images of transverse spinal cords showing afadin and Robo3 expression in e15.5 control (M) and *afadin* $^{fl/fl}$ (N) embryos. Arrows in N point to the two central canals. O-P) Quantification of Robo3 signal at ventral commissure in e12.5 (O) and e13.5 (P) spinal cords (n = 3, mean ± SEM, two-tailed unpaired t-test). Adapted from: Skarlatou et al., 2020.

4.8 CONTRALATERAL AXONAL PROJECTIONS UPON DISRUPTION OF EPHRIN B3 SIGNALING

The repulsive interaction between Ephrin B3 and its receptor EphA4 represents the most prominent example of a signaling system that controls the wiring of spinal neurons. Ephrin B3 that is localized along the whole DV extent of the midline serves as a molecular barrier that repels EphA4^{+} axons, ensuring an ipsilateral projection pattern. Mice, where either Ephrin B3 or EphA4 have been knocked out, display aberrant premotor connectivity and a bound gait (Dottori et al., 1998; Kullander et al., 2001; Satoh et al., 2016). Therefore, axonal projections of interneurons were analyzed in *afadin* $^{fl/fl}$ animals by injection of rhodamine B-dextran (RDA) into one side of the spinal cord at e15.5, the first timepoint when a clear disruption of midline organization is observed (for a detailed description see section 3.11).

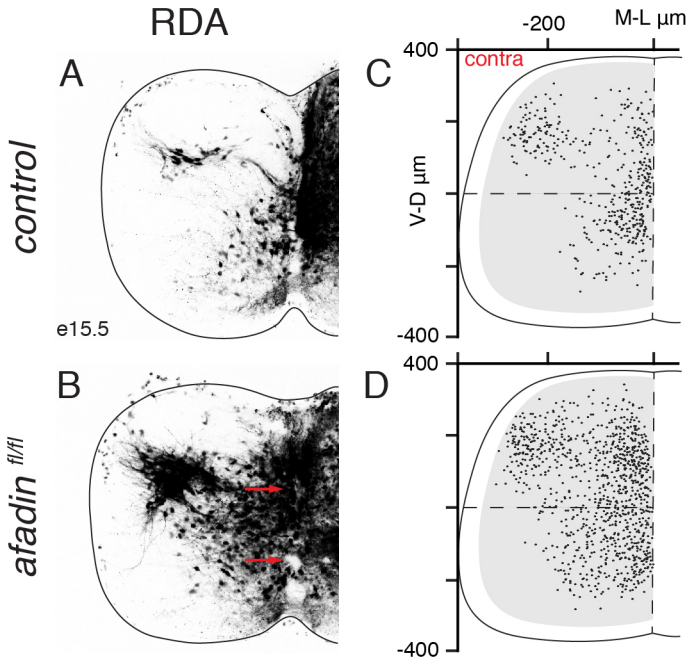

Figure 18. RDA tracing of spinal interneurons at e15.5. A-B) Representative images of transverse hemicords showing RDA-labeled contralateral interneurons and ipsilateral crossing axons in e15.5 control (A) and *afadin* $^{fl/fl}$ (B) embryos. Arrows in B point to the two central canals. E-F) Digital reconstruction of contralateral interneurons in a representative control (E) and *afadin* $^{fl/fl}$ (F) embryo. Adapted from: Skarlatou et al., 2020.

RDA can be taken up both antero- and retrogradely, thus enabling the visualization of contralateral cell bodies as well as crossing axons from ipsilateral neurons. In control embryos, a ventromedial and a dorsolateral cluster of RDA-labeled cells could be observed (Figures 18A and 18C), which were also found in *afadin* $^{fl/fl}$ animals. However, in mutant mice there was additionally an increase in contralaterally labeled cell bodies in the dorsal and intermediate spinal cord (Figures 18B and 18D). Similarly, numerous interneurons projected to the contralateral side through the expanded grey matter in *afadin* $^{fl/fl}$ embryos (Figures 18B), in contrast to control animals that exhibited only sparse crossing axons (Figures 18A).

Together, these data suggest that the loss of Ephrin B3 in between the two central canals in *afadin* $^{fl/fl}$ animals allows aberrant projections to the contralateral side, thus altering the structure of the spinal networks.

4.9 ANALYSIS OF FORELIMB PREMOTOR CONNECTIVITY

The observation that more spinal neurons send contralateral projections through the gap between the two central canals in *afadin* $^{fl/fl}$ mice suggests that the resulting changes in neuronal connectivity are causing the switch from alternation to synchronization of paired limbs. This would imply that motor neurons receive ectopic input that activates them simultaneously on both sides. Indeed, altered premotor connectivity patterns have been demonstrated in other mouse models with similar gait patterns (Satoh et al., 2016). Thus, the distribution of premotor interneurons at forelimb levels was investigated in control and *afadin* $^{fl/fl}$ animals by injecting a genetically modified RV into the extensor carpis radialis (ECR) muscle.

RV is a strictly neurotropic virus that retrogradely infects neurons in the CNS through axon terminals. For its propagation from primarily infected cells to presynaptic partners, it relies on the rabies glycoprotein (G). Accordingly, G-deficient RV cannot spread following initial infection unless the G protein is provided by an external source. Here, the *RΦGT* mouse line was employed, which drives the expression of the G protein in a cre-dependent manner, i.e. *afadin* $^{fl/fl}$ animals crossed with *RΦGT* express G specifically in Olig2^{+} motor neurons. Upon

intramuscular injection of G-deficient RV (for a detailed description see section 3.15), the corresponding motor neurons are infected and, by supplying the missing G protein, restore the RV's ability to spread to monosynaptically connected interneurons. These interneurons do not produce G protein and, consequently, the infection is restricted to first-order connections only.

To begin with, three control replicates were analyzed to test the efficiency and reproducibility of the tracing method. In addition, ChAT staining was used to identify targeted motor neurons. In the analyzed range of 2 mm, comparable numbers of starter cells ($ChAT^+$; RV^+ motor neurons) and RV-labeled premotor neurons were obtained for all animals (Figure 19A and Appendix III). Moreover, digital reconstruction of the ECR premotor network from individual datasets displayed a consistent pattern. The majority of premotor interneurons were located ipsilaterally in Rexed's laminae VI, VII and X while contralateral interneurons were confined to Rexed's lamina VIII, consistent with previous reports (Figure 19D and Stepien et al., 2010). The reproducibility of the experiments was additionally confirmed by ML density distribution analysis, which revealed similar distributions in all controls (Figure 19B), and the high degree of correlation between their positional coordinates (Figure 19C, $R \geq 0.91$). In order to look for differences in premotor connectivity, *afadin* $^{fl/fl}$ mice were evaluated in the same way. Motor neuron targeting and labeling efficiency did not differ from controls (Figures 19E, 19G and Appendix III). The overall distribution of premotor neurons was also similar (Figure 19F), however, afadin mutants exhibited a higher number of contralateral cells found in the intermediate and dorsal spinal cord (Figures 19H - J). This was confirmed by DV density distribution analysis that uncovered an ectopic dorsal peak in *afadin* $^{fl/fl}$ animals compared to the controls (Figure 19K). Futhermore, quantification of the relative incidence of premotor connections in each quadrant of the spinal cord revealed no significant differences on the ipsilateral side, but an approximately 4-fold increase of dorsal contralateral neurons contacting the same motor neurons in *afadin* $^{fl/fl}$ mice (Figure 19L).

In summary, these data show that the premotor connectivity pattern is altered in afadin mutants. In particular, there are aberrant connections onto motor neurons emerging from the contralateral side, which could modify motor output.

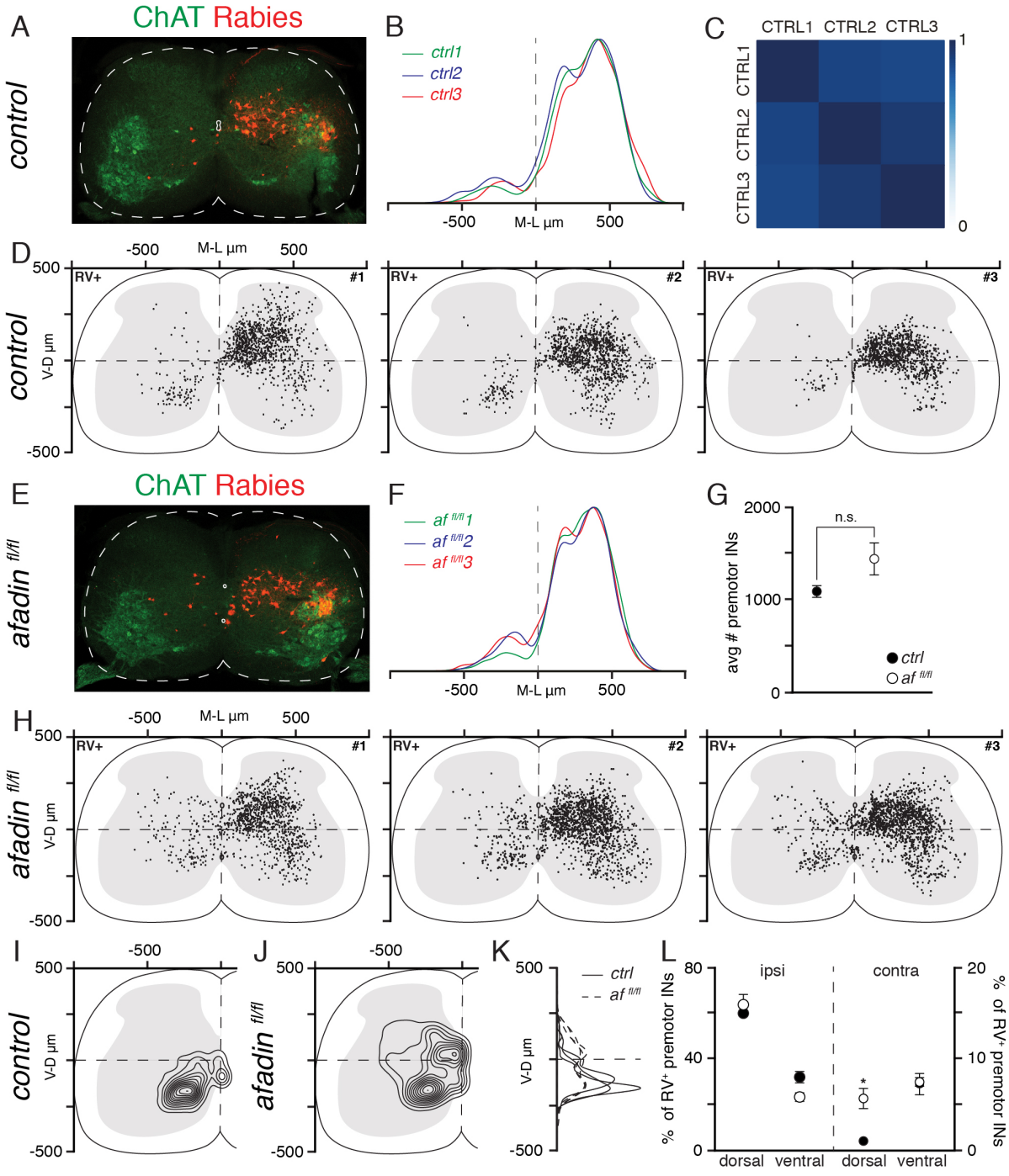

Figure 19. Comparison of ECR premotor connectivity in control and *afadin* $^{fl/fl}$ mice. A) Representative image of a transverse spinal cord showing ChAT expression and RV-labeled ECR premotor interneurons in a p10 control. B) ML density analysis of ECR premotor interneurons in control mice (each trace represents one animal). C) Correlation analysis of ECR premotor interneurons coordinates in three control mice. The scale bar indicates correlation values. D) Digital reconstruction of ECR premotor interneurons positions of three control mice. E) Representative image of a transverse spinal cord showing ChAT expression and RV-labeled ECR premotor interneurons in a p10 *afadin* $^{fl/fl}$. F) ML density analysis of ECR premotor interneurons in *afadin* $^{fl/fl}$ mice (each trace

represents one animal). G) Average number of RV-labeled ECR premotor interneurons in control and *afadin* $^{fl/fl}$ mice (n = 3, mean ± SEM, two-tailed unpaired t-test, p > 0.05). H) Digital reconstruction of ECR premotor interneurons positions of three *afadin* $^{fl/fl}$ mice. I-J) Transverse contour density plot of contralateral ECR premotor interneurons in control (I) and *afadin* $^{fl/fl}$ (J) mice (n = 3). K) DV density analysis of contralateral ECR premotor interneurons in control and *afadin* $^{fl/fl}$ mice (n = 3, each trace represents one animal). L) Percentage of premotor interneurons in the dorsal and ventral quadrants in the ipsilateral (left) and contralateral (right) side of the spinal cord in control and *afadin* $^{fl/fl}$ mice (n = 3, mean ± SEM, two-tailed unpaired t-test, * = p < 0.05). Adapted from: Skarlatou et al., 2020.

4.10 IDENTIFICATION OF ABERRANTLY WIRED INTERNEURONS POPULATIONS

In order to understand the differences in circuit configuration between normal alternating animals and synchronizing *afadin* $^{fl/fl}$ mice, it is necessary to identify the interneurons with altered connectivity that could elicit the changes in motor neuron activation. For this purpose, RV-tracing was combined with immunohistochemistry for markers that are active at postnatal stages and specifically label interneurons populations with known roles in the control of locomotion. This allowed a systematic screening of different classes of interneurons in the quest for those that aberrantly connect to motor neurons in afadin mutants.

As a proof of principle, the distribution of premotor interneurons arising from the Lbx1 progenitor domain was analyzed first. Dorsal contralateral Lbx1$^+$ interneurons, corresponding to dI4s and dI5s, have been recently shown to form abnormal connections to motor neurons upon genetic disruption of Ephrin B3/EphA4 signaling (Satoh et al., 2016). Given the lack of Ephrin B3 between the two central canals in the *afadin* $^{fl/fl}$ model, the same connectivity defect was anticipated here as well. Indeed, digital reconstruction of Lbx1-labeled premotor interneurons showed an increase in contralaterally localized cells in *afadin* $^{fl/fl}$ mice (Figures 20A - D), which was confirmed by quantitative and density distribution analyses that revelead an additional dorsal cluster in the mutants (Figures 20E - F and Appendix III). In contrast, ventral Lbx1$^+$ cells, that represent dI6 neurons, were not significantly different, indicating that they do not play a role in the coordination of left/right movements under the given circumstances. Thus, the presence of a double central canal that interferes with the expression pattern of Ephrin B3 recapitulates the previously studied scenario of EphA4 elimination and results in a similar connectivity

phenotype. However, comparison of total and Lbx1^{+} only contralateral interneurons maps in *afadin* $^{fl/fl}$ animals suggested that dI4 and dI5 neurons cannot account for all of the ectopically wired cells (Figures 20G - H).

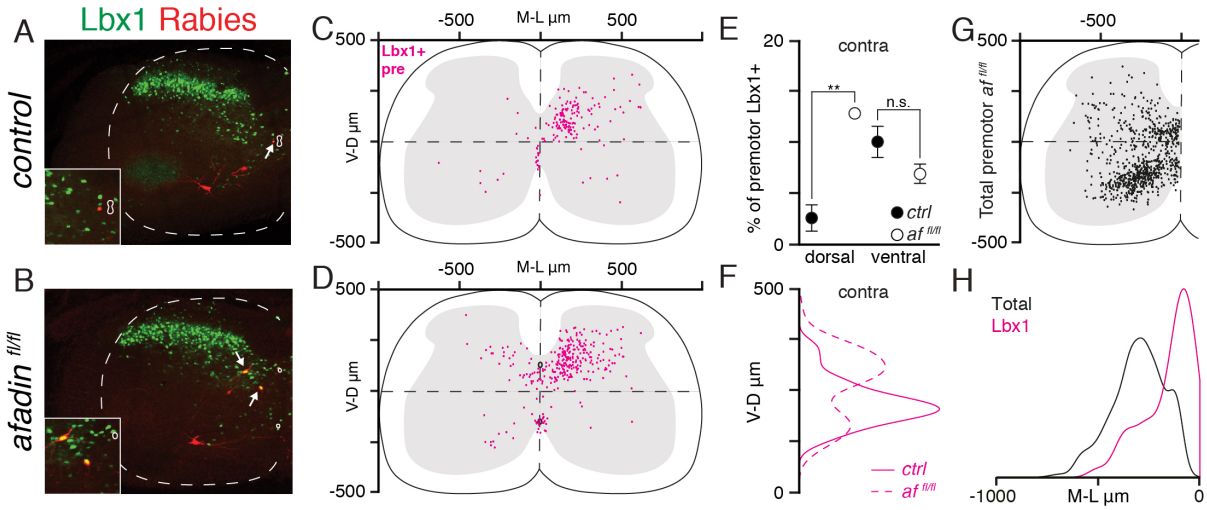

Figure 20. Premotor connectivity of Lbx1^{+} interneurons in control and *afadin* $^{fl/fl}$ mice. A-B) Representative images of transverse contralateral hemicords showing Lbx1 expression and RV-labeled interneurons in a p10 control (A) and *afadin* $^{fl/fl}$ (B). Insets show magnification of representative neurons marked by arrows. C-D) Digital reconstruction of Lbx1^{+} premotor interneurons positions in control (C) and *afadin* $^{fl/fl}$ (D) mice (n = 3). E) Percentage of Lbx1^{+} premotor interneurons in the dorsal and ventral contralateral quadrant in control and *afadin* $^{fl/fl}$ mice (n = 3, mean ± SEM, two-tailed unpaired t-test, ** = $p < 0.01$). F) DV density analysis of contralateral Lbx1^{+} premotor interneurons in control and *afadin* $^{fl/fl}$ mice (n = 3). G) Digital reconstruction of total contralateral premotor interneurons in *afadin* $^{fl/fl}$ mice (n = 3). H) ML density analysis in the dorsal contralateral quadrant of total (black) and Lbx1^{+} (magenta) premotor interneurons in *afadin* $^{fl/fl}$ mice (n = 3 for each). Adapted from: Skarlatou et al., 2020.

The second class of interneurons that was investigated was the one arising from the V0 progenitor domain, which has been implicated in the control of left/right alternation at different locomotor frequencies (Lanuza et al., 2004; Talpalar et al., 2013). In addition, a subset of V0s expresses EphA4, making them susceptible to a lack of Ephrin B3 (Lundfald et al., 2007). V0 interneurons can be identified by expression of Dbx1 during development, but there is no unique marker for them postnatally. Therefore, these cells were approximated by combinatorial analysis of Lhx1, which labels V0s, V1s and subsets of dorsal populations including dI4s and dIL$_A$s, and FoxD3, which allows the exclusion of V1 interneurons. With this approach,

a dorsal contralateral cluster of Lhx1^{+}/FoxD3^{-} premotor neurons was located in *afadin* $^{fl/fl}$ mice, which was missing in control littermates (Figures 21A - D and 21F). The percentage of cells exhibiting this molecular signature in that particular quadrant was increased by a factor of 50 in the mutants while ventral Lhx1^{+}/FoxD3^{-} premotor neurons numbers and positions were indistinguishable from controls (Figure 21E and Appendix III). Interestingly, these putative V0 neurons were positioned more laterally than the Lbx1^{+} population, indicating that they represent a different group of interneurons (Figure 21G - H).

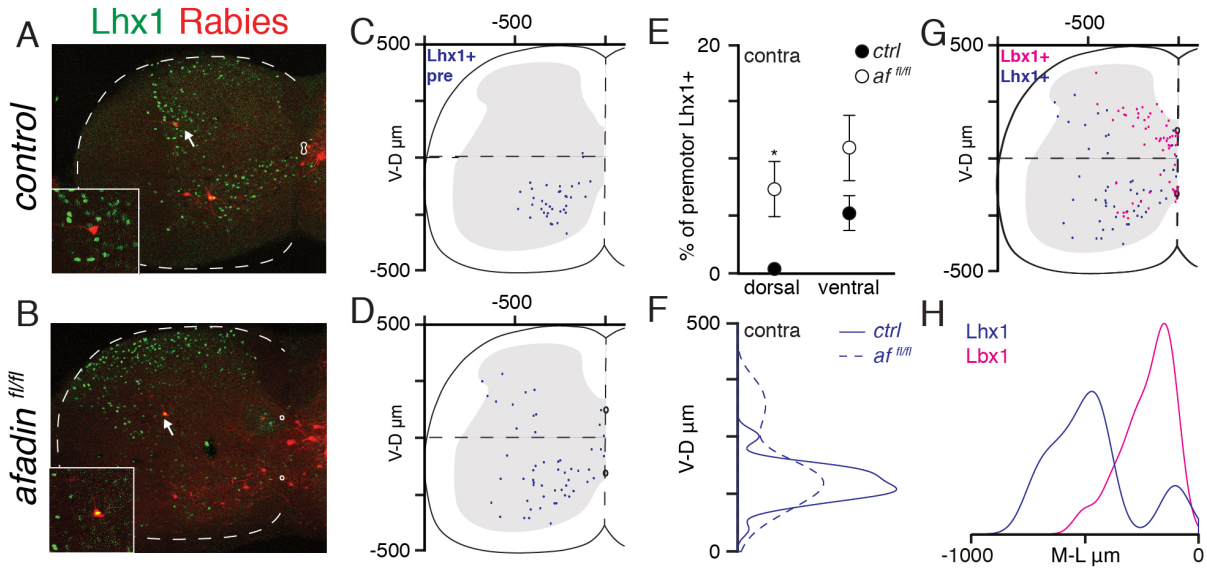

Figure 21. Premotor connectivity of Lhx1^{+}/FoxD3^{-} interneurons in control and *afadin* $^{fl/fl}$ mice. A-B) Representative images of transverse contralateral hemicords showing Lhx1 expression and RV-labeled interneurons in a p10 control (A) and *afadin* $^{fl/fl}$ (B). Insets show magnification of representative neurons marked by arrows. C-D) Digital reconstruction of contralateral Lhx1^{+}/FoxD3^{-} premotor interneurons positions in control (C) and *afadin* $^{fl/fl}$ (D) mice (n = 3). E) Percentage of Lhx1^{+}/FoxD3^{-} premotor interneurons in the dorsal and ventral contralateral quadrant in control and *afadin* $^{fl/fl}$ mice (n = 3, mean ± SEM, two-tailed unpaired t-test, * = $p < 0.05$). F) DV density analysis of contralateral Lhx1^{+}/FoxD3^{-} premotor interneurons in control and *afadin* $^{fl/fl}$ mice (n = 3). G) Digital reconstruction of contralateral Lhx1^{+}/FoxD3^{-} (blue) and Lbx1^{+} (magenta) premotor interneurons in *afadin* $^{fl/fl}$ mice (n = 3). H) ML density analysis in the dorsal contralateral quadrant of Lhx1^{+}/FoxD3^{-} (blue) and Lbx1^{+} (magenta) premotor interneurons in *afadin* $^{fl/fl}$ mice (n = 3 for each). Adapted from: Skarlatou et al., 2020.

On the other hand, analysis of Lhx1^{+}/FoxD3^{+} premotor cells, that mainly comprise inhibitory V1 interneurons, did not display any obvious differences between control and *afadin* $^{fl/fl}$ animals (Figures 22A - B). A prominent ventral cluster was found in the ipsilateral side, which most likely consists of Renshaw neurons, along with some sparse dorsal cells (Figures 22C - D). V1s are known to have ipsilateral projections, however, the analysis of Lhx1^{+}/FoxD3^{+} cells also revealed some contralaterally localized premotor neurons. These contralateral FoxD3^{+} cells were confined to the ventromedial area (Figures 22C - D). Moreover, the relative number of neurons found on each side of the spinal cord as well as their ML distribution did not significantly differ (Figure 22E-F). These observations are in agreement with the fact that V1 interneurons have been shown to control the activity of flexor motor neurons and instead have no described roles in left/right alternation (Arber, 2012; Britz et al., 2015).

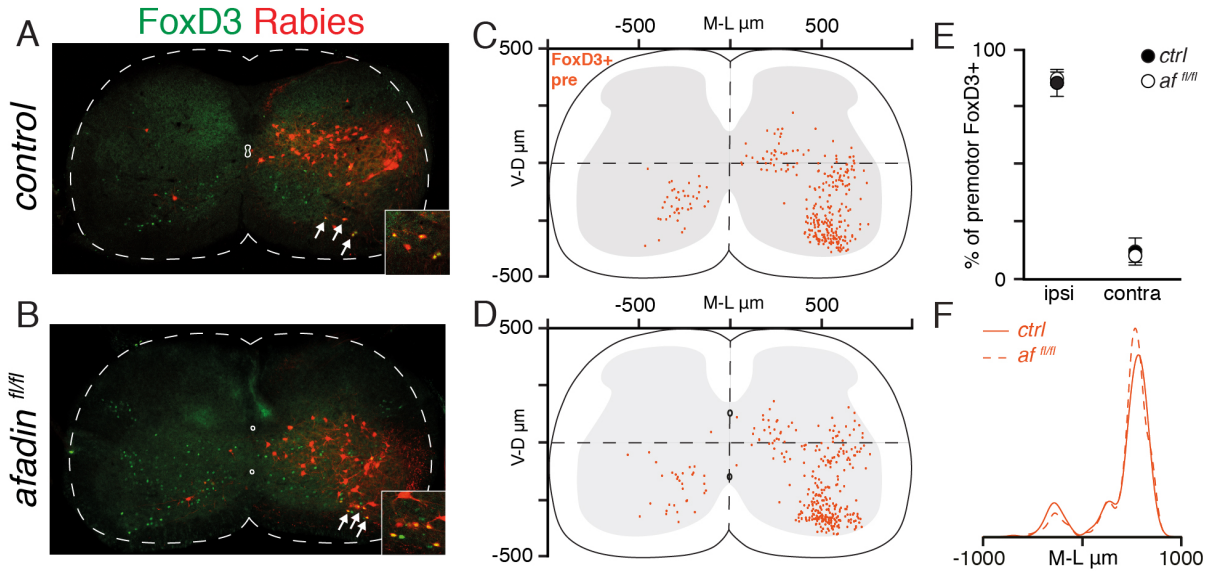

Figure 22. Premotor connectivity of Lhx1^{+}/FoxD3^{+} interneurons in control and *afadin* $^{fl/fl}$ mice. A-B) Representative images of transverse spinal cords showing FoxD3 expression and RV-labeled interneurons in a p10 control (A) and *afadin* $^{fl/fl}$ (B). Insets show magnification of representative neurons marked by arrows. C-D) Digital reconstruction of Lhx1^{+}/FoxD3^{+} premotor interneurons positions in control (C) and *afadin* $^{fl/fl}$ (D) mice (n = 3). E) Percentage of Lhx1^{+}/FoxD3^{+} premotor interneurons in the ipsilateral and contralateral side in control and *afadin* $^{fl/fl}$ mice (n = 3, mean ± SEM, two-tailed unpaired t-test, $p > 0.05$). F) ML density analysis of Lhx1^{+}/FoxD3^{+} premotor interneurons in control and *afadin* $^{fl/fl}$ mice (n = 3). Adapted from: Skarlatou et al., 2020.

A small fraction of V0 interneurons located in Rexed's lamina X has cholinergic character and modulates motor output via C-boutons ($V0_C$, Zagoraiou et al., 2009). The connectivity of these cells was examined by looking at the expression of ChAT within the premotor populations of controls and afadin mutants. Despite the disrupted midline organization in *afadin* $^{fl/fl}$ mice the overall distribution of $V0_C$s was not affected as they were still found at DV positions around the central canal and slightly extending along the ML axis, similar to controls (Figures 23A - B and 23I - L). ChAT-labeled premotor neurons were observed in both control and *afadin* $^{fl/fl}$ animals (Figures 23A - B), however, the latter exhibited a slight but significant increase in contralateral premotor $V0_C$s. In contrast, the ipsilateral numbers remained the same, hinting at a wiring rather than a migrational defect (Figures 23C - D, 23G - H and Appendix III). Their DV distribution did not present remarkable differences between control and mutant mice (Figures 23E - F).

Finally, the connectivity of V2as was analyzed. V2a interneurons are a population of strictly ipsilaterally projecting, excitatory neurons that are characterized by the expression of Chx10. Moreover, approximately 80% of V2as are $EphA4^+$ during development (Lundfald et al., 2007), making them the ideal candidates for misguided axons in the absence of Ephrin B3 signaling. As expected, in control animals premotor V2as were found exclusively in the ipsilateral side (Figures 24A, 24C and Appendix III), but while the number of ipsilateral $Chx10^+$ premotor neurons in afadin mutants was similar to that in controls (Figure 24D and Appendix III), some were also localized contralateral to the point of injection (Figures 24B, 24D and 24H). Accordingly, the emergence of these V2as with contralateral projections in *afadin* $^{fl/fl}$ mice was significant (Figure 24G). On the other hand, similar to $V0_C$s, the distribution of the whole V2a population as well as that of the premotor subset was not altered in mutant mice (Figures 24E - F and 24I - L), indicating that the double central canal does not affected their stereotyped positioning.

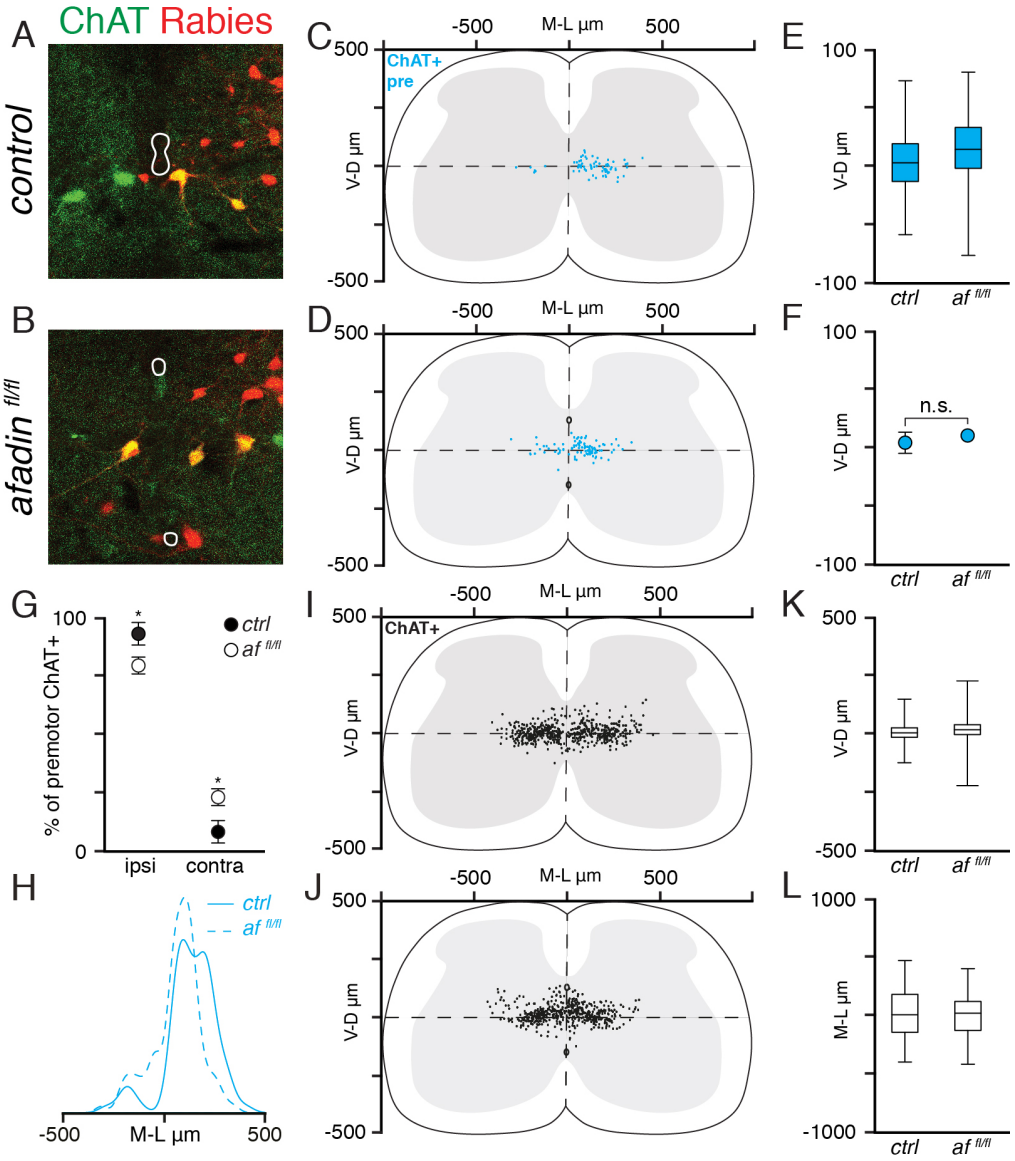

Figure 23. Premotor connectivity of ChAT$^+$ interneurons in control and *afadin* $^{fl/fl}$ mice. A-B) Representative images of central canal area showing ChAT expression and RV-labeled interneurons in a p10 control (A) and *afadin* $^{fl/fl}$ (B). C-D) Digital reconstruction of ChAT$^+$ premotor interneurons positions in control (C) and *afadin* $^{fl/fl}$ (D) mice (n = 3). E) Box plots showing DV distribution of ChAT$^+$ premotor interneurons in control and *afadin* $^{fl/fl}$ mice (n = 3, whiskers represent min/max). F) Average DV positions of ChAT$^+$ premotor interneurons in control and *afadin* $^{fl/fl}$ mice (n = 3, mean ± SEM, two-tailed unpaired t-test, p > 0.05). G) Percentage of ChAT$^+$ premotor interneurons in the ipsilateral and contralateral side in control and *afadin* $^{fl/fl}$ mice (n = 3, mean ± SEM, two-tailed unpaired t-test, * = p < 0.05). H) ML density analysis of ChAT$^+$ premotor interneurons in control and *afadin* $^{fl/fl}$ mice (n = 3). I-J) Digital reconstruction of ChAT$^+$ interneurons positions in control (I) and *afadin* $^{fl/fl}$ (J) mice (n = 3). K-L) Box plots showing DV (K) and ML (L) distribution of ChAT$^+$ interneurons in control and *afadin* $^{fl/fl}$ mice (n = 3, whiskers represent min/max). Adapted from: Skarlatou et al., 2020.

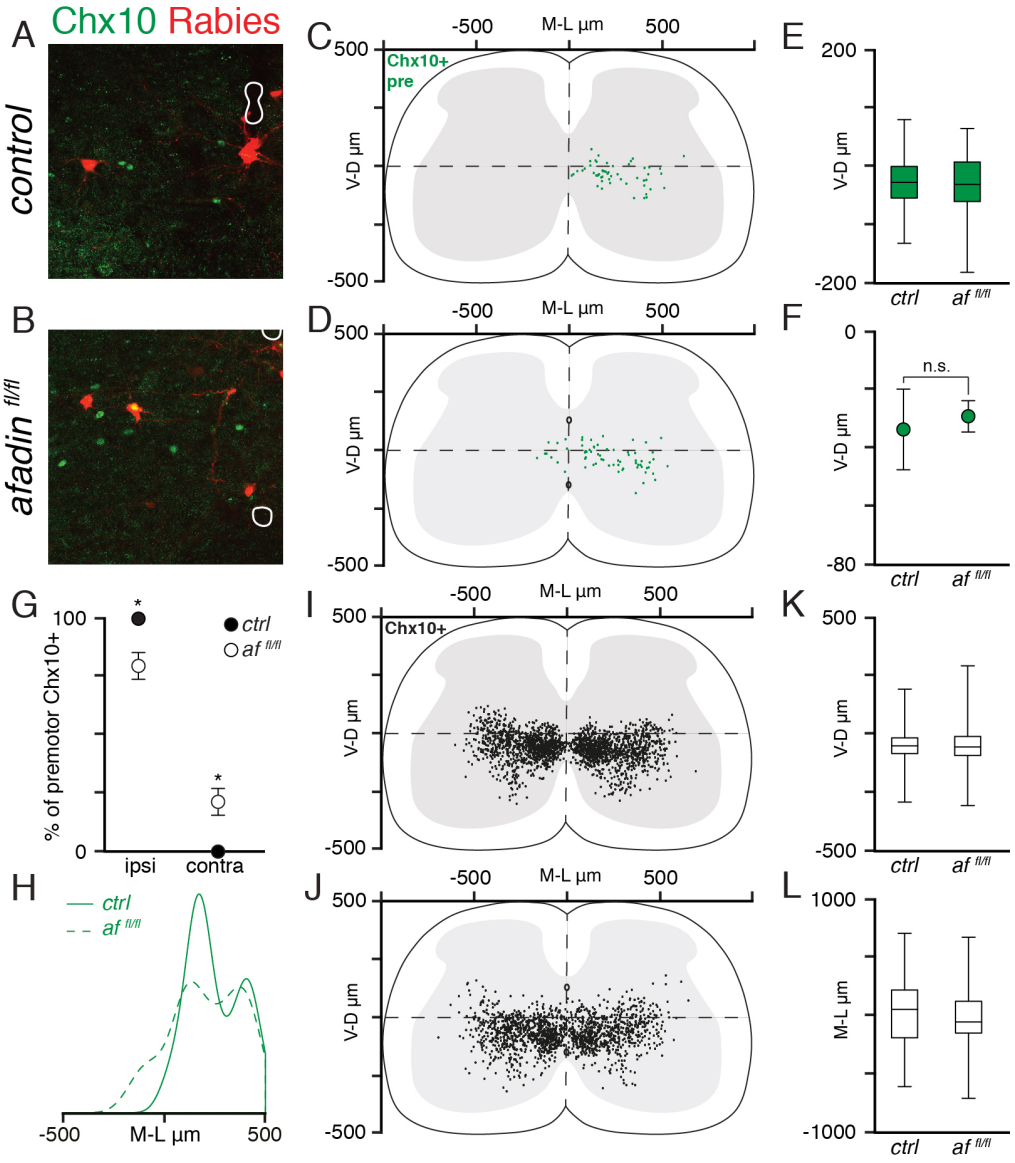

Figure 24. Premotor connectivity of Chx10^{+} interneurons in control and *afadin* $^{fl/fl}$ mice. A-B) Representative images of central canal area showing Chx10 expression and RV-labeled interneurons in a p10 control (A) and *afadin* $^{fl/fl}$ (B). C-D) Digital reconstruction of Chx10^{+} premotor interneurons positions in control (C) and *afadin* $^{fl/fl}$ (D) mice (n = 4). E) Box plots showing DV distribution of Chx10^{+} premotor interneurons in control and *afadin* $^{fl/fl}$ mice (n = 4, whiskers represent min/max). F) Average DV positions of Chx10^{+} premotor interneurons in control and *afadin* $^{fl/fl}$ mice (n = 4, mean ± SEM, two-tailed unpaired t-test, p > 0.05). G) Percentage of Chx10^{+} premotor interneurons in the ipsilateral and contralateral side in control and *afadin* $^{fl/fl}$ mice (n = 4, mean ± SEM, two-tailed unpaired t-test, * = p < 0.05). H) ML density analysis of Chx10^{+} premotor interneurons in control and *afadin* $^{fl/fl}$ mice (n = 4). I-J) Digital reconstruction of Chx10^{+} interneurons positions in control (I) and *afadin* $^{fl/fl}$ (J) mice (n = 4). K-L) Box plots showing DV (K) and ML (L) distribution of Chx10^{+} interneurons in control and *afadin* $^{fl/fl}$ mice (n = 4, whiskers represent min/max). Adapted from: Skarlatou et al., 2020.

Together, these experiments demonstrate aberrant wiring in multiple classes of interneurons in *afadin* $^{fl/fl}$ mutants and highlight their importance for the coordination of left and right appendages during locomotion. Nevertheless, the screening with available markers was not sufficient to identify all of the ectopic populations. Artificial superimposition of the digitally reconstructed contralateral premotor interneuron map of three controls and the pooled contralateral maps of the analyzed interneurons in *afadin* $^{fl/fl}$ mice shows a distribution pattern that resembles that of the mutants, but is still not as densely populated, particularly in the dorsal and intermediate spinal cord (Figures 25A - B). This implies that further, probably as yet uncharacterized, interneurons subtypes must be involved as well.

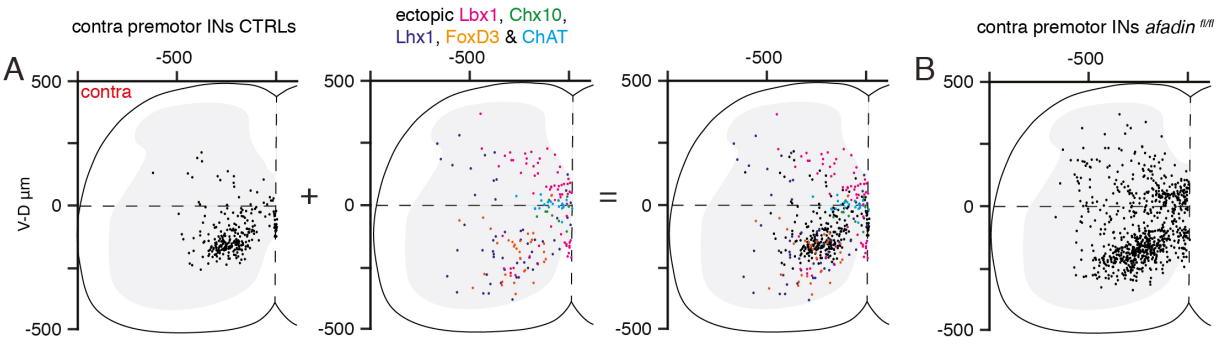

Figure 25. Identified ectopic interneurons complement control premotor map. A-B) Ectopic contralateral interneurons in *afadin* $^{fl/fl}$ mice complement control contralateral premotor interneuron map and approximate it to the *afadin* $^{fl/fl}$ contralateral premotor map (B). However, some aberrantly wired interneurons remained unidentified.

4.11 ANALYSIS OF HINDLIMB PREMOTOR CONNECTIVITY

The fact that *afadin* $^{fl/fl}$ animals display synchronized limb movements at both cervical and lumbar segments of the spinal cord suggests that the locomotor networks controlling the activity of forelimbs and hindlimbs should present the same wiring structure. By applying the RV-based tracing approach described in section 4.9 to lumbar motor neurons, the organization and composition of lumbar premotor circuits could be investigated.

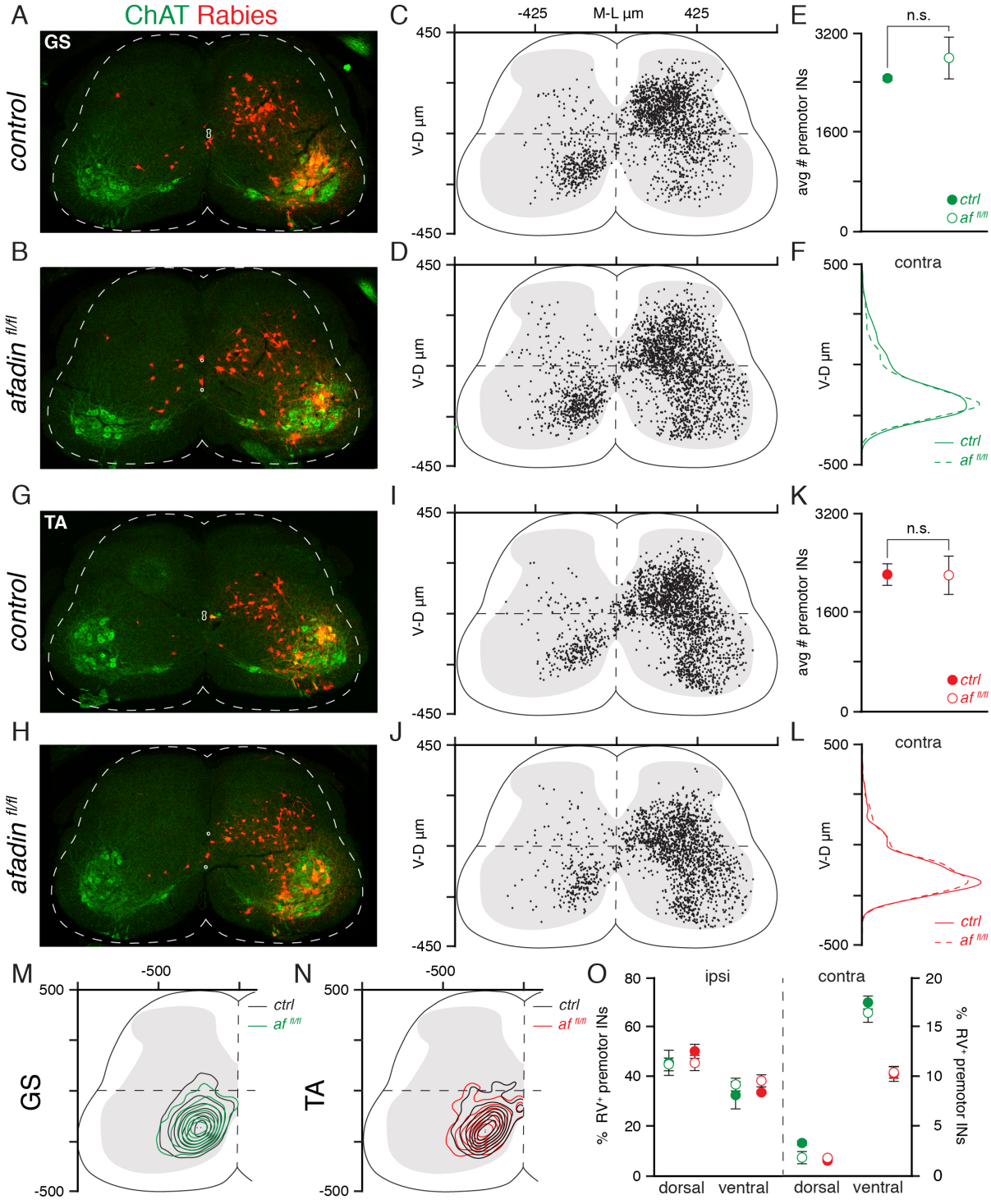

Figure 26. Comparison of GS and TA premotor connectivity in control and *afadin* $^{fl/fl}$ mice. A-B) Representative images of transverse spinal cords showing ChAT expression and RV-labeled GS premotor interneurons in a p10 control (A) and *afadin* $^{fl/fl}$ (B) mouse. C-D) Digital reconstruction of GS premotor interneurons positions of a representative control (C) and *afadin* $^{fl/fl}$ (D) mouse. E) Average number of RV-labeled GS premotor interneurons in control and *afadin* $^{fl/fl}$ mice (n = 3, mean ± SEM, two-tailed unpaired t-test, $p > 0.05$). F) DV density analysis of contralateral GS premotor interneurons in control and *afadin* $^{fl/fl}$ mice (n = 3). G-H) Representative images of transverse spinal cords showing

ChAT expression and RV-labeled TA premotor interneurons in a p10 control (G) and *afadin* $^{fl/fl}$ (H) mouse. I-J) Digital reconstruction of TA premotor interneurons positions of a representative control (I) and *afadin* $^{fl/fl}$ (J) mouse. K) Average number of RV-labeled TA premotor interneurons in control and *afadin* $^{fl/fl}$ mice (n = 3, mean ± SEM, two-tailed unpaired t-test, $p > 0.05$). L) DV density analysis of contralateral TA premotor interneurons in control and *afadin* $^{fl/fl}$ mice (n = 3). M) Transverse contour density plot of contralateral GS premotor interneurons in control (black) and *afadin* $^{fl/fl}$ (green) mice (n = 3). N) Transverse contour density plot of contralateral TA premotor interneurons in control (black) and *afadin* $^{fl/fl}$ (red) mice (n = 3). O) Percentage of premotor interneurons in the dorsal and ventral quadrants in the ipsilateral (left) and contralateral (right) side of the spinal cord in control and *afadin* $^{fl/fl}$ mice (n = 3, mean ± SEM, two-tailed unpaired t-test, $p > 0.05$).

First, the premotor connectivity of GS motor neurons was analyzed. The labeling and tracing efficiency in GS-injected control and *afadin* $^{fl/fl}$ mice was similar to that of ECR experiments (Figures 26A - B, 26E and Appendix III). However, the digital reconstruction of the corresponding premotor interneurons revealed no differences between controls and mutants (Figures 26C - D). In particular, the number of neurons found in the dorsal contralateral quadrant was comparable in all examined animals (Figure 26O). Further analysis of contralateral premotor neurons showed an almost identical distribution of cells along the DV axis (Figures 26F and 26M), supporting the observation that the connectivity of GS premotor neurons seems to be unaffected by the presence of a double central canal. Since the GS is a flexor muscle and the experiments at cervical levels were carried out on an extensor muscle, one possibility could be that extensor motor neurons preferentially receive input from EphA4^{+} interneurons and are, thus, more vulnerable to perturbations in Ephrin B3/EphA4 signaling. In order to test this hypothesis, premotor neurons were traced by injecting the RV into the TA muscle. Similar to GS experiments, the premotor network of TA motor neurons did not display any remarkable differences in terms of number or distribution of cells between control and *afadin* $^{fl/fl}$ animals (Figures 26G - K and Appendix III). Moreover, the location of contralateral neurons did not significantly vary (Figures 26I - J, 26L and 26N) and also their relative incidence in each quadrant was comparable to that in controls (Figure 26O).

Together, these data show that the organization of lumbar circuits is not affected in *afadin* $^{fl/fl}$ mutants, thus indicating that cervical CPGs are able to impose their rhythmogenity.

5. DISCUSSION

The execution of coordinated movements relies on a precise rhythm and pattern of muscle activation, which is determined by spinal motor circuits and modulated by supraspinal and sensory feedback systems. The underlying neuronal networks have a modular organization, where defined, interweaved sets of interneurons are in charge of specific aspects of motor output (Arber, 2012; Kiehn, 2016). Previous studies have been able to identify some of the key players engaged in the circuits controlling motion, but the exact molecular mechanisms operating during their assembly are far from being completely understood. One of the main determinants of circuit formation, namely motor neuron positioning, depends, amongst others, on the function of the scaffold protein afadin (Dewitz et al., 2018). However, former afadin mouse models were perinatally lethal and precluded analysis of motor behavior. Using a model, where the protein has been conditionally eliminated from motor neuron progenitors, the present work reveals that afadin is required for correct assembly and function of spinal locomotor circuits. Conditional afadin mutants exhibit an increase of synchronous segmental limb movements during locomotion. Surprisingly, the data presented here show that this phenotype is not due to a mispositioning of motor neurons, but rather a perturbed anatomical organization of the spinal cord. A lack of afadin at the motor neuron progenitor zone leads to the development of a double central canal, which in turn alters the expression pattern of axon guidance cues, such as Ephrin B3, thus enabling aberrant projections that contribute to the changes in motor neuron activation resulting in simultaneous left and right movements.

5.1 CELL-CELL ADHESION AND THE ORGANIZATION OF MOTOR NEURONS

The control of timing of neurogenesis and migration is one of the strategies used during development of the CNS to position neuronal subtypes at specific coordinates. Similar to the developing cortex, motor neurons at limb levels in the spinal cord first undergo an inside-out layering process to give rise to the medial and

lateral LMC divisions. LMCm neurons are born earlier and migrate radially away from the progenitor zone until they settle at their stereotypic location followed by later-born LMCl neurons that have to move through the LMCm population in order to reach their lateral position in the ventral horn (Hollyday & Hamburger, 1977; Sockanathan & Jessell, 1998). An additional independent step further segregates motor neurons along the DV axis and clusters them into muscle-specific motor pools (Dewitz et al., 2018; Dewitz et al., 2019). It was previously shown that afadin has a selective role in the ML settling of motor neurons. Elimination of afadin perturbs divisional organization by hindering LMCl migration while LMCm neurons remain unaffected. As a consequence, positional coordinates of different motor neuron subtypes increasingly overlap (Dewitz et al., 2018). Surprisingly, the herein presented study of LMC divisions arrangement in fully conditional *afadin* $^{fl/fl}$ mutants reveals that the positional defect uncovered at embryonic stages is indeed only a developmental delay that recovers with time.

The importance of cell adhesive functions of the classical cadherin/catenin and nectin/afadin families for neuronal migration has become increasingly apparent in recent years. In the developing brain, the maintenance of adherens junctions plays a critical role for cortical lamination. Accordingly, genetic deletion of N-cadherin or afadin severely compromises the structural integrity of the ventricular zone and the positioning of projection neurons, resulting in a so-called double cortex (Gil-Sanz et al., 2014; Yamamoto et al., 2015). Cadherins have been also shown to regulate different modes of cortical neuron motility through interactions with nectins and Reelin (Kawauchi et al., 2010; Franco et al., 2011; Jossin & Copper, 2011; Gil-Sanz et al., 2013). Notably, knock-down of cadherins, nectins or afadin function does not completely abolish the neurons' initial ability to migrate, but rather delays the onset or reduces the speed of movement as cells still manage to exit the ventricular zone (Gil-Sanz et al., 2013). The interplay between cadherin/catenin and afadin signaling has also been implicated in the migration of spinal motor neurons, suggesting a conserved mechanism across different CNS structures (Dewitz et al., 2018). The present findings confirm a role for afadin in organizing the spinal topographic map. However, contrary to previous expectations, rather than arresting LMCl migration, its elimination merely slows it down, consistent with observations in cortical development. Nevertheless, evidence points towards differential regulation of

neuronal migration in the cortex and the spinal cord, because, in contrast to motor neurons, differentiated projection neurons are unable to organize into layers even as development proceeds (Gil-Sanz et al., 2014). The exact molecular mechanisms behind afadin function and its relationship to cadherin/catenin signaling requires further investigation. Interestingly, loss of afadin has no effect on the expression of N-cadherin or β-catenin in the spinal cord. Moreover, nectins are not strongly expressed in the spinal cord during development (Dewitz et al., 2018), thus rather hinting at an afadin-mediated, nectin-independent process regulating motor neuron settlement (Miyata, et al., 2009). Since afadin lacks close structural homologs, one possibility could be that other cytoplasmic or surface proteins can promote cadherin function and keep the migrational machinery going even in the absence of afadin. Such roles have been proposed for example in neural tube development and synapse formation for S-SCAM and protocadherin-19 (Biswas et al., 2010; Stan, et al., 2010).

It must be noted, however, that the conclusions here were drawn from the analysis of only two representative adult motor pools. Considering the fact that LMCm and LMCl neurons are not completely intermixed at e13.5, it would be worthwhile to confirm whether the developmental delay hypothesis holds true by evaluating the positions of motor neurons controlling further muscles.

5.2 AFADIN AS A REGULATOR OF LUMEN FORMATION

The generation of tubular networks is a fundamental morphogenetic process, essential for the functional organization of many organs. Such tubules consist of a layer of polarized epithelial cells that surround an internal hollow space or lumen that serves a variety of functions, ranging from the transport of fluids or gases to digestion. Although lumens arise from diverse mechanisms depending on the organ and its environment, they all share some common principles that involve cytoskeleton remodelling and the spatiotemporally coordinated polarization of adjacent cells (Datta et al., 2011). It has already been shown that afadin is essential for pancreatic and renal lumen morphogenesis. In its absence apical-basal polarity is perturbed, thus disrupting the continuity of progressing tubule formation (Yang et al., 2013; Azizoglu

et al., 2017; Gao et al., 2017). The present findings concerning the development of the central canal in the spinal cord complement and expand this view. Afadin is expressed along the midline neuroepithelium, which undergoes apical constriction starting at e14.5 in order to give rise to the tubular organization of the central canal. By eliminating afadin from the pMN, adjoining neuroepithelial areas lose the ability to coalesce and instead form two independent luminal structures. The fact that afadin deletion from dorsal spinal progenitors influences tubulogenesis in a similar manner and results in a ventral displacement of the central canal demonstrates that afadin's role in lumen formation is not confined to a specific area of the spinal neuroepithelium. Conversely, removing afadin from motor neurons after they have exited the progenitor zone leaves the neuroepithelium intact and central canal development unaffected.

How does afadin influence the development of cellular tubes? The underlying morphogenetic process requires dynamic regulation of cell adhesion and cell shape changes, which are coordinated by AJs and tight junctions that link cells to their neighbors and to the apical actin cytoskeleton (Gates & Peifer, 2005). Cadherin/catenin as well as nectin/afadin complexes colocalize at AJs (Takat et al., 2008; Rikitake et al., 2012), raising the hypothesis that lack of one of those components might disrupt the establishment of stable cell connections. However, work in *Drosophila* has shown that the afadin homologue Canoe (Cno) is not necessary for AJs assembly or maintenance during mesoderm invagination. Instead, Cno seems to be the link between AJs and the apical actomyosin and in its absence cell and cytoskeletal constriction events are uncoupled (Sawyer et al., 2009). A cadherin/catenin-independent function is consistent with the observation that in *afadin* $^{fl/fl}$ mice N-cadherin and β-catenin expression patterns are unperturbed (Dewitz et al., 2018). Localization of nectin-1, -2 and -3 at the pMN is lost after removal of afadin with *Olig2::cre*, but single nectin mutants do not present anatomical or locomotor phenotypes similar to the ones described here (Takai et al., 2008; Mandai et al., 2015), suggesting functional redudancy between different nectin family members upstream of afadin. On the other hand, previous work examining the effect of RhoA elimination from the spinal cord neuroepithelium found analogous disruption of midline integrity (Katayama et al., 2012; Mulherkar, et al., 2013). Interestingly, in the developing pancreas and kidney, cytoskeletal remodelling was also shown to rely

on concomitant activities of afadin and RhoA (Yang et al., 2013; Azizoglu et al., 2017), indicating that the intracellular signaling pathway that controls tubulogenesis is conserved across different tissues. Further studies are needed to elucidate the precise mechanistic underpinnings of these processes. First findings deriving from different *in vivo* and *in vitro* systems point towards the regulation of mitotic spindle orientation, a feature that correlates with the positioning of the apical surface and the formation of continuous lumen (Wee et al., 2011; Carminati et al., 2016; Gao et al., 2017; Rakotomamonjy et al., 2017).

5.3 ROLES OF AFADIN IN MOTOR NEURON SYNAPTIC SPECIFICITY

The establishment and maintenance of synapses is pivotal for CNS development and function. In particular, the choice of correct synaptic partners poses a challenging endeavor given the multitude of potential candidates. In the spinal cord, proprioceptive sensory afferents are charged with the task of identifying motor neurons innervating synergistic muscles and avoiding motor neurons with antagonistic roles (Eccles, 1951). Failing to do so, leads to profound impairments in limb coordination as exemplified by conditional FoxP1 mutants (Sürmeli et al., 2011). Given the large number of limb muscles and resulting monosynaptic sensory-motor connections, there is likely a wide range of molecules regulating synaptogenesis in the spinal cord. As intercellular signaling junctions, synapses contain CAMs that orchestrate their formation and restructuring and support the recognition of appropriate interacting pairs (Südhof, 2018). The data presented in this work suggest that afadin is not involved in the organization of synaptic input onto motor neurons. Selective elimination of afadin from postmitotic motor neurons does not affect the assembly of locomotor circuitry and the animals exhibit normal walking gait. However, a detailed analysis of synaptic components will be necessary to affirm this assumption, which at present is only based on behavioral observations.

Intriguingly, nectins and their scaffold protein afadin have been shown to be involved in cadherin-based cell-cell adhesion at puncta adherentia junctions (PAJs). While nectin-1 and nectin-3 asymmetrically localize at the pre- and post-synaptic side, respectively, afadin is found on both sides of PAJs in hippocampal neurons

(Mizoguchi et al., 2002). In addition, afadin deletion significantly decreases the density of synapses in the hippocampus (Beaudoin et al., 2012). Together, this would suggest that different signaling pathways control synaptogenesis in the brain and the spinal cord. On the other hand, a recent paper demonstrated that loss of Cdc42, a small Rho GTPase implicated in the regulation of cytoskeletal remodelling like afadin, causes defects in monosynaptic sensory-motor connections. Notably, the role of Cdc42 was specific to the presynaptic partner, in this case the sensory neurons, as knocking it out in motor neurons did not interfere with synapse formation (Imai et al., 2016). Thus, it would be interesting to examine whether afadin has a similar presynaptic function in the establishment of sensory-motor circuits.

5.4 DOUBLE CENTRAL CANAL AND THE WIRING OF SPINAL MOTOR CIRCUITS

Understanding the cellular and molecular mechanisms that control the wiring of spinal circuits during development is essential in order to decipher the logic behind their functional organization. In particular, the machinery regulating spinal cord laterality, i.e. the decision of neurons to extend their axons either ipsilaterally or contralaterally, plays an important role as it establishes a fine balance between excitation and inhibition across the two halves that ensures coordinated left/right movements. The loss of limb alternation in favor of synchronous activation is one possible consequence of perturbed axon guidance in the spinal cord and has been reported in several mouse models with diverse genetic backgrounds (Dottori et al., 1998; Kullander et al., 2001; Rabe et al., 2009; Katayama et al., 2012; Mulherkar et al., 2013; Satoh et al., 2016), indicating that the precise interplay between different developmental programs is crucial for the formation of motor circuits. In the present study, a correlation between the morphology and location of the central canal and the locomotor output is evidenced. The presence of a double central canal in *afadin* $^{fl/fl}$ mice perturbs the localization patterns of axon guidance molecules, such as Netrin-1 and Ephrin B3. However, only the latter was found to be relevant for the generation of aberrant connectivity. In contrast, interneurons residing in the intermediate spinal cord settled at their stereotypic locations, suggesting that the impairment in lumen morphogenesis leads to changes in circuit architecture due to compromised midline

signaling and not due to mislocalized premotor partners. Furthermore, the disruption in Ephrin B3 expression is not seen in *afadin* $^{fl/fl}$*; ChAT* mice, which do not display any locomotor defect, thus highlighting the causative relationship between Ephrin B3 signal and the gait pattern (Skarlatou et al., 2020).

Ephrin B3 is known to be important for the establishment of ipsilateral CST and interneuron projections by repelling axons that express the receptor EphA4 (Kullander et al., 2001; Kullander et al., 2003; Borgius et al., 2014). The identity of the cells providing the Ephrin B3 signal is unclear, but its developmental expression timeline has been studied. Ephrin B3 mRNA is found at the roof and floor plates as early as e11 and gradually expands towards the center until the midline is formed (Imondi et al., 2000; Kullander et al., 2001). This process runs in parallel to the closure of the ventricular zone and the generation of the central canal. In contrast, protein expression is not seen until e14.5, when first signs of the disorganization of the tissue in *afadin* $^{fl/fl}$ mutants become apparent, accompanied by a prevention of Ephrin B3 expression in the dysplastic region between the two developing central canals. RhoA conditional KO mice, using the *Olig2::Cre* driver line to eliminate the protein, exhibit similar anatomical and locomotor phenotypes (Katayama et al., 2012). Thus, the proper organization of the neuroepithelium maintained by afadin and RhoA activities seems to be important for correct development of the midline. The nature of the underlying mechanisms needs to be further addressed. On the other hand, the development of ipsilateral circuits cannot be solely dependent on Ephrin B3/EphA4 signaling since many interneuron populations with axonal projections confined to the side of their cell body location are not EphA4^{+} (Lundfald et al., 2007). Other families of repellent guidance molecules that could potentially be maintaining ipsilateral projections, such as Slit/Robo, as it has been shown for CST axons (Bagri et al., 2002; López-Bendito et al., 2007), were not analyzed. However, they could complement our understanding of ipsilateral circuits.

In contrast to axon trajectories that are directed by expression patterns of midline cues, the positioning of interneurons in the spinal cord is unaffected by disrupted localization of guidance molecules. Nevertheless, it would be interesting to investigate in the future whether the same CAMs-dependent migratory mechanisms that control motor neuron organization underlie the settlement of different interneurons populations as well.

5.5 EPHRIN B3 DEPENDENCY OF INTERNEURONS WIRING PROFILES

Ephrin B3 and EphA4 KO mice exhibit loss of limb alternation that can be explained by increased crossing of CST and interneurons processes due to the missing repulsive interaction at the spinal cord midline (Dottori et al., 1998; Kullander et al., 2001; Kullander et al., 2003; Paixão et al., 2013; Borgius et al., 2014). However, previous work studying these mutants has mostly focused on axon overshooting instead of premotor connectivity patterns that could alter motor neuron activation. As a consequence, the precise identity of neurons with projection defects is still largely unknown. Dorsal interneurons originating from the Lbx1 progenitor domain have so far been the only subtypes for which aberrant connections upon disruption of Ephrin B3/EphA4 signaling have been demonstrated *in vivo* (Satoh et al., 2016). Nevertheless, selective elimination of EphA4 from Lbx1 progenitors only partially recapitulates the constitutive synchronizing motor phenotype of EphA4 null mice, suggesting that other interneurons subtypes must be involved. The present findings confirm and extend these studies. In addition to $Lbx1^{+}$ dI4-dI5 interneurons that ectopically contact contralateral motor neurons in *afadin* $^{fl/fl}$ mutants as predicted by the literature, a dorsal population with V0 character, cholinergic V0cs and ipsilaterally projecting V2as show altered connectivity, indicating that these interneurons are necessary for a complete switch to synchrony during locomotion.

Dorsal CPG components are likely relay interneurons that integrate incoming sensory information and adjust motor neuron activity accordingly. The current data prove the existence of dorsally located premotor neurons with roles in left/right alternation, a fraction of which are $Lhx1^{+}$/$FoxD3^{-}$. These cells reside lateral to the Lbx1-derived ectopic cluster, raising the question about their origin. Their molecular profile matches that of V0 interneurons during development (Lu et al., 2015) and a small portion of V0s have been shown to express EphA4 (Lundfald et al., 2007), making them good candidates for extending ectopic projections across an Ephrin B3-deficient midline. However, lineage tracing analysis of V0 progenitors shows a distribution confined to the ventromedial area of the spinal cord (Moran-Rivard et al., 2001). Thus, it remains to be clarified whether this novel source of ectopic input onto motor neurons indeed belongs to the V0 family or rather represents a yet

uncharacterized subtype. Nevertheless, V0cs, another subset of V0 interneurons that is cholinergic, display an increase in contralateral connectivity in *afadin* $^{fl/fl}$ mice, indicating that their miswiring can contribute to the deregulation of the circuits controlling gait choice. V0c neurons were previously shown to modulate motor output by regulating the excitability of motor neurons (Zagoraiou et al., 2009), but had not been implicated in the control of left/right alternation.

Although the V2a population, being excitatory, strictly ipsilateral and mostly EphA4^{+}, possesses the ideal characteristics for aberrantly crossing processes in absence of Ephrin B3 signaling, contralateral V2a neurons have not been reported in EphA4 null mice (Lundfald et al., 2007). The herein presented analysis of Chx10 expression within the premotor network of *afadin* $^{fl/fl}$ mutants, on the other hand, demonstrates the presence of ectopic V2a interneurons in the contralateral side of the spinal cord. Due to their proximity to the midline, it could be argued that the loss of structural integrity between the two central canals affects the settling behavior of V0c and V2a neurons, thus positioning the cell bodies in the opposing side while retaining unilateral connectivity. Two lines of evidence make this interpretation unlikely. First, the overall location of V0c and V2a interneurons does not show any remarkable differences between control and *afadin* $^{fl/fl}$ animals. Second, if the ratio of ipsilateral to contralateral premotor V0c and V2a neurons was merely shifted in the mutants, the total number of premotor cells should not change, which is not the case here. Thus, the data suggest that the motor circuits are reconfigured in a way that could interfere with the side-specific control of behavioral responses. Simultaneous analysis of bilateral premotor connectivity could provide definitive proof of wiring defects for the populations in question as it has been done for EphA4-deficient Lbx1 interneurons (Satoh et al., 2016).

Despite the fact that the marker screening performed in this study uncovered the relevance of three interneuron groups for the regulation of left/right alternating movements, it is limited by the fact that most transcription factors are downregulated in the course of development and, thus, lacks the resolution to identify all aberrantly connected neurons. The ectopic neurons presented here do not fully complement the control contralateral premotor interneuron map, indicating a high diversity of neuronal subtypes with wiring defects. Their characterization will therefore require high-throughput unbiased screening methods, such as single-cell transcriptome profiling.

5.6 INFLUENCE OF ECTOPIC CONNECTIONS ON SENSORY-MOTOR INTEGRATION

Proper coordination of muscle contractions on the left and right sides provides the dynamic stability required for speed modulation or adjustment to environmental constraints during locomotion. While the intrinsic activities of motor neurons are controlled for each limb individually by its own CPG, the regulation of neuronal connections between limbs is conducted mainly by sensory feedback systems (Frigon et al., 2017). Unilateral processing of proprioceptive information is evolutionarily conserved and one of the hallmarks of motor circuit structure that ensures appropriate responses (Eccles et al., 1957). Thus, the increased connectivity arising from the dorsal contralateral quadrant of the spinal cord in *afadin* $^{fl/fl}$ animals could also impact sensory input integration into locomotor CPGs. In mice with EphA4^{-} dorsal Lbx1 neurons, these cells receive direct one-sided proprioceptive input while contacting motor neurons on both sides, which hampers ongoing alternating locomotor patterns (Satoh et al., 2016). Whether similar bilateral routing of muscle sensory information takes place in *afadin* $^{fl/fl}$ mutants needs to be further investigated. In addition, experimental setups that challenge the ability to adjust motor output on the two sides of the body separately, for example using split-belt treadmills, could provide insights into the degree of plasticity retained by the modified circuits.

Moreover, distinct modes of body propulsion employ different proprioceptive feedback depending on the weight load applied to the limbs in each case: terrestrial locomotion relies on signals from both GTOs and muscle spindles; on the other hand, during swimming, GTO input is attenuated and muscle spindles are mainly in charge of regulating motor output (Gruner & Altman, 1980; Akay et al., 2014). The present study only focuses on one behavioral readout, namely on-ground locomotion in freely walking mice. It would be interesting to test the behavior of *afadin* $^{fl/fl}$ mice in other contexts as well in order to dissect specific functions for particular proprioceptive signaling systems in the generation of alternative gait patterns. Although the spinal targets of different sensory afferents are not known, the selective emergence of synchronous movements of paired appendages during swimming in conditional Lbx1-EphA4 KO mice implies that sensory input to non-Lbx1 premotor neurons plays a more dominant role during on-ground locomotion (Satoh et al., 2016). Further

functional analysis of the identified Lhx1^{+}/FoxD3^{-} cluster could reveal novel aspects of sensory-motor integration.

5.7 ORGANIZATION OF INTERSEGMENTAL CONTROL OF LOCOMOTION

Bound gait is characterized by a pattern, where the front and rear limbs are consistently moved in synchrony (Bellardita and Kiehn, 2015). The trigger for this kind of movements in wild-type animals is an increase in locomotor frequency that induces the neuronal pathways favoring simultaneous activation of paired limbs in order to reduce the accompanying biomechanical constraints (Lemieux et al., 2016). The configuration of the CPGs controlling the activity of forelimbs and hindlimbs should therefore reflect their ability to transition to coupled left and right activation when needed. Accordingly, genetic animal models that exhibit a constitutive loss of left/right alternation in forelimbs and hindlimbs are expected to display network modifications at both cervical and lumbar spinal levels. Surprisingly, the premotor connectivity of two hindlimb muscles in *afadin* $^{fl/fl}$ mice is indistinguishable from that in control animals, suggesting that a cervico-lumbar drive is able to impose the cervical rhythmic pattern on the lumbar circuits.

Quadrupedal locomotion is defined by the activity of interlimb pathways represented by short-range commissural interneurons that regulate left/right interactions and reciprocal LPNs that connect cervical to lumbar levels and viceversa (Danner et al., 2017). Previous work in isolated spinal cords has proposed a model where rostrocaudal coordination is mediated by a strong ascending influence that integrates thoracic circuitry and ultimately matches cervical rhythmogenesis to that of the lumbar region (Juvin et al., 2005; Gordon et al., 2008; Juvin et al., 2012). This view is difficult to reconcile with the anatomical evidence from afadin conditional mutants. Interestingly, long descending projection neurons were recently found to be involved in postural stability and interlimb coordination at high speeds. Upon ablation of cervico-lumbar neurons, the animals showed selective disruption of left/right alternation in the hindlimbs (Ruder et al., 2016). Thus, ectopic inhibition of these cells at cervical levels could be a possible mechanism resulting in abnormal synchronization of the hindlimbs, independently of the local lumbar circuits. However,

the highly diverse molecular nature of long-projecting neurons makes it hard to test this idea with the currently available genetic tools and also suggests that different subsets might fulfill different roles. Future work should molecularly and functionally characterize this population of neurons in an unbiased manner and study their role in the intersegmental control of locomotion. In addition, a detailed electrophysiological study of motor rhythm generation in *afadin* $^{fl/fl}$ spinal cords could provide useful insights into the coordination of cervical and lumbar CGPs.

5.8 FUTURE PERSPECTIVES

Unravelling the basic developmental and wiring concepts as well as identifying cellular key players of neuronal networks that control movement and other behaviors is one of the biggest challenges in neuroscience. Though in recent years our knowledge about spinal motor circuits has rapidly advanced, growing evidence reveals an unanticipated cellular diversity and modularity (Talpalar et al., 2013; Bikoff et al., 2016; Sweeney et al., 2017; Chopek et al., 2018; Hayashi et al., 2018). On the one hand, this suggests that our current understanding is still largely incomplete, but on the other, it also highlights the importance of ongoing basic research aimed at gaining insight into the intrinsic organization and function of motor circuits, like the present work. In addition, the development of new tools, such as large-scale transcriptome profiling at single cell resolution (Sathyamurthy et al., 2018) or live imaging of big populations of cells in behaving animals (Hamel et al., 2015), will facilitate the identification of circuit components and how they are recruited in order to produce behavior.

Conditions with chronic disturbances in motor and sensory function, such as spinal cord injury, neuropathic pain and neurodegenerative diseases to mention a few, will greatly profit from a better understanding of the network structures underlying movement and sensory perception. Treatment approaches for all of the above mentioned are currently limited to minimizing secondary complications and maximizing residual function by reactivating spared systems (Ramer et al., 2014), but their effectiveness is variable and generally low. Insights from studies investigating the development of spinal circuits have proved valuable in paving the way for stem

cell therapies. Nowadays it is possible to efficiently generate different functional spinal cell types from either embryonic stem cells or reprogrammed somatic cells (Wichterle et al., 2002; Gupta et al., 2018; Hoang et al., 2018). After transplantation, these stem cell-derived populations have the potential to replenish lost cell types, foster axon regeneration, remyelinate surviving axons and reorganize the circuitry, thereby contributing to recovery (Zhou et al., 2019). Although cell therapies are in a very early stage and there are still technical limitations to their clinical use, the advances made so far are promising and will keep on benefiting from a more detailed understanding of how spinal circuits work. Another approach stems from *ex vivo* experiments with spinal cord preparations and uses targeted pharmacological stimulation of CPG networks (Fong et al., 2005; Ichiyama et al., 2008; Cowley et al., 2015; Duru et al., 2015). In particular, enhancing the activity of propriospinal interneurons, that have the ability to circumvent lesion sites and provide an alternative flow of motor commands, could be useful (Cowley et al., 2015). However, a lack of information about the characteristics of relevant populations makes the design of effective treatment strategies at the present time difficult.

The applications described here are just a few examples, but they emphasize the importance of understanding the developmental mechanisms that generate a functional organism. Thus, it is essential that the study of the spinal cord progresses through the integration of novel findings and the use of modern tools. Every contribution to the field will not only expand our comprehension of sensory processing and motor behavior, but will also lay the groundwork for future therapeutic strategies aimed at regenerating spinal neuronal pathways.

REFERENCES

Akai, J., Halley, P. A. & Storey, K. G. (2005). FGF-Dependent Notch Signaling Maintains the Spinal Cord Stem Zone. *Genes and Development*, 2877 - 2887.

Akay, T., Tourtellotte, W. G., Arber, S. & Jessell, T. M. (2014). Degradation of Mouse Locomotor Pattern in the Absence of Proprioceptive Sensory Feedback. *Proceedings of the National Academy of Science of the United States of America*, 16877 - 16882.

Andersson, L. S., Larhammar, M., Memic, F., Wootz, H., Schwochow, D., Rubin, C.-J., Patra, K., Arnason, T., Wellbring, L., Hjälm, G., Imsland, F., Petersen, J. L., McCue M. E., Mickelson, J. R., Cothran, G., Ahituv, N., Roepstorff, L., Mikko, S., Vallstedt, A., Lindgren, G., Andersson, L. & Kullander, K. (2012). Mutations in DMRT3 Affect Locomotion in Horses and Spinal Circuit Function in Mice. *Nature*, 642 - 646.

Appel, B., Givan, L. A. & Eisen, J. S. (2001). Delta-Notch Signaling and Lateral Inhibition in Zebrafish Spinal Cord Development. *BMC Developmental Biology*, 1 - 13.

Arber, S. (2012). Motor Circuits in Action: Specification, Connectivity, and Function. *Neuron*, 975 - 989.

Arshavsky, Y. I., Berkinblit, M. B., Fukson, O. I., Gelfand, I. M. & Orlovsky, G. N. (1972a). Origin of Modulation in Neurones of the Ventral Spinocerebellar Tract During Evoked Locomotion. *Brain Research*, 276 - 279.

Arshavsky, Y. I., Berkinblit, M. B., Fukson, O. I., Gelfand, I. M. & Orlovsky, G. N. (1972b). Recordings of Neurones of the Dorsal Spinocerebellar Tract During Evoked Locomotion. *Brain Research*, 276 - 279.

Ausborn, J., Mahmood, R. & El Manira, A. (2012). Decoding the Rules of Recruitment of Excitatory Interneurons in the Adult Zebrafish Locomotor Network. *Proceedings of the National Academy of Science of the United States of America*, 3631 - 3639.

Azizoglu, D. B., Braitsch, C., Marciano, D. K. & Cleaver, O. (2017). Afadin and RhoA Control Pancreatic Endocrine Mass via Lumen Morphogenesis. *Genes and Development*, 2376 - 2390.

Bagri, A., Marín, O., Plump, A. S., Mak, J., Pleasure, S. J., Rubenstein, J. L. & Tessier-Levigne, M. (2002). Slit Proteins Prevent Midline Crossing and Determine the Dorsoventral Position of Major Axonal Pathways in the Mammalian Forebrain. *Neuron*, 233 - 248.

Balaskas, N., Ribeiro, A., Panovska, J., Dessaud, E., Sasai, N., Page, K. M., Briscoe, J. & Ribes, V. (2012). Gene Regulatory Logic for Reading the Sonic Hedgehog Signaling Gradient in the Vertebrate Neural Tube. *Cell*, 273 - 284.

Balaskas, N., Abbott, L. F., Jessell, T. M. & Ng, D. (2019). Positional Strategies for Connection Specificity and Synaptic Organization in Spinal Sensory-Motor Circuits. *Neuron*, 1 - 14.

Beaudoin III, G. M., Schofield, C. M., Nuwal, T., Zang, K., Ullian, E. M., Huang, B. & Reichardt, L. F. (2012). Afadin, a Ras/Rap Effector That Controls Cadherin Function, Promotes Spine and Excitatory Synapse Density in the Hippocampus. *Development*, 99 - 110.

Beg, A. A., Sommer, J. E., Martin, J. H. & Scheiffele, P. (2007). α2-Chimaerin Is an Essential EphA4 Effector in the Assembly of Neuronal Locomotor Circuits. *Neuron*, 768 - 778.

Bellardita, C. & Kiehn, O. (2015). Phenotypic Characterization of Speed-Associated Gait Changes in Mice Reveals Modular Organization of Locomotor Networks. *Current Biology*, 1426 - 1436.

Beloozerova, I. N. & Sirota, M. G. (2003). Integration of Motor and Visual Information in Parietal Area 5 During Locomotion. *The Journal of Neurophysiology*, 961 - 971.

Beloozerova, I. N. & Sirota, M. G. (1993). The Role of the Motor Cortex in the Control of Accuracy of Locomotor Movements in the Cat. *The Journal of Physiology*, 1 - 25.

Beloozerova, I. N., Sirota, M. G., Orlovsky, G. N. & Deliagina, T. G. (2005). Activity of Pyramidal Tract Neurons in the Cat During Postural Corrections. *The Journal of Neurophysiology*, 1831 - 1844.

Bel-Vialar, S., Itasaki, N. & Krumlauf, R. (2002). Initiating Hox Gene Expression: In the Early Chick Neural Tube Differential Sensitivity to FGF and RA Signaling Subdivides the HoxB Genes in Two Distinct Groups. *Development*, 103 - 115.

Benito-Gonzalez, A. & Alvarez, F. J. (2012). Renshaw Cells and Ia Inhibitory Interneurons are Generated at Different Times from p1 Progenitors and Differentiate Shortly After Exiting the Cell Cycle. *The Journal of Neuroscience,* 1156 - 1170.

Bernhardt, N., Memic, F., Gezelius, H., Thiebes, A.-L., Vallstedt, A. & Kullander, K. (2012). DCC Mediated Axon Guidance of Spinal Interneurons Is Essential for Normal Locomotor Central Pattern Generator Function. *Developmental Biology*, 279 - 289.

Bertuzzi, M. & Ampatzis, K. (2018). Spinal Cholinergic Interneurons Differentially Control Motoneuron Excitability and Alter the Locomotor Network Operational Range. *Scientific Reports*, 1 - 10.

Bikoff, J. B., Gabitto, M. I., Rivard, A. F., Drobac, E., Machado, T. A., Miri, A., Brenner-Morton, S., Famojure, E., Diaz, C., Alvarez, F. J., Mentis, G. Z. & Jessell, T. M. (2016). Spinal Inhibitory Interneuron Diversity Delineates Variant Motor Microcircuits. *Cell*, 207 - 219.

Biswas, S., Edmond, M. R. & Jontes, J. D. (2010). Protocadherin-19 and N-Cadherin Interact to Control Cell Movements During Anterior Neurulation. *The Journal of Cell Biology*, 1029 - 1041.

Bjursten, L.-M., Norrsell, K. & Norrsell, U. (1976). Behavioural Repertory of Cats without Cerebral Cortex from Infancy. *Experimental Brain Research*, 115 - 130.

Borgius, L., Nishimaru, H., Caldeira, V., Kunugise, Y., Löw, P., Reig, R., Itohara, S., Iwasato, T. & Kiehn, O. (2014). Spinal Glutamatergic Neurons Defined by EphA4 Signaling Are Essential Components of Normal Locomotor Circuits. *The Journal of Neuroscience*, 3841 - 3853.

Borowska, J., Jones, C. T., Zhang, H., Blacklaws, J., Goulding, M. & Zhang, Y. (2013). Functional Subpopulations of V3 Interneurons in the Mature Mouse Spinal Cord. *The Journal of Neuroscience*, 18553 - 18565.

Bouvier, J., Caggiano, V., Leiras, R., Caldeira, V., Bellardita, C., Balueva, K., Fuchs, A. & Kiehn, O. (2015). Descending Command Neurons in the Brainstem that Halt Locomotion. *Cell*, 1191 - 1203.

Briscoe, J., Pierani, A., Jessell, T. M. & Ericson, J. (2000). A Homeodomain Protein Code Specifies Progenitor Cell Identity and Neuronal Fate in the Ventral Neural Tube. *Cell*, 435 - 445.

Britz, O., Zhang, J., Grossmann, K. S., Dyck, J., Kim, J. C., Dymecki, S., Gosgnach, S. & Goulding, M. (2015). A Genetically Defined Asymmetry Underlies the Inhibitory Control of Flexor-Extensor Locomotor Movements. *eLIFE* , 1 - 22.

Caldeira, V., Dougherty, K. J., Borgius, L. & Kiehn, O. (2017). Spinal Hb9::Cre-Derived Excitatory Interneurons Contribute to Rhythm Generation in the Mouse. *Scientific Reports*, 1 - 12.

Capelli, P., Pivetta, C., Esposito, M. S. & Arber, S. (2017). Locomotor Speed Control Circuits in the Caudal Brainstem. *Nature*, 373 - 377.

Carminati, M., Gallini, S., Pirovano, L., Alfieri, A., Bisi, S. & Mapelli, M. (2016). Concomitant Binding of Afadin to LGN and F-actin Directs Planar Spindle Orientation. *Nature Structural & Molecular Biology*, 155 - 163.

Carpenter, M. B. (1984). Interconnections Between the Corpus Striatum and Brain Stem Nuclei. In *The Basal Ganglia.* Plenum Press.

Catela, C., Shin, M. M. & Dasen, J. S. (2015). Assembly and Function of Spinal Circuits for Motor Control. *Annual Review of Cell and Developmental Biology*, 669 - 698.

Charron, F., Stein , E., Jeong, J., McMahon, A. P. & Tessier-Lavigne, M. (2003). The Morphogen Sonic Hedgehog is an Axonal Chemoattractant that Collaborates with Netrin-1 in Midline Axon Guidance. *Cell*, 11 - 23.

Chopek, J. W., Nascimento, F., Beato, M., Brownstone, R. M. & Zhang, Y. (2018). Sub-Populations of Spinal V3 Interneurons Form Focal Modules of Layered Pre-Motor Microcircuits. *Cell Reports*, 146 - 156.

Cowley, K. C., MacNeil, B. J., Chopek, J. W., Sutherland, S. & Schmidt, B. J. (2015). Neurochemical Excitation of Thoracic Propriospinal Neurons Improves Hindlimb Stepping in Adult Rats with Spinal Cord Lesions. *Experimental Neurology*, 174 - 187.

Cregg, J. M., Leiras, R., Montalant, A., Wickersham, I. R. & Kiehn, O. (2019). Brainstem Neurons that Command Left/Right Locomotor Asymmetries. *bioRxiv*.

Crone, S., Quinlan, K., Zagoraiou, L., Droho, S., Restrepo, C., Lundfald, L., Endo, T., Setlak, J., Jessell, T. M., Kiehn, O. & Sharma, K. (2008). Genetic Ablation of V2a Ipsilateral Interneurons Disrupts Left-Right Locomotor Coordination in Mammalian Spinal Cord. *Neuron*, 70 - 83.

Crone, S., Zhong, G., Harris-Warrick, R. & Sharma, K. (2009). In Mice Lacking V2a Interneurons, Gait Depends on Speed of Locomotion. *The Journal of Neuroscience*, 7098 - 7109.

Danner, S. M., Shevtsova, N. A., Frigon, A. & Rybak, I. A. (2017). Computational Modeling of Spinal Circuits Controlling Limb Coordination and Gaits in Quadrupeds. *eLife*, 1 - 25.

Dasen, J. S. (2017). Master or Servant? Emerging Roles for Motor Neuron Subtypes in the Construction and Evolution of Locomotor Circuits. *Current Opintion in Neurobiology*, 25 - 32.

Dasen, J. S., Liu, J.-P. & Jessell, T. M. (2003). Motor Neuron Columnar Fate Imposed by Sequential Phases of Hox-c Activity. *Nature*, 926 - 933.

Datta, A., Bryant, D. M. & Mostov, K. E. (2011). Molecular Regulation of Lumen Morphogenesis. *Current Biology*, 126 - 136.

De Marco Garcia, N. V. & Jessell, T. M. (2008). Early Motor Neuron Pool Identity and Muscle Nerve Trajectory Defined by Postmitotic Restrictions in Nkx6.1 Activity. *Neuron*, 217 - 231.

Degtyarenko, A. M., Simon, E. S., Norden-Krichmar, T. & Burke, R. E. (1998). Modulation of Oligosynaptic Cutaneous and Muscle Afferent Reflex Pathways During Fictive Locomotion and Scratching in the Cat. *The Journal of Neurophysiology*, 447 - 463.

DeLong, M. R. (1972). Activity of Basal Ganglia Neurons During Movement. *Brain Research*, 127 - 135.

Demireva, E., Shapiro, L., Jessell, T. & Zampieri, N. (2011). Motor Neuron Position and Topographic Order Imposed by β- and γ-Catenin Activities. *Cell*, 641 - 652.

Deniau, J. M. & Chevalier, G. (1985). Disinhibition as a Basic Process in the Expression of Striatal Functions. II. The Striato-Nigral Influence on Thalamocortical Cells of the Ventromedial Thalamic Nucleus. *Brain Research*, 227 - 233.

Deska-Gauthier, D., & Zhang, Y. (2019). The Functional Diversity of Spinal Interneurons and Locomotor Control. *Current Opinion in Physiology*, 99 - 108.

Dessaud, E., Yang, L. L., Hill, K., Cox, B., Ulloa, F., Ribeiro, A., Mynett, A., Novitch, B. G. & Briscoe, J. (2007). Interpretation of the Sonic Hedgehog Morphogen Gradient by a Temporal Adaptation Mechanism. *Nature, 450*, 717-720.

Dewitz, C., Duan, X. & Zampieri, N. (2019). Organization of Motor Pools Depends on the Combined Function of N-Cadherin and Type II Cadherins. *Development*, 1 - 7.

Dewitz, C., Pimpinella, S., Hackel, P., Akalin, A., Jessell, T. M. & Zampieri, N. (2018). Nuclear Organization in the Spinal Cord Depends on Motor Neuron Lamination Orchestrated by Catenin and Afadin Function. *Cell Reports*, 1681 - 1694.

Dottori, M., Hartley, L., Galea, M., Paxinos, G., Polizzotto, M., Kilpatrick, T., Bartlett, P. F., Murphy, M., Köntgen, F. & Boyd, A. W. (1998). EphA4 (Sek1) Receptor Tyrosine Kinase Is Required for the Development of the Corticospinal Tract. *Proceedings of the National Academy of Science of the United States of America*, 13248 - 13253.

Dougherty, K. J., Zagoraiou, L., Satoh, D., Rozani, I., Doobar, S., Arber, S., Jessell, T. M. & Kiehn, O. (2013). Locomotor Rhythm Generation Linked to the Output of Spinal Shox2 Excitatory Interneurons. *Neuron*, 920 - 933.

Drew, T. (1993). Motor Cortical Activity During Voluntary Gait Modifications in the Cat. I. Cells Related to the Forelimbs. *The Journal of Neurophysiology*, 179 - 199.

Dubuc, R., Brocard, F., Antri, M., Fénelon, K., Gariépy, J.-F., Smetana, R., Ménard, A., Le Ray, D., Viana Di Prisco, G., Pearlstein, E., Sirota, M. G., Derjean, D., St-Pierre, M., Zielinski, B., Auclair, F. & Veilleux, D. (2008). Initiation of Locomotion in Lampreys. *Brain Research Reviews*, 172 - 182.

Duru, P. O., Tillakaratne, N. J. K., Kim, J. A., Zhong, H., Stauber, S. M., Pham, T. T., Xiao, M. S., Edgerton, V. R. & Roy, R. R. (2015). Spinal Neuronal Activation During Locomotor-Like Activity Enabled by Epidural Stimulation and 5-hydrozytryptamine Agonists in Spinal Rats. *The Journal of Neuroscience*, 1229 - 1239.

Duysens, J. D. & Pearson, K. G. (1980). Inhibition of Flexor Burst Generation by Loading Ankle Extensor Muscles in Walking Cats. *Brain Research*, 321 - 332.

Eccles, J. C., Eccles, R. M. & Lundberg, A. (1957). The Convergence of Monosynaptic Excitatory Afferents on to Many Different Species of Alpha Motoneurones. *The Journal of Physiology*, 22 - 50.

Ericson, J., Briscoe, J., Rashbass, P., van Heyningen, V. & Jessell, T. M. (1997). Graded Sonic Hedgehog Signaling and the Specification of Cell Fate in the Ventral Neural Tube. In *Pattern Formation During Development* (pp. 451 - 566). Cold Spring Harbor Symposia on Quantitative Biology.

Esposito, M. S., Capelli, P. & Arber, S. (2014). Brainstem Nucleus MdV Mediates Skilled Forelimb Motor Tasks. *Nature*, 351 - 356.

Falgairolle, M., Puhl, J. G., Pujala, A., Liu, W. & O'Donovan, M. (2017). Motoneurons Regulate the Central Pattern Generator During Drug-Induced Locomotor-Like Activity in the Neonatal Mouse. *eLIFE*, 1 - 29.

Ferreira-Pinto, M. J., Ruder, L., Capelli, P. & Arber, S. (2018). Connecting Circuits for Supraspinal Control of Locomotion. *Neuron*, 361 - 374.

Flynn, J. R., Conn, V. L., Boyle, K. A., Hughes, D. I., Watanabe, M., Velasquez, T., Goulding, M. D., Callister, R. J. & Graham, B. A. (2017). Anatomical and Molecular Properties of Long Descending Propriospinal Neurons in Mice. *Frontiers in Neuroanatomy*, 1 - 13.

Fong, A. J., Cai, L. L., Otoshi, C. K., Reinkensmeyer, D. J., Burdick, J. W., Roy, R. R. & Edgerton, V. R. (2005). Spinal Cord-Transected Mice Learn to Step in Response to Quipazine Treatment and Robotic Training. *Frontiers in Neuroanatomy*, 1 - 13.

Forssberg, H., Grillner, S. & Rossignol, S. (1975). Phase Dependent Reflex Reversal During Walking in Chronic Spinal Cats. *The Journal of Neuroscience*, 11738 - 11747.

Franco, S. J., Martinez-Garay, I., Gil-Sanz, C., Harkins-Perry, S. R. & Müller, U. (2011). Reelin Regulates Cadherin Function via Dab1/Rap1 to Control Neuronal Migration and Lamination in the Neocortex. *Neuron*, 482 - 497.

Frigon, A., Desrochers, É., Thibaudier, Y., Hurteau, M.-F. & Dambreville, C. (2017). Left–Right Coordination from Simple to Extreme Conditions During Split-Belt Locomotion in the Chronic Spinal Adult Cat. *The Journal of Physiology*, 341 - 361.

Fukuhara, K., Imai, F., Ladle, D. R., Katayama, K.-i., Leslie, J. R., Arber, S., Jessell, T. M. & Yoshida, Y. (2013). Specificity of Monosynaptic Sensory-Motor Connections Imposed by Repellent Sema3E-PlexinD1 Signaling. *Cell Reports*, 748 - 758.

Gao, L., Yang, Z., Hiremath, C., Zimmerman, S. E., Long, B., Brakeman, P. R., Mostov, K. E., Bryant, D. M., Luby-Phelps, K. & Marciano, D. K. (2017). Afadin Orients Cell Division to Position the Tubule Lumen in Developing Renal Tubules. *The Company of Biologists*, 3511 - 3520.

Garcia-Rill, E., Skinner, R. D. & Gilmore, S. A. (1981). Pallidal Projections to the Mesencephalic Locomotor Region (MLR) in the Cat. *American Journal of Anatomy*, 311 - 321.

Gates, J. & Peifer, M. (2005). Can 1000 Reviews Be Wrong? Actin, a-Catenin, and Adherens Junctions. *Cell*, 769 - 772.

Gil-Sanz, C., Franco, S. J., Martinez-Garay, I., Espinosa, A., Harkins-Perry, S. & Müller, U. (2013). Cajal-Retzius Cells Instruct Neuronal Migration by Coincidence Signaling Between Secreted and Contact-Dependent Guidance Cues. *Neuron*, 461 - 477.

Gil-Sanz, C., Landeira, B., Ramos, C., Costa, M. R. & Müller, U. (2014). Proliferative Defects and Formation of a Double Cortex in Mice Lacking Mltt4 and Cdh2 in the Dorsal Telencephalon. *The Journal of Neuroscience*, 10475 - 10487.

Goltz, F. (1892). Der Hund ohne Grosshirn. *Archiv für die gesamte Physiologie des Menschen und der Tiere*, 570 - 614.

Gordon, I. T., Dunbar, M. J., Vanneste, K. J. & Whelan, P. J. (2008). Interaction Between Developing Spinal Locomotor Networks in the Neonatal Mouse. *The Journal of Neurophysiology*, 117 - 128.

Gosgnach, S., Bikoff, J. B., Dougherty, K. J., El Manira, A., Lanuza, G. M. & Zhang, Y. (2017). Delineating the Diversity of Spinal Interneurons in Locomotor Circuits. *The Journal of Neuroscience*, 10835 - 10841.

Gosgnach, S., Lanuza, G. M., Butt, S. J., Saueressig, H., Zhang, Y., Velasquez, T., Riethmacher, D., Callaway, E. M., Kiehn, O., Goulding, M. (2006). V1 Spinal Neurons Regulate the Speed of Vertebrate Locomotor Outputs. *Nature*, 215 - 219.

Goulding, M. (2009). Circuits Controlling Vertebrate Locomotion: Moving in a New Direction. *Nature Reviews Neuroscience*, 507 - 518.

Graham Brown, T. (1914). On the Nature of the Fundamental Activity of the Nervous Centres; Together with an Analysis of the Conditioning of Rhythmic Activity in Progression, and a Theory of the Evolution of Function in the Nervous System. *The Journal of Physiology*, 18 - 46.

Graham Brown, T. (1911). The Intrinsic Factors in the Act of Progression in the Mammal. *Proceedings of the Royal Society London B*, 308 - 319.

Grillner, S. (2006). Biological Pattern Generation: The Cellular and Computational Logic of Networks in Motion. *Neuron*, 751 - 766.

Grillner, S. & El Manira, A. (2020). Current Principles of Motor Control, with Special Reference to Vertebrate Locomotion. *Physiological Reviews*, 271 - 320.

Grillner, S. & Jessell, T. M. (2009). Measured Motion: Searching for Simplicity in Spinal Locomotor Networks. *Current Opinion in Neurobiology*, 572 - 586.

Gross, M. K., Dottori, M. & Goulding, M. (2002). Lbx1 Specifies Somatosensory Association Interneurons in the Dorsal Spinal Cord. *Neuron*, 535 - 549.

Gruner, J. A. & Altman, J. (1980). Swimming in the Rat: Analysis of Locomotor Performance in Comparison to Stepping. *Experimental Brain Research*, 374 - 382.

Gupta, S., Sivalingam, D., Hain, S., Makkar, C., Sosa, E., Clark, A. & Butler, S. J. (2018). Deriving Dorsal Spinal Sensory Interneurons from Human Pluripotent Stem Cells. *Stem Cell Reports*, 390 - 405.

Hägglund, M., Borgius, L., Dougherty, K. J. & Kiehn, O. (2010). Activation of Groups of Excitatory Neurons in the Mammalian Spinal Cord or Hindbrain Evokes Locomotion. *Nature Neuroscience*, 246 - 252.

Hägglund, M., Dougherty, K. J., Borgius, L., Itohara, S., Iwasato, T. & Kiehn, O. (2013). Optogenetic Dissection Reveals Multiple Rhythmogenic Modules Underlying Locomotion. *Proceedings of the National Academy of Science of the United States*, 11589 - 11594.

Hamel, E. J., Grewe, B. F., Parker, J. G. & Schnitzer, M. J. (2015). Cellular Level Brain Imaging in Behaving Mammals: An Engineering Approach. *Neuron*, 140 - 159.

Haque, F., Rancic, V., Zhang, W., Clugston, R., Ballanyi, K. & Gosgnach, S. (2018). WT1-Expressing Interneurons Regulate Left-Right Alternation During Mammalian Locomotor Activity. *The Journal of Neuroscience*, 5666 - 5676.

Hayashi, M., Hinckley, C. A., Driscoll, S. P., Moore, N. J., Levine, A. J., Hilde, K. L., Sharma, K. & Pfaff, S. L. (2018). Graded Arrays of Spinal and Supraspinal V2a Interneuron Subtypes Underlie Forelimb and Hindlimb Motor Control. *Neuron*, 869 - 884.

Helmbacher, F., Schneider-Maunoury, S., Topilko, P., Tiret, L. & Charnay, P. (2000). Targeting of the EphA4 Tyrosine Kinase Receptor Affects Dorsal/Ventral Pathfinding of Limb Motor Axons. *Development*, 3313 - 3324.

Hemmati-Brivanlou, A. & Melton, D. A. (1994). Inhibition of Activin Receptor Signaling Promotes Neuralization in Xenopus. *Cell*, 273 - 281.

Hemmati-Brivanlou, A., Kelly, O. G. & Melton, D. A. (1994). Follistatin, an Antagonist of Activin, Is Expressed in the Spemann Organizer and Displays Direct Neuralizing Activity. *Cell*, 283 - 295.

Hinckley, C. A., Alaynick, W. A., Gallarda, B. W., Hayashi, M., Hilde, K. L., Driscoll, S. P., Dekker, J. D., Tucker, H. O., Sharpee, T. O. & Pfaff, S. L. (2015). Spinal Locomotor Circuits Develop Using Hierarchical Rules Based on Motorneuron Position and Identity. *Neuron*, 1008 - 1021.

Hoang, P. T., Chalif, J. I., Bikoff, J. B., Jessell, T. M., Mentis, G. Z. & Wichterle, H. (2018). Subtype Diversification and Synaptic Specificity of Stem Cell-Derived Spinal Interneurons. *Neuron*, 135 - 149.

Hollyday, M. & Hamburger, V. (1977). An Autoradiographic Study of the Formation of the Lateral Motor Column in the Chick Embryo. *Brain Research*, 197 - 208.

Ichiyama, R. M., Gerasimenko, Y., Jindrich, D. L., Zhong, H., Roy, R. R. & Edgerton, V. R. (2008). Dose Dependence of the 5-HT Agonist Quipazine in Facilitating Spinal Stepping in the Rat with Epidural Stiumlation. *Neuroscience Letters*, 281 - 285.

Ikeda, W., Nakanishi, H., Miyoshi, J., Mandai, K., Ishizaki, H., Tanaka, M., Togawa, A., Takahashi, K., Nishioka, H., Yoshida, H., Mizoguchi, A., Nishikawa, S. & Takai, Y. (1999). Afadin: A Key Molecule Essential for Structural Organization of Cell-Cell Junctions of Polarized Epithelia During Embryogenesis. *The Journal of Cell Biology*, 1117 - 1131.

Imai, F., Ladle, D. R., Leslie, J. R., Duan, X., Rizvi, T. A., Ciraolo, G. M., Zheng, Y. & Yoshida, Y. (2016). Synapse Formation in Monosynaptic Sensory-Motor

Connections Is Regulated by Presynaptic Rho GTPase Cdc42. *The Journal of Neuroscience*, 5724 - 5735.

Imondi, R., Wideman, C. & Kapriellan, Z. (2000). Complementary Expression of Transmembrane Ephrins and their Receptors in the Mouse Spinal Cord: a Possible Role in Constraining the Orientation of Longitudinally Projecting Axons. *Development*, 1397 - 1410.

Iwasato, T., Katoh, H., Nishimaru, H., Ishikawa, Y., Inoue, H., Saito, Y. M., Ando, R., Iwama, M., Takahashi, R., Negishi, M. & Itohara, S. (2007). Rac-GAP α-Chimaerin Regulates Motor-Circuit Formation as a Key Mediator of EphrinB3/EphA4 Forward Signaling. *Cell*, 742 - 753.

Jessell, T. M. (2000). Neuronal Specification in the Spinal Cord: Inductive Signals and Transcriptional Codes. *Nature Reviews Genetics*, 20 - 29.

Jordan, L., Liu, J., Hedlund, P., Akay, T. & Pearson, K. (2008). Descending Command Systems for the Initiation of Locomotion in Mammals. *Brain Research Reviews*, 183 - 191.

Jossin, Y. & Copper, J. A. (2011). Reelin, Rap1 and N-Cadherin Orient the Migration of Multipolar Neurons in the Developing Neocortex. *Nature Neuroscience*, 697 - 704.

Juvin, L., Le Gal, J.-P., Simmers, J. & Morin, D. (2012). Cervicolumbar Coordination in Mammalian Quadrupedal Locomotion: Role of Spinal Thoracic Circuitry and Limb Sensory Input. *The Journal of Neuroscience*, 953 - 965.

Juvin, L., Simmers, J. & Morin, D. (2005). Propriospinal Circuitry Underlying Interlimb Coordination in Mammalian Quadrupedal Locomotion. *The Journal of Neuroscience*, 6025 - 6035.

Kandel, E. R., Schwartz, J. H., Jessell, T. M., Siegelbaum, S. A. & Hudspeth, A. J. (2013). Locomotion. In *Principles of Neural Science* (Fifth Edition ed., pp. 812 - 833). The McGraw-Hill Companies, Inc.

Katayama, K.-i., Leslie, J. R., Lang, R. A., Zheng, Y. & Yoshida, Y. (2012). Left-Right Locomotor Circuitry Depends Upon RhoA-Driven Organization of the Neuroepithelium in the Developing Spinal Cord. *The Journal of Neuroscience*, 10396 - 10407.

Kawauchi, T., Sekine, K., Shikanai, M., Chihama, K., Tomita, K., Kubo, K.-I., Nakahima, K., Nabeshima, Y.-I. & Hoshino, M. (2010). Rab GTPases-Dependent Endocytic Pathways Regulate Neuronal Migration and Maturation Through N-Cadherin Trafficking. *Neuron*, 588 - 602.

Kiehn, O. (2016). Decoding the Organization of Spinal Circuits that Control Locomotion. *Nature Reviews Neuroscience*, 224 - 238.

Kiehn, O. (2006). Locomotor Circuits in the Mammalian Spinal Cord. *Annual Reviews*, 279 - 306.

Kjaerulff, O. & Kiehn, O. (1996). Distribution of Networks Generating and Coordinating Locomotor Activity in the Neonatal Rat Spinal Cord In Vitro: A Lesion Study. *The Journal of Neuroscience*, 5777 - 5794.

Kudo, N. & Yamada, T. (1987). N-Methyl-D,L-Aspartate-Induced Locomotor Activity in a Spinal Cord-Hindlimb Muscles Preparation of the Newborn Rat Studied in vitro. *Neuroscience Letters*, 43 - 48.

Kullander, K., Butt, S. J., Lebret, J. M., Lundfald, L., Restrepo, C. E., Rydstrom, A., Klein, R. & Kiehn, O. (2003). Role of EphA4 and EphrinB3 in Local Neuronal Circuits that Control Walking. *Science*, 1889 - 1892.

Kullander, K., Croll, S., Zimmer, M., Pan, L., McClain, J., Hughes, V., Zabski, S., DeChiara, T. M., Klein, R., Yancopoulos, G. D. & Gale, N. W. (2001). Ephrin-B3 is the Midline Barrier that Prevents Corticospinal Tract Axons from Recrossing, Allowing for Unilateral Motor Control. *Genes & Development*, 877 - 888.

Landmesser, L. (1978). The Distribution of Motoneurones Supplying Chick Hind Limb Muscles. *The Journal of Physiology*, 371 - 389.

Langworthy, O. R. (1924). A Physiological Study of the Reactions of Young Decerebrate Animals. *The Journal of Physiology*, 254 - 264.

Lanuza, G. M., Gosgnach, S., Pierani, A., Jessell, T. M. & Goulding, M. (2004). Genetic Identification of Spinal Interneurons that Coordinate Left-Right Locomotor Activity Necessary for Walking Movements. *Neuron*, 375 - 386.

Laussu, J., Audouard, C., Kischel, A., Assis-Nascimento, P., Escalas, N., Liebl, D. J., Soula, C. & Davy, A. (2017). Eph/Ephrin Signaling Controls Progenitor Identities In The Ventral Spinal Cord. *Neural Development*, 1 - 11.

Leber, S. M. & Sanes, J. R. (1995). Migratory Paths of Neurons and Glia in the Embryonic Chick Spinal Cord. *The Journal of Neuroscience*, 1236 - 1248.

Lemieux, M., Josset, N., Roussel, M., Couraud, S. & Bretzner, F. (2016). Speed-Dependent Modulation of the Locomotor Behavior in Adult Mice Reveals Attractor and Transitional Gaits. *Frontiers in Neuroscience*, 1 - 16.

Lemon, R. N. (2008). Descending Pathways in Motor Control. *Annual Review of Neuroscience*, 195 - 218.

Lin, J. H., Salto, T., Anderson, D. J., Lance-Jones, C., Jessell, T. M. & Arber, S. (1998). Functionally Related Motor Neuron Pool and Muscle Sensory Afferent Subtypes Defined by Coordinate ETS Gene Expression. *Cell*, 393 - 407.

Liu, J.-P., Laufer, E. & Jessell, T. M. (2001). Assigning the Positional Identity of Spinal Motor Neurons: Rostrocaudal Patterning of Hox-c Expression by FGFs, Gdf11, and Retinoids. *Neuron*, 997 - 1012.

Livet, J., Sigrist, M., Stroebel, S., De Paola, V., Price, S. R., Henderson, C. E., Jessell, T. M. & Arber, S. (2002). ETS Gene Pea3 Controls the Central Position and Terminal Arborization of Specific Motor Neuron Pools. *Neuron*, 877 - 892.

Lu, D. C., Niu, T. & Alaynick, W. A. (2015). Molecular and Cellular Development of Spinal Cord Locomotor Circuitry. *Frontiers in Molecular Neuroscience*, 1 - 18.

Lundberg, A. (1979). Multisensory Control of Spinal Reflex Pathways. *Brain Research*, 11 - 28.

Lundfald, L., Restrepo, C., Butt, S., Peng, C.-Y., Droho, S., Endo, T., Zeilhofer, H. U., Sharma, K. & Kiehn, O. (2007). Phenotype of V2-Derived Interneurons and their Relationship to the Axon Guidance Molecular EphA4 in the Developing Mouse Spinal Cord. *European Journal of Neuroscience*, 2989 - 3002.

López-Bendito, G., Flames, N., Ma, L., Fouquet, C., Di Meglio, T., Chedotal, A., Tessier-Levigne, M. & Marín, O. (2007). Robo1 and Robo2 Cooperate to Control the Guidance of Major Axonal Tracts in the Mammalian Forebrain. *The Journal of Neuroscience*, 3395 - 3407.

Luria, V., Krawchuk, D., Jessell, T. M., Laufer, E. & Kania, A. (2008). Specification of Motor Axon Trajectory by Ephrin-B/EphB Signaling: Symmetrical Control of Axonal Patterning in the Developing Limb. *Neuron*, 1039 - 1053.

Machado, T. A., Pnevmatikakis, E., Paninski, L., Jessell, T. M. & Miri, A. (2015). Primacy of Flexor Locomotor Pattern Revealed by Ancestral Reversion of Motor Neuron Identity. *Cell*, 338 - 350.

Mandai, K., Rikitake, Y., Mori, M. & Takai, Y. (2015). Nectins and Nectin-Like Molecules in Development and Disease. In *Cellular Adhesion in Development and Disease* (pp. 197 - 231).

Marigold, D. S. & Drew, T. (2011). Contribution of the Cells in the Posterior Parietal Cortex to the Planning of Visually Guided Locomotion in the Cat: Effects of Temporary Visual Interruption. *The Journal of Neurophysiology*, 2457 - 2470.

Marple-Horvat, D. E. & Armstrong, D. M. (1999). Central Regulation of Motor Cortex Neuronal Responses to Forelimb Nerve Inputs During Precision Walking in the Cat. *The Journal of Physiology*, 279 - 299.

Marple-Horvat, D. E., Amos, A. J., Armstrong, D. M. & Criado, J. M. (1993). Changes in Discharge Patterns of Cat Motor Cortex Neurones During Unexpected Perturbations of On-Going Locomotion. *The Journal of Physiology*, 87 - 113.

Mayer, W. P. & Akay, T. (2018). Stumbling Corrective Reaction Elicited by Mechanical and Electrical Stimulation of the Saphenous Nerve in Walking Mice. *Journal of Experimental Biology*, 1 - 10.

McHanwell, S. & Biscoe, T. J. (1981). The Sizes of Motoneurons Supplying Hindlimb Muscles in the Mouse. *Proceedings of the Royal Society of London. Series B, Biological Sciences*, 201 - 216.

McVea, D. A. & Pearson, K. G. (2006). Long-Lasting Memories of Obstacles Guide Leg Movements in the Walking Cat. *The Journal of Neuroscience*, 1175 -1178.

Mendes, C., Bartos, I., Marka, Z., Akay, T., Marka, S. & Mann, R. (2015). Quantification of Gait Parameters in Freely Walking Rodents. *BMC Biology*, 1 - 11.

Miles, G. B., Hartley, R., Todd, A. J. & Brownstone, R. M. (2007). Spinal Cholinergic Interneurons Regulate the Excitability of Motoneurons During Locomotion. *Proceedings of the National Acabdemy of Science of the United States of America*, 2448 - 2453.

Miyata, M., Maruo, T., Kaito, A., Wang, S., Yamamoto, H., Fujiwara, T., Mizoguchi, A., Mandai, K. & Takai, Y. (2017). Roles of Afadin in the Formation of the Cellular Architecture of the Mouse Hippocampus and Dentate Gyrus. *Molecular and Cellular Neurosciences*, 34 - 44.

Miyata, M., Ogita, H., Komura, H., Nakata, S., Okamoto, R., Ozaki, M., Majima, T., Matsuzawa, N., Kawano, S., Minami, A., Waseda, M., Fujita, N., Mizutani, K., Rikitake, Y. & Takai, Y. (2009). Localization of Nectin-Free Afadin at the Leading Edge and its Involvement in Directional Cell Movement Induced by Platelet-Derived Growth Factor. *Journal of Cell Science*, 4319 - 4329.

Mizoguchi, A., Nakanishi, H., Kimura, K., Matsubara, K., Ozaki-Kuroda, K., Katata, T., Honda, T., Kiyohara, Y., Heo, K., Higashi, M., Tsutsumi, T., Sonoda, S., Ide, D. & Takai, Y. (2002). Nectin: an Adhesion Molecule Involved in Formation of Synapses. *The Journal of Cell Biology*, 555 - 565.

Moran-Rivard, L., Kagawa, T., Saueressig, H., Gross, M. K., Burrill, J. & Goulding, M. (2001). Evx1 Is a Postmitotic Determinant of V0 Interneuron Identity in the Spinal Cord. *Neuron*, 385 - 399.

Moschovakis, A. K., Solodkin, M. & Burke, R. E. (1992). Anatomical and Physiological Study of Interneurons in an Oligosynaptic Cutaneous Reflex Pathway in the Cat Hindlimb. *Brain Research*, 311 - 318.

Mulherkar, S., Liu, F., Chen, Q., Narayanan, A., Couvillon, A. D., Shine, H. D., Tolias, K. F., (2013). The Small GTPase RhoA Is Required for Proper Locomotor Circuit Assembly. *PLoS One*, 1 - 11.

Nascimento, F., Broadhead, M. J., Tetringa, E., Tsape, E., Zagoraiou, L. & Miles, G. B. (2020). Synaptic Mechanisms Underlying Modulation of Locomotor-Related Motoneuron Output by Premotor Cholinergic Interneurons. *eLIFE*, 1 - 26.

Ni, Y., Nawabi, H., Liu, X., Yang, L., Miyamichi, K., Tedeschi, A., Xu, B., Wall, N. R., Callaway, E. M. & He, Z. (2014). Characterization of Long Descending Premotor Propriospinal Neurons in the Spinal Cord. *The Journal of Neuroscience*, 9404 - 9417.

Okabe, N., Shimizu, K., Ozaki-Kuroda, K., Nakanishi, H., Morimoto, K., Takeuchi, M., Katsumaru, H., Murakami, F. & Takai, Y. (2004). Contacts Between the Commissural Axons and the Floor Plate Cells are Mediated by Nectins. *Developmental Biology*, 244 - 256.

Orlovsky, G. N. (1969). Spontaneous and Induced Locomotion of the Thalamic Cat. *Biophysics*, 1154 - 1162.

Orlovsky, G., Deliagina, T. & Grillner, S. (1999). Neuronal Control of Locomotion: From Mollusc to Man. *Oxford University Press*.

Paixão, S., Balijepalli, A., Serradj, N., Niu, J. & Luo, W. (2013). EphrinB3/EphA4-Mediated Guidance of Ascending and Descending Spinal Tracts. *Neuron*, 1407 - 1420.

Pearson, K. G. (2004). Generating the Walking Gait: Role of Sensory Feedback. *Progress in Brain Research*, 123 - 129.

Pearson, K. G. (1995). Proprioceptive Regulation of Locomotion. *Current Opinion in Neurobiology*, 786 - 791.

Pecho-Vrieseling, E., Sigrist, M., Yoshida, Y., Jessell, T. M. & Arber, S. (2009). Specificity of Sensory-Motor Connections Encoded by Sema3e-Plxnd1 Recognition. *Nature*, 842 - 846.

Peng, J., Ferent, J., Li, Q., Liu, M., Da Silva, R. V., Zeilhofer, H. U., Kania, A., Zhang, Y. & Charron, F. (2018). Loss of Dcc in the Spinal Cord Is Sufficient to Cause a Deficit in Lateralized Motor Control and the Switch to a Hopping Gait. *Developmental Dynamics*, 620 - 629.

Philippson, M. (1905). *L'Autonomie et la Centralisation dans le Système Nerveux des Animaux.* Falk.

Pignata, A., Ducuing, H. & Castellani, V. (2016). Commissural Axon Navigation: Control of Midline Crossing in the Vertebrate Spinal Cord by the Semaphorin 3B Signaling. *Cell Adhesion & Migration*, 604 - 617.

Price, S. R., De Marco Garcia, N. V., Ranscht, B. & Jessell, T. M. (2002). Regulation of Motor Neuron Pool Sorting by Differential Expression of Type II Cadherins. *Cell*, 205 - 216.

Rabe, N., Gezelius, H., Vallstedt, A., Memic, F. & Kullander, K. (2009). Netrin-1-Dependent Spinal Interneuron Subtypes Are Required for the Formation of Left-Right Alternating Locomotor Circuitry. *The Journal of Neuroscience*, 15642 - 15649.

Rabe-Bernhardt, N., Memic, F., Gezelius, H., Thiebes, A.-L., Vallstedt, A. & Kullander, K. (2012). DCC Mediated Axon Guidance of Spinal Interneurons Is Essential for Normal Locomotor Central Pattern Generator Function. *Developmental Biology*, 279 - 289.

Rakotomamonjy, J., Brunner, M., Juschke, C., Zang, K., Huang, E. J., Reichardt, L. F. & Chenn, A. (2017). Afadin Controls Cell Polarization and Mitotic Spindle Orientation in Developing Cortical Radial Glia. *Neural Development*, 1 - 10.

Ramer, L. M., Ramer, M. S. & Bradbury, E. J. (2014). Restoring Function After Spinal Cord Injury: Towards Clinical Translation of Experimental Strategies. The *Lancet Neurology*, 1241 - 1256.

Rikitake, Y., Mandai, K. & Takai, Y. (2012). The Role of Nectins in Different Types of Cell-Cell Adhesion. *Journal of Cell Science*, 3713 - 3722.

Roberts, A., Li, W.-C., Soffe, S. R. & Wolf, E. (2008). Origin of Excitatory Drive to a Spinal Locomotor Network. *Brain Research Reviews*, 22 - 28.

Romanes, G. (1951). The Motor Cell Columns of the Lumbo-Sacral Spinal Cord of the Cat. *The Journal of Comparative Neurology*, 313 - 363.

Romanes, G. (1964). The Motor Pools of the Spinal Cord. *Progress in Brain Research*, 93 - 119.

Rossi, J., Balthasar, N., Olson, D., Scott, M., Berglund, E., Lee, C., Choi, M. J., Lauzon, D., Lowell, B. B. & Elmquist, J. K. (2011). Melanocortin-4 Receptors Expressed by Cholinergic Neurons Regulate Energy Balance and Glucose Homeostasis. *Cell Metabolism*, 195 - 204.

Rossignol, S., Dubuc, R. & Gossard, J.-P. (2006). Dynamic Sensorimotor Interactions in Locomotion. *Physiological Reviews*, 89 - 154.

Rowitch, D. H., St.-Jacques, B., Lee, S. M., Flax, J. D., Snyder, E. Y. & McMahon, A. P. (1999). Sonic Hedgehog Regulates Proliferation and Inhibits Differentiation of CNS Precursor Cells. *The Journal of Neuroscience*, 8954 - 8965.

Ruder, L., Takeoka, A. & Arber, S. (2016). Long-Distance Descending Spinal Neurons Ensure Quadrupedal Locomotor Stability. *Neuron*, 1 - 16.

Sathyamurthy, A., Johnson, K. R., Matson, K. J. E., Dobrott, C. I., Li, L., Ryba, A. R., Bergman, T. B., Kelly, M. C., Kelley, M. W. & Levine, A. J. (2018). Massively Parallel Single Nucleus Transcriptional Profiling Defines Spinal Cord Neurons and Their Activity During Behavior. *Cell Reports*, 2216 - 2225.

Satoh, D., Pudenz, C. & Arber, S. (2016). Context-Dependent Gait Choice Elicited by EphA4 Mutation in Lbx1 Spinal Interneurons. *Neuron*, 1046 - 1058.

Sawyer, J. K., Harris, N. J., Slep, K. C., Gaul, U. & Peifer, M. (2009). The Drosophila afadin Homologue Canoe Regulates Linkage of the Actin Cytoskeleton to Adherens Junctions During Apical Constriction. *The Journal of Cell Biology*, 57 - 73.

Schaltenbrand, G. & Cobb, S. (1930). Clinical and Anatomical Studies on Two Cats without Neocortex. *Brain*, 449 - 487.

Schnerwitzki, D., Perry, S., Ivanova, A., Caixeta, F. V., Cramer, P., Günther, S., Weber, K., Tafreshiha, A., Becker, L., Vargas Panesso, I. L., Klopstock, T., Hrabe de Angelis, M., Schmidt, M. Kullander, K. & Englert, C. (2018). Neuron-Specific Inactivation of Wt1 Alters Locomotion in Mice and Changes Interneuron Composition in the Spinal Cord. *Life Science Alliance*, 1 - 14.

Serafini, T., Colamarino, S. A., Leonardo, E. D., Wang, H., Beddington, R., Skarnes, W. C. & Tessier-Lavigne, M. (1996). Netrin-1 is Required for Commissural Axon Guidance in the Developing Vertebrate Nervous System. *Cell*, 1001 - 1014.

Sharma, K., Leonard, A. E., Lettieri, K. & Pfaff, S. L. (2000). Genetic and Epigenetic Mechanisms Contribute to Motor Neuron Pathfinding. *Nature*, 515 - 519.

Sherrington, C. S. (1910). Flexion-Reflex of the Limb, Crossed Extension-Reflex, and Reflex Stepping and Standing. *The Journal of Physiology*, 28 - 121.

Sherrington, C. S. (1906). *The Integrative Action of the Nervous System.* Yale University Press.

Shirasaki, R., Lewcock, J. W., Lettieri, K. & Pfaff, S. L. (2006). FGF as a Target-Derived Chemoattractant for Developing Motor Axons Genetically Programmed by the LIM Code. *Neuron*, 841 -853.

Sockanathan, S. & Jessell, T. M. (1998). Motor Neuron-Derived Retinoid Signaling Specifies Subtype Identity of Spinal Motor Neurons. *Cell*, 503 - 514.

Song, J., Ampatzis, K., Björnfors, E. & El Manira, A. (2016). Motor Neurons Control Locomotor Circuit Function Retrogradely via Gap Junctions. *Nature*, 399 - 402.

Spemann, H. & Mangold, H. (1924). Über Induktion von Embryonalanlagen Durch Implantation Artfremder Organisatoren. *Archiv für mikroskopische Anatomie und Entwicklungsmechanik*, 599 - 638.

Stam, F. J., Hendricks, T. J., Zhang, J., Geiman, E. J., Francius, C., Labosky, P. A., Clotman, F. & Goulding, M. (2012). Renshaw Cell Interneuron Specialization is Controlled by a Temporally Restricted Transcription Factor Program. *Development*, 179 - 190.

Stan, A., Pierlarski, K. N., Brigadski, T., Wittenmayer, N., Fedorchenko, O., Gohla, A., Lessmann, V., Dresbach, T. & Gottmann, K. (2010). Essential Cooperation of N-Cadherin and neuroligin-1 in the Transsynaptic Control of Vesicle Accumulation. *Proceedings of the National Academy of Science of the United States of America*, 11116 - 11121.

Stepien, A., Tripodi, M. & Arber, S. (2010). Monosynaptic Rabies Virus Reveals Premotor Network Organization and Synaptic Specificity of Cholinergic Partition Cells. *Neuron*, 456 - 472.

Südhof, T. C. (2018). Towards an Understanding of Synapse Formation. *Neuron*, 274 - 293.

Sürmeli, G., Akay, T., Ippolito, G., Tucker, P. & Jessell, T. M. (2011). Patterns of Spinal Sensory-Motor Connectivity Prescribed by a Dorsoventral Positional Template. *Cell*, 653 - 665.

Swanson, L. W., Morgenson, G. J., Gerfen, C. R. & Robinson, P. (1983). Evidence for a Projection From the Lateral Preoptic Area and Substantia Innominata to the 'Mesencephalic Locomotor Region' in the Rat. *Brain Research*, 161 - 178.

Sweeney, L. B., Bikoff, J. B., Gabitto, M. I., Brenner-Morton, S., Baek, M., Yang, J. H., Tabak, E. G., Dasen, J. S., Kintner, C. R. & Jessell, T. M. (2017). Origin and Segmental Diversity of Spinal Inhibitory Interneurons. *Neuron*, 341 - 355.

Tachibana, K., Nakanishi, H., Mandai, K., Ozaki, K., Ikeda, W., Yamamoto, Y., Nagafuchi, A., Tsukita, S. & Takai, Y. (2000). Two Cell Adhesion Molecules, Nectin and Cadherin, Interact Through Their Cytoplasmic Domain-Associated Proteins. *The Journal of Cell Biology*, 1161 - 1176.

Takahashi, K., Nakanishi, H., Miyahara, M., Mandai, K., Satoh, K., Satoh, A., Nishioka, H., Aoki, J., Nomoto, A., Mizoguchi, A. & Takai, Y. (1999). Nectin/PRR: an Immunoglobulin-Like Cell Adhesion Molecule Recruited to Cadherin-Based

Adherens Junctions Through Interaction with Afadin, a PDZ Domain-Containing Protein. *The Journal of Cell Biology*, 539 - 549.

Takai, Y., Ikeda, W., Ogita, H. & Rikitake, Y. (2008). The Immunoglobulin-Like Cell Adhesion Molecule Nectin and Its Associated Protein Afadin. *Annual Review of Cell and Developmental Biology*, 309 - 342.

Takakusaki, K. (2013). Neurophysiology of Gait: From the Spinal Cord to the Frontal Lobe. *Movement Disorders*, 1483 - 1491.

Takakusaki, K., Habaguchi, T., Ohtinata-Sugimoto, J., Saitoh, K. & Sakamoto, T. (2003). Basal Ganglia Efferents to the Brainstem Centers Controlling Postural Muscle Tone and Locomotion: a New Concept for Understanding Motor Disorders in Basal Ganglia Dysfunction. *Neuroscience*, 293 - 308.

Takatoh, J., Nelson, A., Zhou, X., Bolton, M., Ehlers, M., Arenkiel, B., Mooney, R. & Wang, F. (2013). New Modules Are Added to Vibrissal Premotor Circuitry with the Emergence of Exploratory Whisking. *Neuron*, 346 – 360.

Talpalar, A. E. & Kiehn, O. (2010). Glutamatergic Mechanisms for Speed Control and Network Operation in the Rodent Locomotor CPG. *Frontiers in Neural Circuits*, 1 - 14.

Talpalar, A., Bouvier, J., Borgius, L., Fortin, G., Pierani, A. & Kiehn, O. (2013). Dual-mode Operation of Neuronal Networks Involved in Left–Right Alternation. *Nature*, 85 - 88.

Tazerart, S., Viemari, J.-C., Darbon, P., Vinay, L. & Brocard, F. (2007). Contribution of Persistent Sodium Current to Locomotor Pattern Generation in Neonatal Rats. *The Journal of Neurophysiology*, 613 - 628.

Ten Cate, J. & Van Herk, A. (1933). Beobachtungen in Kaninchen nach Exstirpationen im Neopallium. *Archives Neerlandaises de Physiologie de l'Homme et des Animaux*, 337 - 386.

Tripodi, M., Stepien, A. E., & Arber, S. (2011). Motor Antagonism Exposed by Spatial Segregation and Timing of Neurogenesis. *Nature*, 61 - 68.

Valle, M. S., Bosco, G. & Poppele, R. E. (2017). Cerebellar Compartments for the Processing of Kinematic and Kinetic Information Related to Hindlimb Stepping. *Experimental Brain Research*, 3437 - 3448.

Wee, B., Johnston, C. A., Prehoda, K. E. & Doe, C. Q. (2011). Canoe Binds RanGTP to Promote Pins(TPR)/Mud-Mediated Spindle Orientation. *The Journal of Cell Biology*, 369 - 376.

Whelan, P., Bonnot, A. & O'Donovan, M. J. (2000). Properties of Rhythmic Activity Generated by the Isolated Spinal Cord of the Neonatal Mouse. *The Journal of Neurophysiology*, 2821 - 2833.

Wichterle, H., Lieberam, I., Porter, J. A. & Jessell, T. M. (2002). Directed Differentiation of Embryonic Stem Cells into Motor Neurons. *Cell*, 385 - 397.

Widajewicz, W., Kably, B. & Drew, T. (1994). Motor Cortical Activity During Voluntary Gait Modifications in the Cat. II. Cells Related to the Hindlimbs. *The Journal of Neurophysiology*, 2070 - 2089.

World Health Organization (2011). World Report on Disability. *WHO Library*, 1 - 276.

Wu, Z., Makihara, S., Yam, P. T., Teo, S., Renier, N., Balekoglu, N., Moreno-Bravo, J. A., Olsen, O., Chédotal, A., Charron, F. & Tessier-Levigne, M. (2019). Long-Range Guidance of Spinal Commissural Axons by Netrin1 and Sonic Hedhehog from Midline Floor Plate Cells. *Neuron*, 635 - 647.

Yamamoto, H., Mandai, K., Konno, D., Maruo, T., Matsuzaki, F. & Takai, Y. (2015). Impairment of Radial Glial Scaffold-Dependent Neuronal Migration and Formation of Double Cortex by Genetic Ablation of afadin. *Brain Research*, 139 - 152.

Yamamoto, H., Maruo, T., Majima, T., Ishizaki, H., Tanaka-Okamoto, M., Miyoshi, J., Mandai, K. & Takai, Y. (2013). Genetic Deletion of Afadin Causes Hydrocephalus by Destruction of Adherens Junctions in Radial Glial and Ependymal Cells in the Midbrain. *PLoS One*, 1 - 10.

Yang, Z., Zimmerman, S., Brakemann, P. R., Beaudoin III, G. M., Reichardt, L. F. & Marciano, D. K. (2013). De novo Lumen Formation and Elongation in the Developing Nephron: a Central Role for afadin in Apical Polarity. *Development*, 1774 - 1784.

Zagoraiou, L., Akay, T., Martin, J., Brownstone, R., Jessell, T. M. & Miles, G. (2009). A Cluster of Cholinergic Premotor Interneurons Modulates Mouse Locomotor Activity. *Neuron*, 645 - 662.

Zampieri, N., Jessell, T. M. & Murray, A. J. (2014). Mapping Sensory Circuits by Anterograde Transsynaptic Transfer of Recombinant Rabies Virus. *Neuron*, 766 - 778.

Zhang, J., Lanuza, G. M., Britz, O., Wang, Z., Siembab, V. C., Zhang, Y., Velasquez, T., Alvarez, F. J., Frank, E. & Goulding, M. (2014). V1 and V2b Interneurons Secure the Alternating Flexor-Extensor Motor Activity Mice Require for Limbed Locomotion. *Neuron*, 138 - 150.

Zhang, Y., Narayan, S., Geiman, E., Lanuza, G., Velasquez, T., Shanks, B., Akay, T., Dyck, J., Pearson, K., Gosgnach, S., Fan, C.-M. & Goulding, M. (2008). V3 Spinal Neurons Establish a Robust and Balanced Locomotor Rhythm During Walking. *Neuron*, 84 - 96.

Zhong, G., Masino, M. A. & Harris-Warrick, R. W. (2007). Persistent Sodium Currents Participate in Fictive Locomotion Generation in Neonatal Mouse Spinal Cord. *The Journal of Neuroscience*, 4507 - 4518.

Zhu, P., Guan, J., Xu, P., Zhao, J., Zhang, C., Zhang, B., Mao, Y. & Cui, W. (2019). Cellular Therapeutic Strategies for Spinal Cord Injury. *Advances in Wound Care*, 585 - 605.

APPENDIX

APPENDIX I

Table 8. Locomotor parameters in control, *afadin* $^{fl/fl}$ and *afadin* $^{fl/fl}$ *; ChAT* mice. F: forelimbs, H: hindlimbs

Genotype	Phenotype	Speed (cm/s)	Step frequency (Hz)	% of sync. steps	Step length (cm)	Stance duration (s)
control 1	alternating	23.5	4.7	0	F: 17.47 H: 17.29	F: 0.16 H: 0.19
control 2	alternating	22.4	5.7	0	F: 14.60 H: 14.92	F: 0.14 H: 0.16
control 3	alternating	18.7	4.0	0	F: 16.93 H: 16.63	F: 0.20 H: 0.21
afadin $^{fl/fl}$ 1	mostly alternating	15.7	3.3	16.3	F: 14.99 H: 14.47	F: 0.21 H: 0.19
afadin $^{fl/fl}$ 2	mostly alternating	20.0	4.7	16.1	F: 14.16 H: 13.75	F: 0.17 H: 0.16
afadin $^{fl/fl}$ 3	mostly alternating	19.3	3.3	5.9	F: 14.90 H: 14.57	F: 0.21 H: 0.21
afadin $^{fl/fl}$ 4	mixed	21.9	4.0	56.8	F: 12.50 H: 12.21	F: 0.18 H: 0.22
afadin $^{fl/fl}$ 5	mixed	12.7	4.7	69.4	F: 12.67 H: 12.72	F: 0.25 H: 0.25
afadin $^{fl/fl}$ 6	mixed	12.3	4.0	60.0	F: 12.34 H: 12.45	F: 0.12 H: 0.14
afadin $^{fl/fl}$ 7	synchronizing	29.5	7.7	90.5	F: 11.70 H: 11.99	F: 0.10 H: 0.10
afadin $^{fl/fl}$ 8	synchronizing	28.7	7.3	97.1	F: 12.35 H: 11.51	F: 0.11 H: 0.11

afadin $^{fl/fl}$ 9	synchronizing	28.7	7.7	95.5	F: 11.20 H: 10.49	F: 0.09 H: 0.10
afadin $^{fl/fl}$ 10	synchronizing	29.8	7.0	100	F: 10.39 H: 10.30	F: 0.11 H: 0.11
afadin $^{fl/fl}$; *ChAT* 1	alternating	20.7	3.2	0	F: 15.98 H: 16.26	F: 0.19 H: 0.19
afadin $^{fl/fl}$; *ChAT* 2	alternating	26.2	3.5	0	F: 17.63 H: 16.77	F: 0.17 H: 0.16
afadin $^{fl/fl}$; *ChAT* 3	alternating	27.82	3.8	0	F: 18.84 H: 19.10	F: 0.15 H: 0.15

APPENDIX II

Table 9. Afadin and grey matter measurements in e14.5 control and *afadin $^{fl/fl}$; Wnt1* mice. GM: grey matter

Genotype	Afadin (µm)	GM top (µm)	GM total (µm)
control 1	155.44	116.08	329.15
control 2	157.26	118.26	337.79
control 3	152.81	122.17	391.16
afadin $^{fl/fl}$; Wnt1 1	139.72	134.88	334.10
afadin $^{fl/fl}$; Wnt1 2	133.45	145.72	327.77
afadin $^{fl/fl}$; Wnt1 3	148.59	165.26	371.49

Table 10. Afadin, Phalloidin and grey matter measurements in e16.5 control and *afadin $^{fl/fl}$; Wnt1* mice. GM: grey matter

Genotype	Afadin (µm)	Phalloidin (µm)	GM top (µm)	GM bottom (µm)	GM total (µm)
control 1	75.11	73.07	137.35	73.66	301.68
control 2	64.67	65.17	136.64	69.51	290.71
control 3	58.98	59.73	145.88	74.35	284.52
afadin $^{fl/fl}$; Wnt1 1	51.38	51.27	149.44	63.16	287.90
afadin $^{fl/fl}$; Wnt1 2	40.77	41.23	159.22	58.49	296.33
afadin $^{fl/fl}$; Wnt1 3	43.80	45.37	150.42	55.72	286.36

APPENDIX III

Table 11. Number of neurons labeled in each ECR RV tracing experiment. ChAT^{+} datasets were also used for total cervical premotor analysis in Figure 19. Numbers in colors represent neurons that were identified for the corresponding marker (color code as in Figures 20 - 24). MNs = motor neurons

Genotype	Experiment	Total	Ipsi	Contra	MNs
control 1	ChAT	1128 33	1017 31	111 2	15
control 2		1179 24	1075 20	104 4	26
control 3		968 18	913 18	55 0	40
afadin $^{fl/fl}$ 1		1101 24	924 17	177 7	33
afadin $^{fl/fl}$ 2		1585 46	1344 36	241 10	46
afadin $^{fl/fl}$ 3		1478 35	1269 25	209 10	36
control 1	Chx10	1740 10	1599 10	141 0	29
control 2		2504 23	2308 23	196 0	23
control 3		1160 16	1102 16	58 0	32
control 4		1635 7	1464 7	171 0	20
afadin $^{fl/fl}$ 1		1782 22	1552 21	230 1	23
afadin $^{fl/fl}$ 2		2066 16	1811 12	255 4	21
afadin $^{fl/fl}$ 3		2190 20	1940 17	250 3	31

afadin $^{fl/fl}$ 4		1791 8	1511 6	280 2	27
control 1	Lbx1	846 80	753 68	93 12	31
control 2		743 51	704 43	39 8	18
control 3		677 43	624 40	53 3	13
afadin $^{fl/fl}$ 1		1070 94	984 74	86 20	29
afadin $^{fl/fl}$ 2		1730 131	1566 105	164 26	33
afadin $^{fl/fl}$ 3		1569 95	1398 78	171 17	22
control 1	Lhx1/FoxD3	1933 231 187	1691 206 161	242 25 26	43
control 2		1175 123 85	1053 113 68	122 10 17	24
control 3		667 41 44	635 40 44	32 1 0	23
afadin $^{fl/fl}$ 1		854 45 55	789 39 46	65 6 9	19
afadin $^{fl/fl}$ 2		1677 150 158	1436 121 142	241 29 16	19
afadin $^{fl/fl}$ 3		1875 123 127	1582 104 120	293 19 7	21

Table 12. Number of neurons labeled in each GS and TA RV tracing experiment. MNs = motor neurons

Genotype	Experiment	Total	Ipsi	Contra	MNs
control 1	GS	1988	1549	439	31
control 2		1928	1585	343	18
control 3		1875	1416	459	17
afadin $^{fl/fl}$ 1		2511	1925	586	36
afadin $^{fl/fl}$ 2		1572	1377	195	45
control 1	TA	1845	1719	126	47
control 2		2399	1929	470	22
control 3		2340	2044	296	17
afadin $^{fl/fl}$ 1		2507	2260	247	45
afadin $^{fl/fl}$ 2		2506	2083	423	28
afadin $^{fl/fl}$ 3		1835	1572	263	30

STATUTORY DECLARATION

"I, Sophie Skarlatou, by personally signing this document in lieu of an oath, hereby affirm that I prepared the submitted dissertation on the topic "The Role of Afadin Signaling in the Assembly of Spinal Locomotor Circuits" ("Die Rolle des Afadin-Signalsystems in der Entwicklung von Spinalen Lokomotorischen Netzwerken") independently and without the support of third parties, and that I used no other sources and aids than those stated.

All parts, which are based on the publications or presentations of other authors, either in letter or in spirit, are specified as such in accordance with the citing guidelines. The sections on methodology (in particular regarding practical work, laboratory regulations, statistical processing) and results (in particular regarding figures, charts and tables) are exclusively my responsibility.

Furthermore, I declare that I have correctly marked all of the data, the analyses, and the conclusions generated from data obtained in collaboration with other persons, and that I have correctly marked my own contribution and the contributions of other persons (cf. declaration of contribution). I have correctly marked all texts or parts of texts that were generated in collaboration with other persons.

My contributions to any publications to this dissertation correspond to those stated in the preface declaration made together with the supervisor. All publications created within the scope of the dissertation comply with the guidelines of the ICMJE (International Committee of Medical Journal Editors; www.icmje.org) on authorship. In addition, I declare that I shall comply with the regulations of Charité – Universitätsmedizin Berlin on ensuring good scientific practice.

I declare that I have not yet submitted this dissertation in identical or similar form to another Faculty.

The significance of this statutory declaration and the consequences of a false statutory declaration under criminal law (Sections 156, 161 of the German Criminal Code) are known to me."

Date: Signature:

Declaration of your own contribution to any publications

Sophie Skarlatou contributed the following to the below listed publications:

Publication 1: Skarlatou, S., Hérent, C., Toscano, E., Mendes, C.S., Bouvier, J., Zampieri, N. Afadin Signaling at the Spinal Neuroepithelium Regulates Central Canal Formation and Gait Selection, Cell Reports (2020, in print)
Contribution: Data acquisition and analysis as well as manuscript and figure design were carried out by Sophie Skarlatou under supervision of Dr. Niccolò Zampieri, except for fictive locomotion experiments and data presentation (Figure 2) and Ephrin B3 *in situ* hybridizations (Figures 5 and S4).

_____

Signature PhD candidate

CURRICULUM VITAE

Mein Lebenslauf wird aus datenschutzrechtlichen Gründen in der elektronischen Version meiner Arbeit nicht veröffentlicht.

PUBLICATIONS LIST

PEER-REVIEWED JOURNAL ARTICLES

2020: Skarlatou, S., Hérent, C., Toscano, E., Mendes, C.S., Bouvier, J., Zampieri, N. Afadin Signaling at the Neuroepithelium Regulates Central Canal Formation and Gait Selection , Cell Reports (in print)

PODIUM PRESENTATIONS

2019: Skarlatou, S., Toscano, E., Bouvier, J., Mendes, C.S., Zampieri, N. "Afadin signaling at the neuroepithelium regulates central canal formation and gait selection".

Society for Neuroscience Annual Meeting, Chicago (USA), October 19 - 23

POSTER PRESENTATIONS

2018: Skarlatou, S., Mendes, C.S., Zampieri, N. "Afadin signaling in the spinal cord regulates central canal formation and gait selection in mice".

11th FENS Forum of Neuroscience, Berlin (Germany), July 7 - 11

2017: Skarlatou, S., Mendes, C.S., Zampieri, N. "Afadin controls central canal formation and gait selection in mice".

AXON2017, Klosterneuburg (Austria), September 11 - 14

2016: Skarlatou, S., Dewitz, C., Zampieri, N. "The role of afadin in motor neuron organization in the spinal cord".

10th FENS Forum of Neuroscience, Copenhagen (Denmark), July 2 - 6

ACKNOWLEDGEMENTS

First and foremost, I want to thank my supervisor Niccolò Zampieri for believing in me when I was a novice with negligible experience in neuroscience. His enthousiastic inquisitiveness transmitted his passion for science to me and his teachings and advice, both in the lab and outside of it, have shaped me as a mature and critical scientist, ready for the next step.

I also want to extend my thanks to Prof. Dr. Britta Eickholt for accepting to be my first supervisor and providing valuable inputs to my project throughout my graduate studies, Dr. Marta Rosario for taking part in my committee meetings and always challenging me to see my work through a different perspective, and NeuroCure for funding part of my PhD.

I am very grateful to my colleagues who helped me not only with technical assistance, but also with fruitful discussions and words of support: Jasmin Bonkowski, Katrin Gerstmann, Liana Kosizki, Stephan Dietrich. But especially, I want to express my gratitude to Isabelle Werner, who saved my project with the best RV batches; Elisa Toscano, who helped me during the last months of extensive data analysis and will be an outstanding successor for the project; and finally, Carola Dewitz, who has not only been my companion and moral support for all aspects of PhD life, but has also become one of those friends I cannot imagine life without!

The past five years would also not have been such a pleasant endeavour had it not been for my amazing friends who have helped me through up and downs and who always do a great job lifting my spirits: Alexandra Mittelstädt, Alfredo Azmitia, Canan Sahin-Sak, Cecilia Cruz, David Murrieta, Fernando Valdivieso, Grace Lee, Itzel Toledo, Jagoda Pogorzelec, Lydia Brusendorf, Malte Hohenbrink, María Clara Cisneros, María Fernanda Aguilar, Rafael Velasco, Stela Ilicic. I love you all!

And last but not least, I am forever indebted to my family, whose whole-hearted, inconditional support is the motor that keeps me going. My mom and my sister see more potential in me that I will ever be able to fathom and would readily do any sacrifice to help me achieve my goals. I don't know what I would do without them! And finally, Lotti and Theo, who have come into our lives to brighten even the darkest days - I hope that someday I will become someone you can aspire to!